NTNU

Norwegian University of
Science and Technology

A compact disk antenna for car-to-car communication

Pablo García Moreno

Master of Science in Electronics
Submission date: July 2008
Supervisor: Jon Anders Langen Aas, IET

Norwegian University of Science and Technology
Department of Electronics and Telecommunications

Problem Description

Q-Free and SINTEF are partners in CVIS , an EU project where technology for communication between vehicles and between vehicles and roadside are developed. The technology development is based on the new CALM standard. The antenna unit to be placed on the vehicle must cover a broad range of frequency bands, and two versions of broadband monopole antennas have been developed and integrated into an antenna unit. This antenna unit will later be used to demonstrate communication between vehicles and roadside infrastructure.

However, there is a need to develop new antenna solutions, which are more compact and which can more easily be integrated into the roof, side mirrors or wind screens of the vehicle. A promising antenna candidate is the compact disk antenna, as described in [1]. The antenna is a circular patch antenna with a shorted central post, and can be operated in the TM01 mode to generate a conical shaped radiation pattern with a lobe zero at zenith and omni-directional coverage in azimuth, as desired for communication between cars.

The work has been placed in two tasks:

Task 1: Comprise a literature survey/study, analysis/design, manufacturing and measurements of a compact disk antenna for operation around 2 GHz. The design will be based on [1].
Task 2: Comprise a literature survey/study and analysis/design of a stacked disk antenna for a compact multi-band antenna solution. The most interesting frequency bands are the GSM/900, UMTS and 5.9 GHz bands.

The Master thesis will include a literature survey to gain knowledge of the fundamentals of the disk antenna and related antenna types. This will also include techniques used to obtain broadband and multi-band antenna solutions. For the analysis and design of antennas the WIPL-D and EMDS tools will be used.

[1] McEvan et al.,"Compact WLAN Disc Antennas," IEEE Trans. AP, vol. 50, pp. 1862-1864, Dec 2002.

Contact person at SINTEF IKT: Irene Jensen, irene.jensen@sintef.no, tlf 73 59 2740
Adviser at NTNU: Jon Anders Langen Aas

Assignment given: 14. January 2008
Supervisor: Jon Anders Langen Aas, IET

Summary

The final goal of this document is the construction of multi-band terminal for the CVIS project to allow the communication among cars and between the cars and the roadside infrastructure. For the construction of this multi-band terminal, this document takes as starting point, a new compact disk antenna described in [1]. It consists in a circular patch antenna shorted by a central metallic post. This allows reducing the dimensions of a classical circular patch antenna so it is very useful for our application given that the terminal is going to be place on the top of a car and it should be small enough to be attractive for the final users. Specifically, we are going to analyze the behaviour of this kind of antenna when it radiates in the TM_{01} mode, because the radiation pattern of this mode is particularly interesting for the applications of the CVIS project.

This document is divided into two main parts. In the first one, a study in depth of the behaviour of the antenna proposed in [1] was performed. Firstly, through an analytical model and afterward with the help of two simulation tools (WIPL-D and EMDS), we analyze the influence of the main parameters of the antenna (outer and inner radiuses, height, electrical permittivity and the position of the feed) on its properties (resonant frequency, bandwidth, entrance impedance, the shape of the radiation pattern and so on). A general methodology for the design of this kind of antennas was proposed, and it was put in practice with the design of a prototype for a band around 2 GHz. In addition to the conclusions about the influence of the different parameters of the antenna, another important conclusion was done. It was discovered that the use of the simulation tool WIPL-D Lite was not suitable for the simulation of this kind of antenna.

In the second part, this document tackles the construction of a dual-frequency antenna for the bands of 2.4-2.484 GHz and 5.75-5.95 GHz. For this, the present document studies the possibility of stacking two compact circular patch antennas, so we put the one which covers the higher band (the smaller) on the top of the one which covers the lower band (the lager). The two patch antennas have a coaxial feed and the feed of the upper antenna goes inside the central post of the lower antenna to minimize the influence of it on the radiation pattern of the lower antenna. This proposal works out not to be feasible, because we need a lower antenna with a large inner radius to allow the variation of the feed position of the upper antenna in a wide range. This is necessary to get a good matching for the upper antenna. The problem is that the radiation pattern becomes very asymmetric when we increase the inner radius of the patch antenna.

To solve that, two alternative were analyzed in this document. The first consists in putting a second feed symmetrically placed with respect to the central post. It leads to a more symmetric radiation pattern so we can choose a larger inner radius. In addition, the introduction of the second feed increases the bandwidth of the antenna. The second alternative is a simplification of the first one. It consists in replacing the upper antenna with a monopole on the top of the lower antenna. It is simpler but it prevents the possibility of stacking other patch antennas to cover more frequency bands in a future. Due to this disadvantage, the first alternative was chosen. Finally, a proposal based on the first alternative, which fulfils quite well all the requirements which were raised in the wording of this master thesis, was presented and studied in depth.

Preface

This master thesis has been written at the Department of Electronics and Telecommunications of the Norwegian University of Science and Technology (NTNU), during the summer of 2008. It arose from a proposal made by SINTEF concerning to the European project Cooperative Vehicle-Infrastructure System (CVIS).

This thesis is the final assignment of a master degree in Telecommunication Engineering at the University of Valladolid (UVA) in Spain, which has been finished at the NTNU as an exchange student.

First of all, I would like to express my gratitude to the Norwegian University of Science and Technology for giving me the opportunity to complete my studies, with this master thesis. Especially, I would like to thank my supervisor, Jon Anders Ass, who with his constant guidance and encouragement, has ensured that this project has been completed successfully. He has always answered all my questions and doubts quickly and efficiently. I would also like to thank SINTEF for its interest in this project and especially to my contact point with SINTEF, Irene Jensen, whose assistance and support have been one of the key pieces that made possible the realization of this project. Last but not least, I would like to thank family and friends for their unconditional support in the good and bad moments.

August 2008
Trondheim, Norway.
Pablo García Moreno.

Table of contents

Figures

1. Introduction

The vial safety has become in an extraordinary importance topic in the lately years. Within the territory of the European Union, there are more than 375 millions traffic infrastructures' users and the traffic accidents mean approximately 40000 deaths each year. These data led to the EU to think about the need of putting the information technologies at the service of traffic needs.

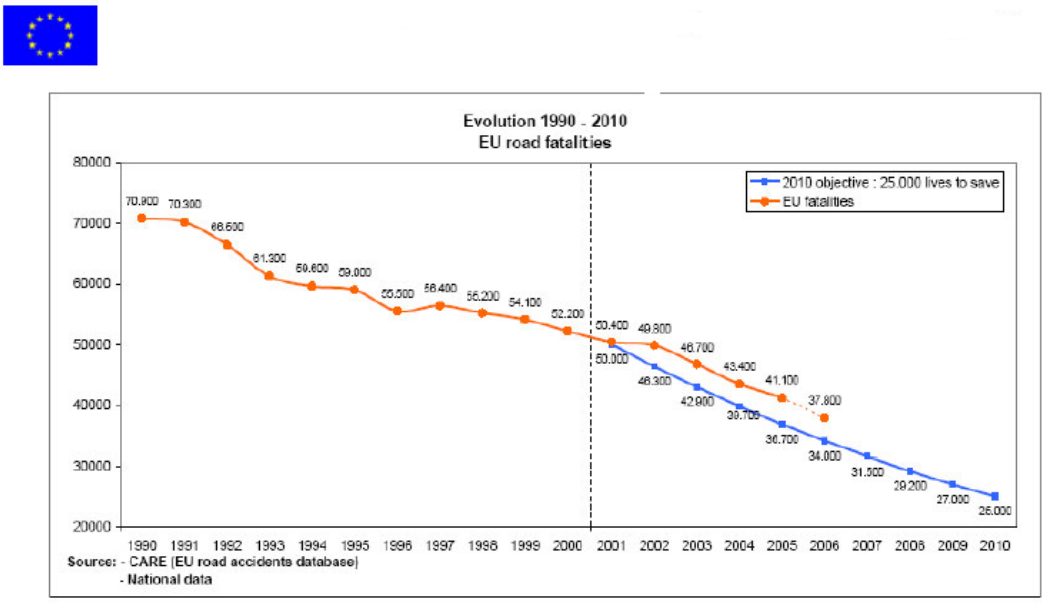

Source : CARE (EU road accidents database) or national publications
European Commission / Directorate General Energy and Transport

Figure 1-1: Road safety evolution in EU

Thus arose the project CVIS (Cooperative Vehicle Infrastructure System) [2]. The main goal of this project is the design of a communication system that allows the transmission of relevant information among cars (V2V: Vehicle-to-vehicle communications) and between cars and roadside infrastructures (V2I: Vehicle-to-Infrastructure communications) in a transparent way.

Although the main goal of this project is to improve the traffic safety, at the same time other reasons justify to carry out this project:

- To increase the efficiency in the driving: The system will be used for the transmission of information about the traffic situation.
- To reduce the environmental impact of vehicles.
- To improve management and control of the road network (both urban and inter-urban). The information which the users send to a national traffic controller entity, can be use to do real time modification over the infrastructures of the road.
- To better and more efficient response to hazards, incidents and accidents. Implementation of automatic emergency calls when an accident happens.

For the implementation of this communication system, cars need a multi-channel terminal that allows them the exchange of information both with other cars as the road side infrastructures.

For the communications between the cars and the infrastructures, the project CVIS has adopted the protocol CALM (Communication Access for Land Mobiles) which is a protocol architecture that allow us to use different wireless technologies with unify criteria and allows as long communications as shorts. Specifically, the main objective of the international standard CLAM is to guarantee the interoperability between:

- Mobile wireless Local Area Networks (WLAN/Wi-Fi)
- Cellular networks (GPRS, UMTS)
- Short-range microwave beacons (DSRC)
- Infrared (IR)

Within the scope of the CVIS project this paper addresses the design of a circular patch antenna for the European project based on a set of several compact circular patches stacked, that fulfil the necessary requirements for the transmission of information over the different wireless protocols that form CALM. This antenna is supposed to be placed on the roof of the cars.

The first part of this project is focused on the study of a single compact patch antenna for the band of 2GHz based on the design proposed in [1]. This article proposes a circular patch antenna shorted by a central cylindrical metal post to its ground plane. The objective in the first part of this master thesis is the evaluation of the viability of the construction of an antenna that fit the special requirements of the terminal. The main requirements are summarize in the following list:

- Radiation pattern: The antenna should present a conical radiation pattern with a null in the zenith, which is favourable for communications, via ceiling reflections. For this purpose, a mode TM_{01} has been chosen [1]. The elevation angle of the radiation pattern should be as low as it is possible.
- Dimensions: Others proposals for the multi-band terminal have been done, but the dimension of the prototypes were very large, what made those proposals very unattractive for the car users. One of the most important objectives of this master thesis is to achieve a prototype with small enough dimensions which make it attractive for the consumers.
- Bandwidth: One of the most important limitations of the patch antennas is that they present a very narrow bandwidth, so in this first part of the project, is important to analyse the bandwidth of the design proposed in [1] and study the influence of the antenna's parameters (dimensions, substrate, feed position...) in its bandwidth.
- Polarization: Given that the conclusion of this first part about the behaviour of the 2GHz prototype are going to be used to the implementation of the final antenna design in the second part, we need a linear polarization because we have to meet the requirements of the CALM protocol.

Trough this first part we are going to improve our knowledge about the antenna behaviour and the influence of the different parameters such as its dimensions, the material of the substrate, etc.

For the implementation of the prototype for the 2 GHz band, we are going to use first of all an analytical model. With this model we will obtain a first approximation which will be refined later through the application of two simulation tools. Once we have finished the design, we will construct and measure the prototype, to finally analyze and study the results.

The second part is focused on the study of a stacked structure for the covering of several bands of the CALM protocol. Specifically, we are going to propose a design for the following bands:

- 2.4 GHz – 2.484 GHz
- 5.75 GHz – 5.95 GHz

Through this section we are going to study the limitations of this structure and the coupling between the two antennas, finally we will propose some modification that solve this problem and lead to a realizable design which could be used for the successful implementation of the project CVIS.

In the same way, we will use the analytical model for designing separately from each of the two antennas. Then we will use the simulation tool to refine the design. When we have the design of the two circular patch antennas, we will stack the two antennas and we will analyze the results with the help of the simulation software.

2. Previous published work

The microstrip patch antennas have a lot of application nowadays because of their reduced dimension and their low profile which make them useful for a wide range of systems thanks to their flexibility and adaptability. This has lead to a lot of investigations about patch antennas for the last years.

Among the various shapes of patch antennas, the rectangular and the circular patches have been two of the models more extensively studied. In our case we are going to focus our study on a circular patch antenna. A lot of studies have been done about the circular patch antenna [3] [4] [5]. One of the problems of this kind of antennas was that for low frequencies the size was extremely large for some applications, so some variations over the original model started to be investigated to reduce the size of a conventional patch antenna.

The first option we find through the literature consist in the use of a ring antenna instead of a conventional patch antenna. We can see the properties of the conventional ring antennas (open ring) in many articles like [6] and [7]. However, the open circuit condition in both the inner and the outer radiuses cause some problems when we want to feed the antenna. This master thesis starts from a particular case of ring antenna which is proposed in an article published in December 2002 [1]. This antenna arises shorting the conventional patch antenna with a central metallic post from the top patch to its ground plane. Although [1] was the starting point, some other previous articles about this kind of patch antenna were found [8] [9]. We can see this kind of patch antenna like a shorted ring antenna where the inner radius is short circuited while the outer radius is open circuited. For the final purpose of this master thesis, this kind of antenna is optimum because it can be put in the roof of a car for the implementation of a compact multi-band antenna solution for the CVIS project.

We are going to study the behaviour of this shorted patch antenna for the TM_{01} because as it is explained in the article [1], it presents a radiation pattern circularly symmetrical in the azimuth and a null in the zenith which is favourable for communications, via ceiling reflections, between terminals in arbitrary azimuthal relationship. Other investigations [9] about other azimuthal modes (TM_{0n} $n>1$) have been carried out. But the design needs a more complex feeding schema to obtain a uniform radiation in the azimuth direction. Another property of the antenna that we should consider is the elevation angle of its radiation pattern. The antenna is going to be mounted in the roof of a car, so it is desired that the elevation angle of its radiation pattern will be low in order to favour the communications with other cars and with the roadside infrastructures. One solution is proposed in [9], where we can see how the electrical permittivity affects directly the elevation angle. Regarding to the feed schema, we are going to use a coaxial feed which is one of the most extended schema to feed any patch antenna [10].

Another problem to solve in the final part of this project is to analyze the global behaviour when we stacked more than one antenna of this kind to cover different bands of frequency. Regarding with this topic, there is a lot of articles like [11] about what happen when we stack two or more conventional circular patch antennas for cover more

than one band of frequencies, but there have been no studies about the stacking of two concentrically shorted patch antennas.

3. Analysis, design and implementation of a compact disk antenna for the band of 2GHz (Part I)

3.1 Analytical Analysis

3.1.1 Introduction

In this section, we are going to use an analytical model to characterize some properties of the antenna structure. Although these kinds of models are less accurate than the numerical models, they are used mainly for the following reasons:

- They facilitate the posterior numerical analysis because with the analytical model, we can delimit the variation of the parameters within a range of interest and rule out the values of the different parameters that produce undesired results. This is very useful because in that way we can reduce the cases that we have to simulate with a computer tool and allowing us reduce design time.
- With an analytical model, we can understand better the effect of the variation of the different parameters of our design. This is a great advantage of these kinds of models because with them, we can improve our knowledge about the structure of the antenna and in that way we can modify and improve our design for getting better results.

There are several analytic models that can forecast the resonant frequency of a circular patch antenna. In our case, we are going to use the cavity model [12], because of its simplicity. The cavity model consists in characterizing the microstrip antenna as a resonant cavity, bounded by electrical walls on the top and the bottom, and by magnetic walls along the periphery.

This model is supported by the assumption that the normal component of the electric current along the peripheral of the patch metallization is zero, so in our model, we can suppose that tangential component of the field H is zero along the edge. This is equivalent to put a PMC wall along the peripheral [13]. Why the electric current is zero along the edge of the patch metallization can be explained in an intuitive way if we see the next figure where we can see the distribution of the charges inside the patch:

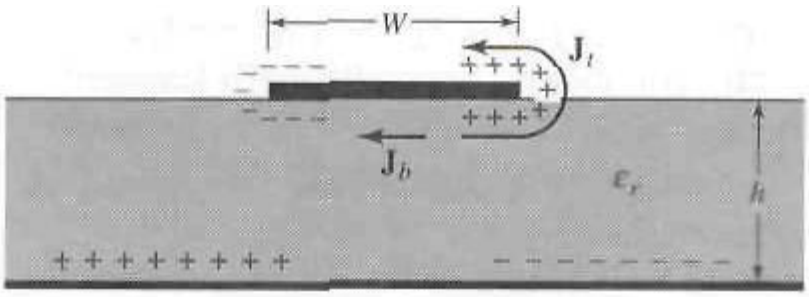

Figure 3-1: Distribution of the charges inside a patch

Since the height of a typical patch antenna is very thin in comparison to the length of the patch, the attraction forces between the charges of the patch and the charges of the ground plane are dominants. So most current flows remain underneath the patch and the amount of current flows around the edges of the patch to its top surface is negligible.

Finally, we are going to simplify the model disregarding the effects of the feed. This simplification allows us to work with the Maxwell equation without considering free charges and currents.

With the previous simplifications, we are ready to analyze our antenna. The first step is to calculate the fields inside the resonant cavity through the application of the Maxwell equations and the boundary conditions for the particular geometry of our antenna.

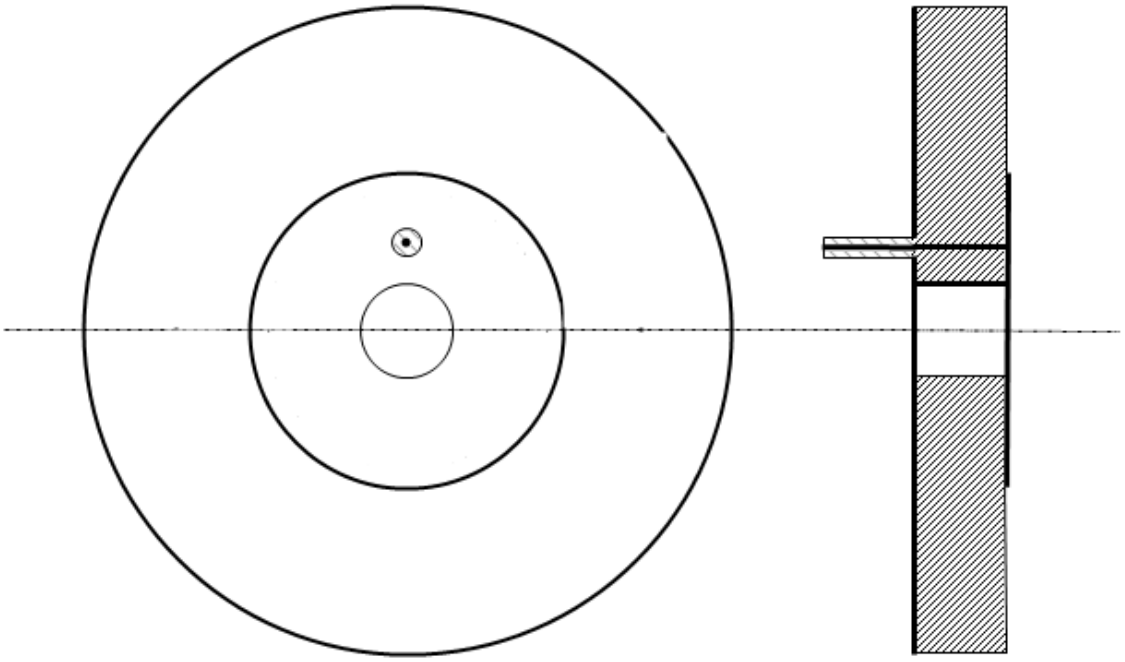

Figure 3-2: Geometry of the compact disk patch antenna

3.1.2 Interior fields

Our starting point is the Maxwell equations without free charges and currents, which we can use instead the general expression of the Maxwell equations if we have into account the simplification of the feed made in the previous section.

$$\nabla XE = -j\omega B \qquad D = \varepsilon E$$
$$\nabla XH = J_c + j\omega D = j\omega\varepsilon_{ef} E \qquad B = \mu H$$
$$\nabla XD = 0 \qquad J_c = \sigma E$$
$$\nabla XB = 0 \qquad \varepsilon_{ef} = \varepsilon' - j\varepsilon'' - j\frac{\sigma}{\omega}$$

From these equations, we can obtain the wave equations of *Helmholtz*:

$$\nabla^2 E + K_m^2 E = 0$$
$$\nabla^2 H + K_m^2 H = 0$$
$$K_m^2 = \omega^2 \mu\varepsilon_{ef}$$

We can generalize in the following way:

$$\nabla^2 F + K_m^2 F = 0$$
$$F = E \,//\, H$$

From this point, we are going to perform a general analysis of the fields inside the cavity. In this analysis we will be gradually introducing the assumptions we advanced in the previous section.

Firstly, we want to separate the longitudinal component (F_z component) and the longitudinal coordinate (z coordinate), from the transversal components (F_T component) and the transversal coordinates (t1 and t2 coordinates):

$$\bar{E}(\bar{r}) = \bar{E}_{aT}(t_1, t_2) f_a(z) + E_{az}(t_1, t_2) f_a(z)\hat{z}$$
$$\nabla^2 = \nabla_T^2 + \frac{\partial^2}{\partial z^2}$$

Substituting this into the wave equation we obtain:

- Equation for the longitudinal component:
  - $f_a \nabla_T^2 E_{az} + E_{az} \frac{\partial^2}{\partial z^2} f_a + K_m^2 E_{az} f_a = 0$
- Equation for the transversal components:
  - $f_a \nabla_T^2 \bar{E}_{aT} + \bar{E}_{aT} \frac{\partial^2}{\partial z^2} f_a + K_m^2 \bar{E}_{aT} f_a = 0$

3.1.2.1 Longitudinal component

We are going to start with the analysis of the longitudinal component equation. If we divide the whole equation by $E_{az}f_a$, then we obtain a new equation where each addend depends on a different variable, so we can identify three constants:

$$\frac{\nabla_T^2 E_{az}}{E_{az}} + \frac{\frac{\partial^2}{\partial z^2} f_a}{f_a} + K_m^2 = 0$$

$$(1)\ \nabla_T^2 E_{az} + K_c^2 E_{az} = 0$$

$$(2)\ \frac{\partial^2}{\partial z^2} f_a - \gamma^2 f_a = 0$$

We can see that the solution of the equation (2) is:

$$f_a(z) = A_1 e^{-\gamma z} + A_2 e^{+\gamma z}$$

$$\gamma = \sqrt{K_c^2 - K_m^2} = \alpha + j\beta$$

- γ = Propagation constant.
- α = Attenuation constant.
- β = Phase constant.

After we obtain the solution of the equation (2) we are going to solve the equation (1). To solve it, we have to consider the coordinate system that we are going to choose for the representation of the geometry of the cavity. Given that the transversal section of our antenna is circular, the most appropriate coordinate system is a cylindrical coordinate system.

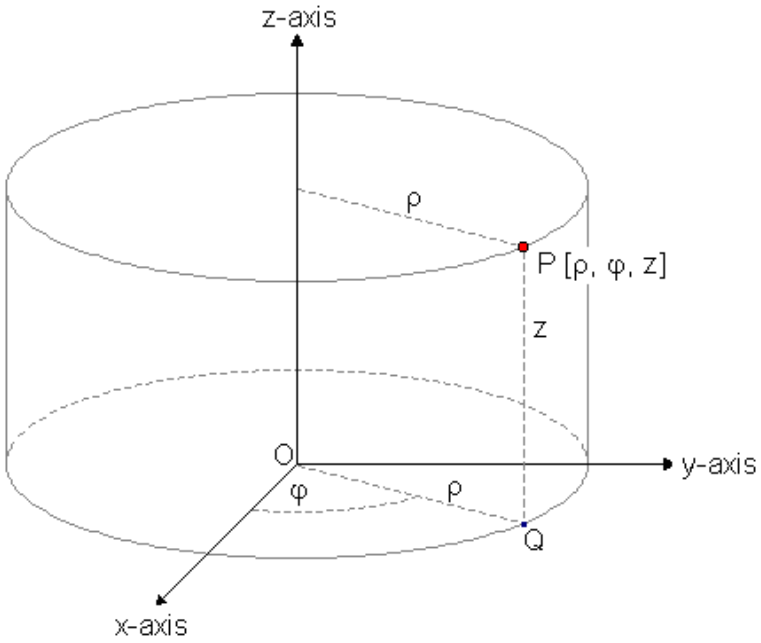

Figure 3-3: Coordinate system

Once we have chosen the coordinate system, next step is to separate the two transversal components for solving the equation. For this purpose we can represent the function F_{az} in the next way:

$$F_{az} = R(\rho)G(\varphi)$$

Taking into account the definition of F_{az}, the expression of ∇_T in cylindrical coordinates and replacing it in the equation (1) we obtain the next result, in which each addend depends on a different variable:

$$\frac{\rho}{R}\frac{d}{d\rho}(\rho\frac{dR}{d\rho}) + \rho^2 K_c^2 + \frac{1}{G}\frac{d^2G}{d\varphi^2} = 0$$

Then we have two new equations:

- (1.1) $\frac{d^2G}{d\varphi^2} + v^2\varphi G = 0$
- (1.2) $\frac{\rho}{R}\frac{d}{d\rho}(\rho\frac{dR}{d\rho}) + \rho^2 K_c^2 - n^2 = 0 \Rightarrow \frac{d^2R}{d\rho^2} + \frac{1}{\rho}\frac{dR}{d\rho} + (K_c^2 - n^2)R = 0$

The solution of the equation 1.1 has the following format:

$$G(\varphi) = A\cos(v\varphi) + B\sin(v\varphi)$$

We have to realize that the previous equation has to be necessary a periodic function, and due to this, v should be an integer:

$$G(\varphi) = G(\varphi + 2\pi) \xrightarrow{v=n(entire\ number)} G(\varphi) = A\cos(n\varphi) + B\sin(n\varphi) = a_n \cos(n\varphi + \alpha_n)$$

To figure out the solution of the equation 1.2 we have to use the Bessel's equation. In particular, the solution has the next format:

$$R_n(\rho) = C_n J_n(K_c\rho) + D_n Y_n(K_c\rho)$$

Where J_n is the Bessel's function of the first kind and Y_n is de Bessel function of the second kind. So, taking into account those expressions, the format of the longitudinal component is this:

$$F_z = (C_n J_n(K_c\rho) + D_n Y_n(K_c\rho))(A_n \cos(n\varphi) + B_n \sin(n\varphi))(A_1 e^{-\gamma z} + A_2 e^{+\gamma z})$$

To solve the longitudinal component, the last step is to apply the boundary conditions of our particular design to restrict the problem. Firstly, we are not going to contemplate the boundary condition of the patch and the ground plane, so the problem is similar to the problem of solving a waveguide with the section of the patch antenna.

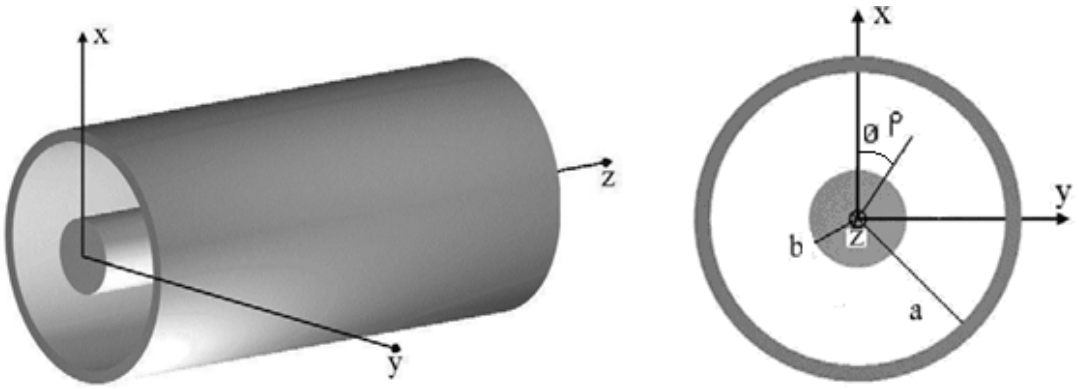

Figure 3-4: Coaxial waveguide

These kinds of antennas only permits are optimums for the transmission of the TM modes. As we can see later, the reason of this behaviour is that we have two PEC surfaces very close to each other, so the electrical field is perpendicular to the patch metallization and the ground plane, and it does not vary along the z axis. So from here, we are going to talk about theses modes. We are particularly interested in the boundary conditions that appear as a consequence of the supposition that the resonant cavity is surrounded by a perfect magnetic wall:

- $\hat{n}X\overline{E} = 0 \Rightarrow$
  - $E_{az}\,|_{\rho=b} = 0 \Rightarrow C_n J_n(K_c b) + D_n Y_n(K_c b) = 0$
  - $\frac{\partial}{\partial r} E_{az}\,|_{\rho=a} = 0 \Rightarrow C_n J_n^{'}(K_c a) + D_n Y_n^{'}(K_c a) = 0$

And solving this equation system, we obtain the next equation:

$$J_n(K_c b)Y_n^{'}(K_c a) - J_n^{'}(K_c a)Y_n(K_c b) = 0$$

To summarize, we have achieved the following equation that models the longitudinal component of field inside the cavity:

$$H_z = 0$$

$$E_z = (C_n J_n(K_{c,nm}\rho) + D_n Y_n(K_{c,nm}\rho))(A_n \cos(n\varphi) + B_n \sin(n\varphi))(A_{1nm}e^{-\gamma_{nm}z} + A_{2nm}e^{+\gamma_{nm}z})$$

And $K_{c,nm}$ is the solution of the following equation:

$$J_n(K_{c,mn}b)Y_n^{'}(K_{c,mn}a) - J_n^{'}(K_{c,mn}a)Y_n(K_{c,mn}b) = 0$$

3.1.2.2 Transversal components

Once we know the longitudinal component of the E field inside the resonant frequency, we can obtain the transversal components applying the Maxwell's equation for a free space region:

- $E_T = \frac{\gamma_{nm}}{K_{c,mn}^2}\nabla_T E_{az,mn}(-A_{1,mn}e^{+\gamma_{nm}z} + A_{2,nm}e^{-\gamma_{nm}z})$
- $H_T = \pm\frac{\hat{z}XE_{T,mn}}{Z_{TM,mn}}; Z_{TM} = \frac{\gamma_{nm}}{j\omega\varepsilon_{ef}}$

Substituting the solution that we found for the longitudinal components into these two expressions we can find the transversal components of the field inside the resonant cavity:

- $$E_T = \frac{\gamma_{nm}}{K_{c,nm}}[(C_n J_n^{'}(K_{c,nm}\rho) + D_n Y_n^{'}(K_{c,nm}\rho))(A_n \cos(n\varphi) + B_n \sin(n\varphi))](-A_1 e^{-\gamma_{nm}z} + A_2 e^{+\gamma_{nm}z})\hat{\rho}$$
$$-\frac{\gamma_{nm}}{K_{c,mn}^2}[(C_n J_n(K_{c,nm}\rho) + D_n Y_n(K_{c,nm}\rho))n(-A_n \sin(n\varphi) + B_n \cos(n\varphi))](-A_1 e^{-\gamma_{nm}z} + A_2 e^{+\gamma_{nm}z})\hat{\varphi}$$

- $$H_T = -\frac{j\omega\varepsilon_{ef}}{K_{c,nm}}[(C_n J_n^{'}(K_{c,nm}\rho) + D_n Y_n^{'}(K_{c,nm}\rho))(A_n \cos(n\varphi) + B_n \sin(n\varphi))](A_1 e^{-\gamma z} + A_2 e^{+\gamma z})\hat{\varphi}$$
$$-\frac{j\omega\varepsilon_{ef}}{K_{c,mn}^2}[(C_n J_n(K_{c,nm}\rho) + D_n Y_n(K_{c,nm}\rho))n(-A_n \sin(n\varphi) + B_n \cos(n\varphi))](A_1 e^{-\gamma z} + A_2 e^{+\gamma z})\hat{\rho}$$

Following the same procedure that we applied with the longitudinal component, we have to define the boundary conditions for the transversal component. Particularly, we are interested in the boundary conditions that appear as a consequence of the metallic walls that close the resonant cavity at the top and at the bottom (the patch metallization and the ground plane respectively).

- $E_T|_{z=0} = 0 \Rightarrow -A_1 e^{-\gamma 0} + A_2 e^{+y0} = 0; A_1 = A_2 = A$
- $E_T|_{z=h} = 0 \Rightarrow -Ae^{-\gamma h} + Ae^{+\gamma h} = A(e^{+\gamma h} - e^{-\gamma h}) = 0; sin(\gamma h) = 0; K_c^2 = \left(\frac{p\pi}{h}\right)^2 + K_m^2$

Since the substrate of a typical microstrip antenna is very thin in comparison to the wavelength (h<0.05λ), we can suppose that the fields inside the resonant cavity are constant along the z axis. This is represented by selecting p=0 in the previous equation so we have:

- $K_{c,mn}^2 = K_m^2 = \omega_r{}^2 \mu\varepsilon_{ef}$

So far, we have calculated the longitudinal and the transversal components of the field inside the resonant cavity that models our circular patch antenna. With this information we can calculate the resonant frequency as a function of the dimension of our antenna.

Then we are going to summarize the solution of the fields inside the cavity, taking into account the last assumption (the electric field is constant along the z axis):

- Longitudinal component
  - $H_z = 0$
  - $E_z = 2A(C_n J_n(K_{c,nm}\rho) + D_n Y_n(K_{c,nm}\rho))(A_n \cos(n\varphi) + B_n \sin(n\varphi))$
  - $K_{c,mn}^2 = \omega_r{}^2 \mu\varepsilon_{ef}$
  - $J_n(K_{c,mn}b)Y_n^{'}(K_{c,mn}a) - J_n^{'}(K_{c,mn}a)Y_n(K_{c,mn}b) = 0$
- Transversal component
  - $H_T = -2A\frac{j\omega\varepsilon_{ef}}{K_{c,nm}}[(C_n J_n^{'}(K_{c,nm}\rho) + D_n Y_n^{'}(K_{c,nm}\rho))(A_n \cos(n\varphi) + B_n \sin(n\varphi))]\hat{\varphi}$
  - $-2A\frac{j\omega\varepsilon_{ef}}{K_{c,mn}^2}[(C_n J_n(K_{c,nm}\rho) + D_n Y_n(K_{c,nm}\rho))n(-A_n \sin(n\varphi) + B_n \cos(n\varphi))]\hat{\rho}$

From these equations, we can obtain the resonant frequency as follows:

$$K_{c,mn}^2 = \omega_r{}^2 \mu\varepsilon_{ef}$$

$$J_n(K_{c,mn}b)Y_n^{'}(K_{c,mn}a) - J_n^{'}(K_{c,mn}a)Y_n(K_{c,mn}b) = 0$$

$$J_n(Kx)Y_n^{'}(x) - J_n^{'}(x)Y_n(Kx) = 0 \qquad K = \frac{b}{a}; x = K_{c,mn}a$$

From the second equation we can obtain the value of x. Given that the equation contains Bessel functions, it has multiple solutions. If we call the different solutions of the equation as $x_{mn} = K_{c,mn}a$, then the resonant frequency has the following value:

$$f_r = \frac{\frac{x_{nm}}{a}}{2\pi\sqrt{\mu\varepsilon_{ef}}}$$

The problem of this expression is that it does not take into account the fringing field at the edges of the patch. Due to that the patch have finite dimensions, the field at the edges of the patch undergo fringing. We can see the lines of the fringing field in the next figure:

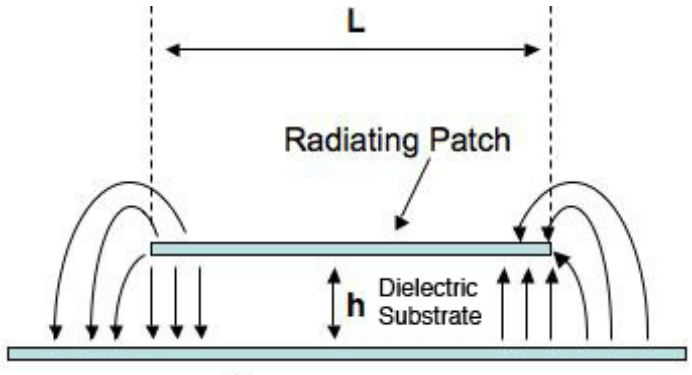

Figure 3-5: Fringing field

The amount of fringing is a function of the dimensions of the patch, the shape of the patch, the height of the substrate and the properties of the substrate. In our case, we are going to use an expression that is quite accurate for our purpose (error less than 2%). This expression takes into account the fringing effect through the definition of an effective radius a_{ef}. The value of $a_{ef} - a$ should be approximately equal to the thickness of the substrate.

$$f_r = \frac{x_{nm}}{2\pi a_{ef}\sqrt{\mu\varepsilon_{ef}}} \text{ Where: } a_{ef} = a\sqrt{\left\{1 + \frac{2h}{\pi a \varepsilon_{efr}}\left[\ln\left(\frac{\pi a}{2h}\right) + 1.7726\right]\right\}}$$

The previous equation is derived from the quasi-static capacitance of the microstrip circular disc:

$$C = \frac{\pi\varepsilon a^2}{h}$$

This expression is valid for a generic circular patch antenna, but our antenna incorporates a shorting rod at the centre of the circular patch antenna. Using the Green's function method, we find out that the quasi-static capacitance of the geometry of our antenna can be modelled by the following expression:

$$C = \frac{\pi\varepsilon(a^2 - b^2)}{h}$$

Taking into account this, we can adapt this expression to the geometry of our antenna as follows [8]:

$$a_{ef} = a\sqrt{\left\{1+\frac{2h}{\pi a_m \varepsilon_{efr}}\left[\ln\left(\frac{\pi a_m}{2h}\right)+1.7726\right]\right\}} \qquad a_m = \sqrt{a^2-b^2}$$

The design process consists in, for a given resonant frequency; calculate the value of the different parameters of the antenna (dimensions and substrate properties). For example, if we know the permittivity, the height of the substrate and the relation between the radiuses b and a, then the design process would be as follows:

1. From $f_r = \frac{\frac{x_{nm}}{a_{ef}}}{2\pi\sqrt{\mu\varepsilon_{ef}}}; a_{ef} = \frac{x_{nm}}{2\pi f_r\sqrt{\mu\varepsilon_{ef}}}$ we find the value $\frac{x_{nm}}{a_{ef}} = K_m$.
2. From $J_n(Kx)Y_n^{'}(x) - J_n^{'}(x)Y_n(Kx) = 0$ we can obtain $x = K_{c,mn}a_{ef}$ because the relation $K = \frac{b}{a}$ is known.
3. Then we can find the effective outer radius $x = K_{c,mn}a_{ef} \Rightarrow a_{ef} = \frac{x}{K_m}$.
4. From $a_{ef} = a\sqrt{\left\{1+\frac{2h}{\pi a_m \varepsilon_{efr}}\left[\ln\left(\frac{\pi a_m}{2h}\right)+1.7726\right]\right\}}$ we can obtain the physical outer radius. To find $a = f(a_{ef})$ we can do a first order approximation which consists in replacing the value of the effective outer radius that we found in the previous step into the variable a_{ef} and substituting $a_m = \sqrt{a_{ef}^2(1-K^2)}$ inside the logarithmic function. Then we get the following equation:
   - $$a = \frac{a_{ef}}{\sqrt{\left\{1+\frac{2h}{\pi a_m \varepsilon_{efr}}\left[\ln\left(\frac{\pi a_m}{2h}\right)+1.7726\right]\right\}}}$$
5. And finally, from $K = \frac{b}{a}$ we find the physical inner radius.

For solving the equation $J_n(Kx)Y_n^{'}(x) - J_n^{'}(x)Y_n(Kx) = 0$ and to evaluate the influence of the different parameters of the antenna in the resonant frequency, a MATLAB program has been implemented. This program receives as input, the resonant frequency of the antenna and plots the possible values of a group of different substrates with different permittivity. The goal of this program is to improve our knowledge of the behaviour of the circular patch antenna and evaluate the different options that could be interesting to fit the design requirements.

Finally, we are going to design the antenna for a particular mode. The mode that has been chosen is the mode TM_{01}. The reasons because we chose this mode are the following:

- Because it gives a radiation pattern that present a revolutionary symmetry around the z axis.

- It gives a radiation pattern with a null in the zenith which is favourable for communication via ceiling reflections.

So the final expression of the fields inside the resonant cavity is:

- Longitudinal component
  - $H_z = 0$
  - $E_z = 2A(C_0 J_0(K_{c,01}\rho) + D_0 Y_0(K_{c,01}\rho))$
  - $K_{c,02}^2 = \omega_r{}^2 \mu\varepsilon_{ef}$
  - $J_0(K_{c,01}b)Y_0^{'}(K_{c,01}a) - J_0^{'}(K_{c,01}a)Y_0(K_{c,01}b) = 0$
- Transversal component
  - $H_T = -2A\frac{j\omega\varepsilon_{ef}}{K_{c,01}}[C_0 J_0^{'}(K_{c,01}\rho) + D_0 Y_0^{'}(K_{c,01}\rho)]\hat{\varphi}$

3.1.3 Exterior fields

For calculating the exterior fields, we are going to apply the Equivalence principle. The key idea is to change the external sources (J, M) of a volume V for superficial currents (J_s, M_s), in a way that the solution in the interior of the volume V keep being the same [13].

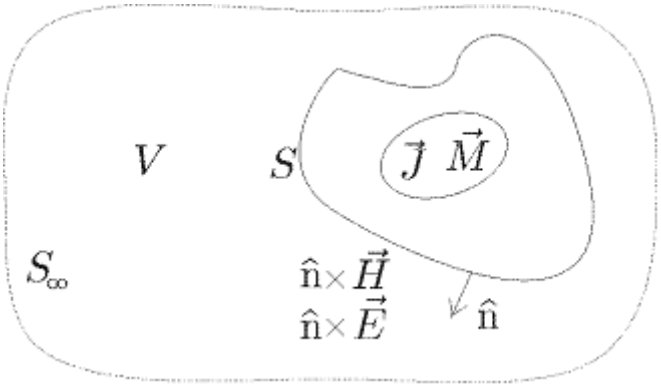

Figure 3-6: Equivalence principle

So, if we want that the fields outside the volume V (we are going to put the antenna outside the volume V so the volume V is the free space), to maintain the tangential components of the fields in S is necessary that some superficial currents appear in that surface, leading to a discontinuity among the tangential components of the fields in that surface.

$$\overline{J_s} = \hat{n}\times\overline{H}$$
$$\overline{M_s} = -\hat{n}\times\overline{E}$$

As we saw before, the fact that in a typical microstrip antenna the substrate is very thin in comparison to the wavelength and the outer radius, cause that the current density at the top of the patch is much smaller than the current density at the bottom of the patch. This allows supposing that the current density at the top of the patch is zero. Also as we explained before, the tangential component of the magnetic field along the edge of the patch is very small, so it can be supposed that is zero too. Due to these assumptions, the corresponding equivalent electric current density Js is very small and we can assume that it is negligible. The only relevant current density is the equivalent magnetic current density along the side periphery of the patch antenna. If we include the effect of the ground plane applying the Image theory, we obtain the next result:

$$\overline{M_s} = -2\hat{n} \times \overline{E}\,|_{\rho=a} = 4A(C_0 J_0(K_{c,01}a) + D_0 Y_0(K_{c,01}a))\hat{\varphi}$$

Since the substrate is very thin we can suppose that the equivalent magnetic current density is uniform along the z axis. In this case we can model this by a filamentary magnetic current:

$$\overline{I_s} = h\overline{M_s} = 4hA(C_0 J_0(K_{c,01}a) + D_0 Y_0(K_{c,01}a))\hat{\varphi}$$

We are going to represent the filamentary magnetic current by the coordinate system $(r', \vartheta', \varphi')$ as we can see in the next figure:

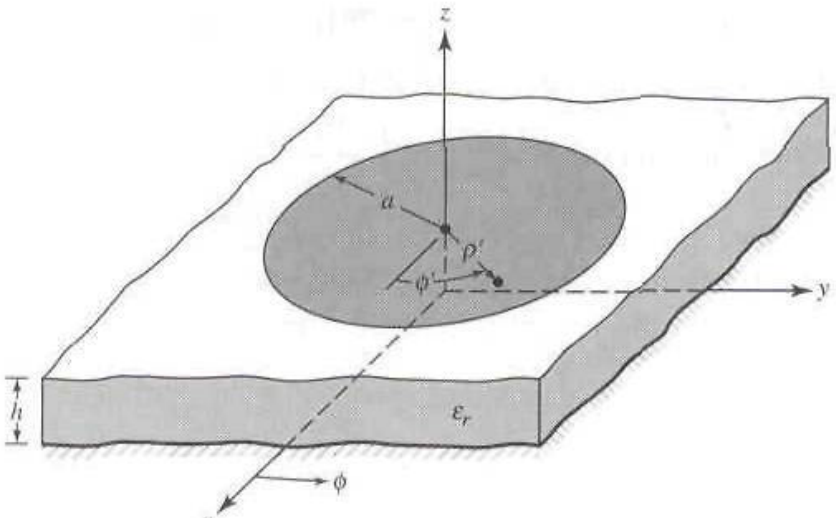

Figure 3-7: Coordinate system of the source

Then we have the next expression for the current:

$$I_m = hM_s = 4hA(C_0 J_0(K_{c,01}a) + D_0 Y_0(K_{c,01}a))\widehat{\varphi'} = V_0\widehat{\varphi'}$$

Once we know the expression of the magnetic current, we can calculate the far fields through the magnetic radiation vector:

$$L = \int_L I_m e^{jka\sin(\vartheta)\cos(\varphi-\varphi')} a d\varphi' = \int_{\phi'=0}^{\varphi'=2\pi} V_0\widehat{\varphi'} e^{jka\sin(\vartheta)\cos(\varphi-\varphi')} a d\varphi'$$

The next step is to put the vector $\widehat{\varphi}'$ as a function of the coordinate system (r,ϑ,φ), because this vector has a different direction depends on the point that we are evaluating and that property makes very difficult to solve the previous expression:

$$\widehat{\varphi}' = \sin(\vartheta)\sin(\varphi-\varphi')\hat{r} + \cos(\vartheta)\sin(\varphi-\varphi')\hat{\vartheta} + \cos(\varphi-\varphi')\hat{\varphi}$$

I we apply this equivalence we can express the magnetic radiation vector in the next way:

$$L_r = V_0 a \sin(\vartheta)\int_{\phi'=0}^{\varphi'=2\pi} \sin(\varphi-\varphi')e^{jka\sin(\vartheta)\cos(\varphi-\varphi')}d\varphi' = 0$$
$$L_\vartheta = V_0 a \cos(\vartheta)\int_{\phi'=0}^{\varphi'=2\pi} \sin(\varphi-\varphi')e^{jka\sin(\vartheta)\cos(\varphi-\varphi')}d\varphi' = 0$$
$$L_\varphi = V_0 a \int_{\phi'=0}^{\varphi'=2\pi} \cos(\varphi-\varphi')e^{jka\sin(\vartheta)\cos(\varphi-\varphi')}d\varphi' \neq 0$$

For simplifying the equation, we are going to calculate the radiation pattern only for $\varphi = 0$, because we know that the radiation pattern has revolutionary symmetry around the z axis:

$$J_n(x) = \frac{j^{-n}}{\pi}\int_0^\pi \cos(n\varphi)e^{jx\cos\varphi}d\varphi \Rightarrow L_r = V_0 a\int_{\phi'=0}^{\varphi'=2\pi} \cos(\varphi-\varphi')e^{jka\sin(\vartheta)\cos(\varphi-\varphi')}d\varphi' \neq 0$$
$$\varphi = 0 \Rightarrow L_\varphi = V_0 a\int_{\phi'=0}^{\varphi'=2\pi} \cos(\varphi')e^{jka\sin(\vartheta)\cos(\varphi')}d\varphi' \neq 0$$
$$L_\varphi = V_0 a\int_{\phi'=0}^{\varphi'=\pi} \cos(\varphi')e^{jka\sin(\vartheta)\cos(\varphi')}d\varphi' + V_0 a\int_{\phi'=\pi}^{\varphi'=2\pi} \cos(\varphi')e^{jka\sin(\vartheta)\cos(\varphi')}d\varphi' \neq 0$$
$$\varphi'' = \varphi' + \pi$$
$$L_\varphi = V_0 a\int_{\phi'=0}^{\varphi'=\pi} \cos(\varphi')e^{jka\sin(\vartheta)\cos(\varphi')}d\varphi' - V_0 a\int_{\phi''=0}^{\varphi''=\pi} \cos(\varphi')e^{-jka\sin(\vartheta)\cos(\varphi')}d\varphi'$$
$$L_\varphi = V_0 a\pi j[J_1(ka\sin(\vartheta)) - J_1(-ka\sin(\vartheta))] = 2V_0 a\pi j J_1(ka\sin(\vartheta))$$
$$k = \sqrt{\mu_0\varepsilon_0}\omega = 2\pi f\sqrt{\mu_0\varepsilon_0} = \frac{2\pi f}{c} = \frac{2\pi}{\lambda}$$

Then the final expression of the far fields of the patch antenna, for φ=0, is the followings:

- Magnetic field:
  - $H_r = 0$
  - $H_\vartheta = -j\omega\frac{\varepsilon}{4\pi}\frac{e^{-jkr}}{r}L_\vartheta = 0$
  - $H_\varphi = -j\omega\frac{\varepsilon}{4\pi}\frac{e^{-jkr}}{r}L_\varphi = -j\omega\frac{\varepsilon}{4\pi}\frac{e^{-jkr}}{r}2V_0 a\pi j J_1(ka\sin(\vartheta))$
- Electric field:
  - $E_r = 0$

- $E_\vartheta = \eta H_\varphi = -j\eta\omega \frac{\varepsilon}{4\pi} \frac{e^{-jkr}}{r} 2V_0 a\pi\, jJ_1(ka\sin(\vartheta))$
- $E_\varphi = -\eta H_\vartheta = 0$

With this result, we can plot a cut of the radiation pattern at and study the influence of the different parameters in it. For this purpose a new MATLAB program has been designed. In the next section we are going to analyze the most important conclusions that we can extract from this analytical study.

3.1.4 Results of the analytical analysis

In this section we are going to study, through a couple of MATLAB programs based on the previous section, the effect of vary the different parameters of our antenna in the resonant frequency and in the shape of the radiation pattern. This analysis is very important because it allows us to understand deeply how to act over the antenna's dimensions and the material of the substrate in order to fit the requirements for a particular design.

Firstly, we are going to analyze how the dimension of our antenna affects the resonant frequency. In the next two figures, we can see the influence of the size of the outer and inner radius in the resonant frequency.

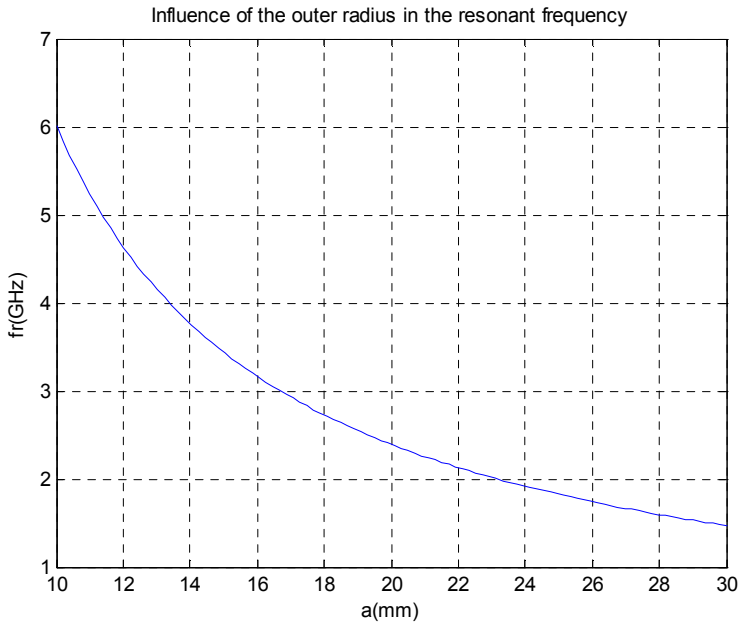

Figure 3-8: Influence of the outer radius (Inner radius= 3 mm, height=5 mm, εr=1, μr=1)

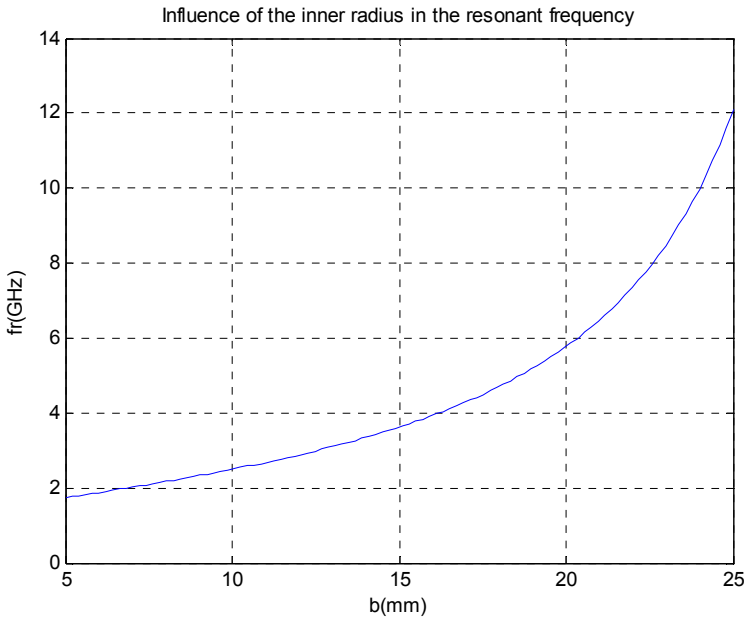

Figure 3-9: Influence of the inner radius (Outer radius=30 mm, height=5 mm, εr=1, μr=1)

We can observe that when the outer radius decreases, the resonant frequency increases. With the inner radius, we have the inverse relationship, when the radius decrease the resonant frequency also decrease. We can also see that the influence that the variation of the inner radius has on the resonant frequency is sensibly stronger than the influence of the variation of the outer radius. These are going to be the main two parameters that we are going to design to achieve the desired resonant frequency.

As we can see in the next figure, there is a small dependence between the height of the substrate and the resonant frequency. When the height decreases, the resonant frequency is higher. But the influence is not so strong and the range of variation is very small, because in our model we did the assumption than the height was smaller than 0.05λ. So is better to choose it on the basis on other criteria like the radiation efficiency, the mechanical properties, etc. and set the resonant frequency by the relationship between the outer and the inner radiuses.

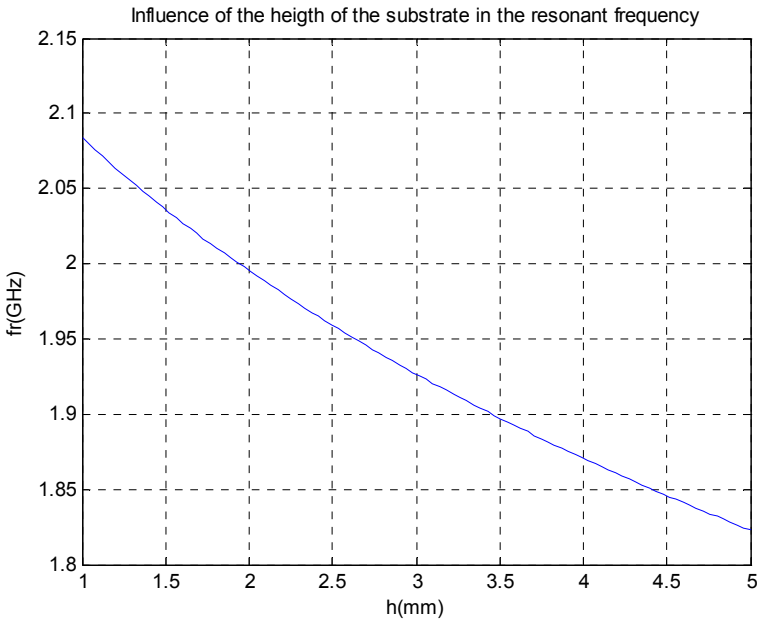

Figure 3-10: Influence of the height (Outer radius=25 mm, inner radius=3 mm, εr=1, μr=1)

Other important parameter that we can vary in order to fit the desired resonant frequency is the electric permittivity. In the next figure we can see that if we increase the electric permittivity the resonant frequency decreases. So one way in which we can try to construct very compact patch antennas for lower resonant frequencies is to choose a substrate with a high electrical permittivity.

.

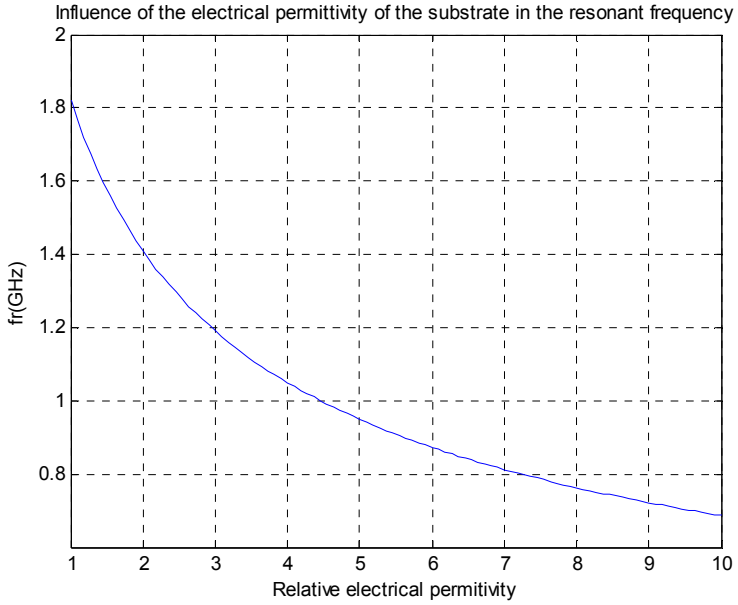

Figure 3-11: Influence of the electrical permittivity (Outer radius=25 mm, inner radius=3 mm, height=5 mm, μr=1)

Moreover, this parameter has an especial influence in the shape of the radiation pattern that makes itself very useful as we see in the next figure. This figure is obtained through a simple MATLAB program that implements the equations of the far fields that we calculated in the previous section.

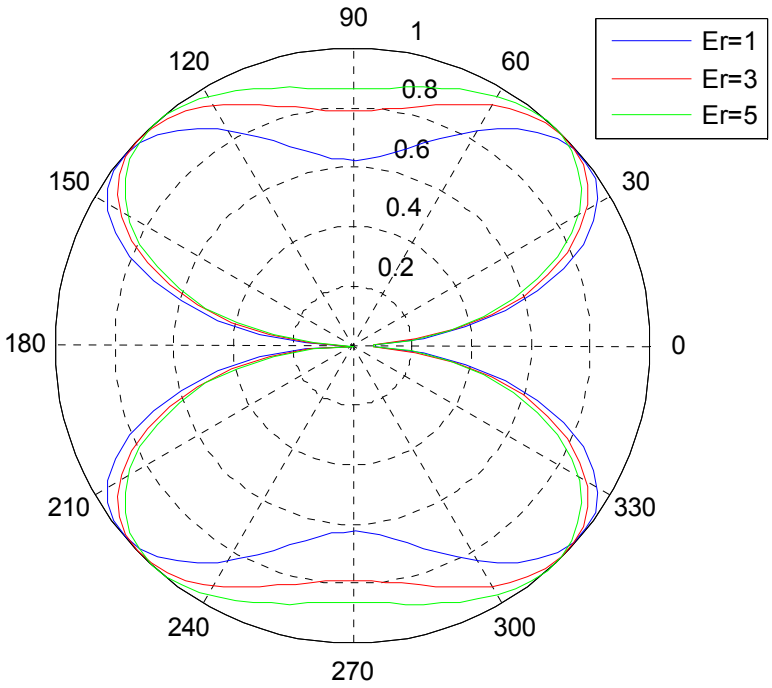

Figure 3-12: Influence of the permittivity in the radiation pattern (fr=2GHz, b=45mm)

In the next sections we will see that the forecast of the radiation pattern basis on this theoretical equation is quite different for the final radiation pattern of the prototype. This is due to:

1. The finite size of the ground plane. In the model, we have supposed that the ground plane is infinite, but in the practice, the ground plane has a finite dimension. This affect specially the shape of the radiation pattern in the proximities of the horizontal plane (Theta=90).
2. The presence of the feed. The model does not take into account the presence of the feed. This fact will lead to a slight asymmetry in the radiation pattern of the final prototype.

But, in spite of that, we can extract some conclusions that will be still valid. For example, in the figure we can see that when we increase the relative electrical permittivity of the substrate, the elevation angle at which the radiation pattern present a maximum increase. So we are interested in substrates with a high relative electrical permittivity for achieving an end-fire radiation pattern, which is optimum for the applications of our circular patch antenna.

Finally, we have done another program that receives as input the resonant frequency and plots the dimensions of the outer and the inner radiuses that allow that resonant frequency for different substrates. Here is an example of the typical output of this program:

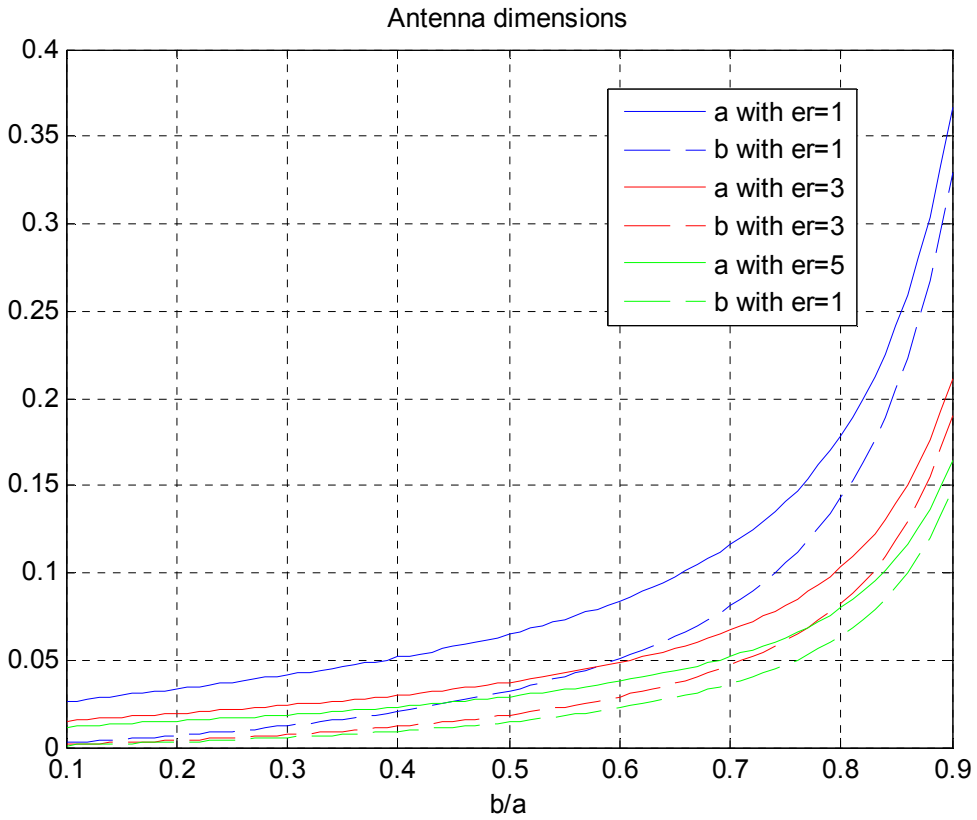

Figure 3-13: Possible dimensions and substrate materials that led to a particular resonant frequency (height=5 mm, μr=1)

This kind of plot is very useful for the process design because we can see the relationship between the different parameters and the resonant frequency. One way to design our patch antenna is presented below:

1. Choose a high relative electrical permittivity to achieve an end-fire radiation pattern.
2. Choose the height for the substrate. A thick substrate gives antennas with better radiation efficiency, but for modelling a very thick antenna our model is not very accurate.
3. Plot the possibly values of the outer and the inner radiuses that lead to the desired resonant frequency.

In the next section we are going to use this analysis to set the basis for the construction of a prototype that satisfies the requirements of the first part of this project.

3.1.5 Analytic design of the prototype

As we already advanced in the introduction, the goal of the first part of our project is the designing of a prototype for a compact circular patch antenna which should operates at the frequency of 2 GHz, as directed by [1], whose proposal is to short-circuit the patch antenna with a metallic central rod for reducing the dimensions of the antenna.

The first step is to get an approximation with the conclusions and the programmes of the previous section, for improving it through the use of simulation tools in the next section.

Inside the large amount of parameter that we can vary in order to fit the requirements, we will focus our design in the variation of a subgroup of them, making the rest of the parameter constant and choosing its values basis on the following other criteria:

1. Although we have seen that a dielectric with a high electrical permittivity was desirable, we are going to use air as the dielectric between the patch metallization and the ground plane for the construction of this first prototype. The reason is that this lead to a cheaper design and we can construct the prototypes in a short period of time without the need of a very accurate fabrication process. This allows us to construct several prototypes without spend a lot of resources and study the differences between the theorist design and the real prototype. In addition is known that thick substrates with a low permittivity lead to antennas with a wide bandwidth and a high radiation efficiency [15].
2. We have seen that the height does not affect very much the resonant frequency but it affect other parameters as the bandwidth as we will see in the next section when we use the simulation tools. For the construction of our prototype, we are going to choose a value large enough to avoid that some movements of the plane of the patch metallization due to the impact of the air on the antenna structure when the car is moving, could affect too much the value of the resonant frequency. In addition, we have to take into account that in our analytical model, we did the simplification of supposing that the height was very small in comparison to the dimensions of the wavelength. Following these criteria we are going to choose a height of 5 mm.

To achieve the resonant frequency, once we have set the previous parameters, we can only play with the dimensions of the outer and the inner radiuses. Using the program MATLAB we can obtain the possible relations between the outer and the inner radiuses that lead to the desired resonant frequency of 2 GHz.

In the next figure we can see that there are a lot of combinations for the outer and the inner radiuses that leads to the desired resonant frequency. In the next sections we are going to use simulation tools for deciding the most appropriate combination, taking into account the position of the feed, for the matching of the antenna, because as we will see, no all the combinations of the inner and the outer radiuses allow a good matching of the antenna.

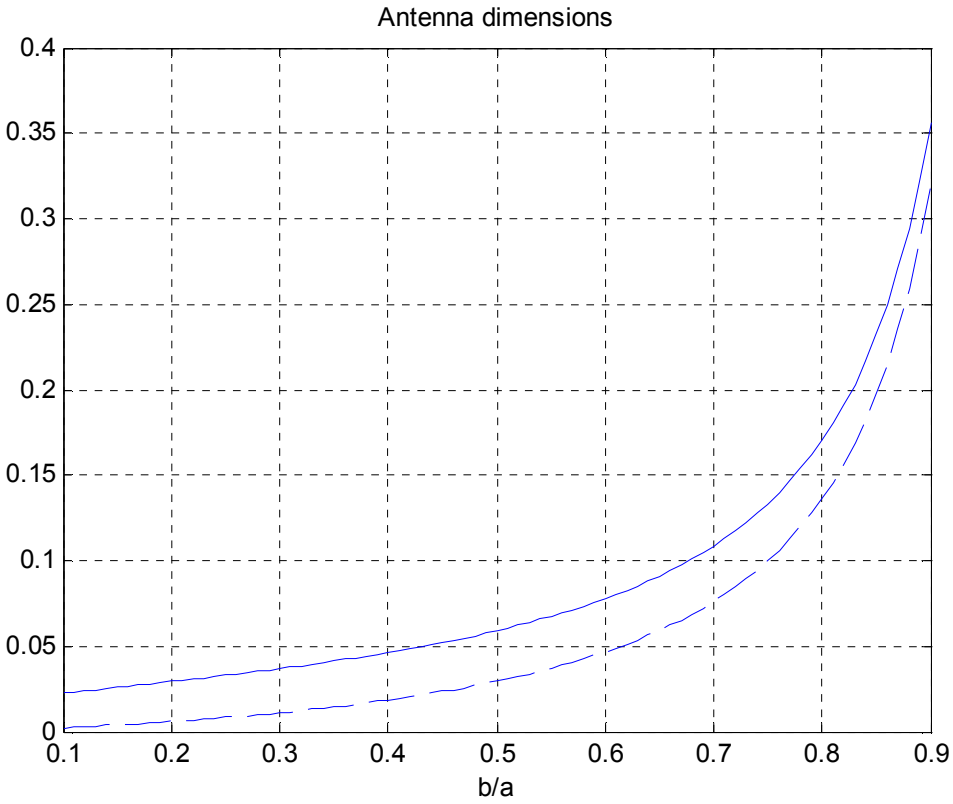

Figure 3-14: Analytical design of a 2GHz prototype (height=5 mm, εr=1, μr=1)

3.2 Simulation tools

3.2.1 Introduction

The analytical model that we developed in the previous section has some limitations that prevent to shape the antenna with the enough accuracy. For example, that model does not take into account the feed schema, so it cannot model the entrance impedance. This is the reason because we have to use simulation tools which use numerical methods, to do the final adjustment over the dimensions of the antenna for satisfying the requirements.

Within large amount of simulations tools that are offered, we are going to use the following two:

- *WIPL-D*: Commercial software for high frequency electromagnetic modelling and simulation. The main features of the software are [16]:
  - Circuit solver with schematic capture
  - 3D Electromagnetic solver
  - Component Library
  - Design optimization tool

  We are particularly interested in the 3D Electromagnetic. This software employs a method of moments technique and allows you to define the geometry of a structure as a combination of wires, plates, material objects and more, and provides information on that structure's current distribution, far-field radiation pattern, near-field distribution, and multiport admittance, impedances, and/or s-parameters at pre-defined feed points. The main advantages of this software respect to EMDS is that has a lower requirements of memory (256MB RAM and 50MB Hard disk space) and it consumes less time in each simulation.

- *EMDS (Electromagnetic Design System*): This software is a complete solution for electromagnetic simulation of arbitrarily-shaped, passive three-dimensional structures, which make it optimum for the antennas design [17]. EMDS simulation technique is based on the finite element method (FEM) which divides the full problem space into thousands of smaller regions and represents the field in each element with a local function. The principal advantage of EMDS over WIPL-D is that it is more accurate.

The reason why we use WIPL-D before EMDS is because; although WIPL-D is less accurate it is faster. Thus, we can do a lot of simulations for different values of the outer and the inner radiuses in a short time with a fairly good accuracy with WIPL-D. We can do the last adjustments with EMDS when we have a quasi-final design, given that is more accurate.

3.2.2 WIPL-D

Within the group of values for the inner and the outer radiuses that we obtained at the end of the section 3.1.5, we are going to evaluate the influence over other properties of the antenna that were not considered by the analytical model like:

- Bandwidth
- Entrance impedance
- The shape of the radiation pattern
- Radiation efficiency

Beside the influence of the inner and the outer radiuses in those properties, we are going to analyze the influence of other parameters like:

- The position of the feed, that is the main parameter to vary the entrance impedance and thus, to match the antenna
- The size of the ground plane, that as we can see affects the elevation angle of the radiation pattern

The WIPL-D model used for the simulation is shown in the next figure:

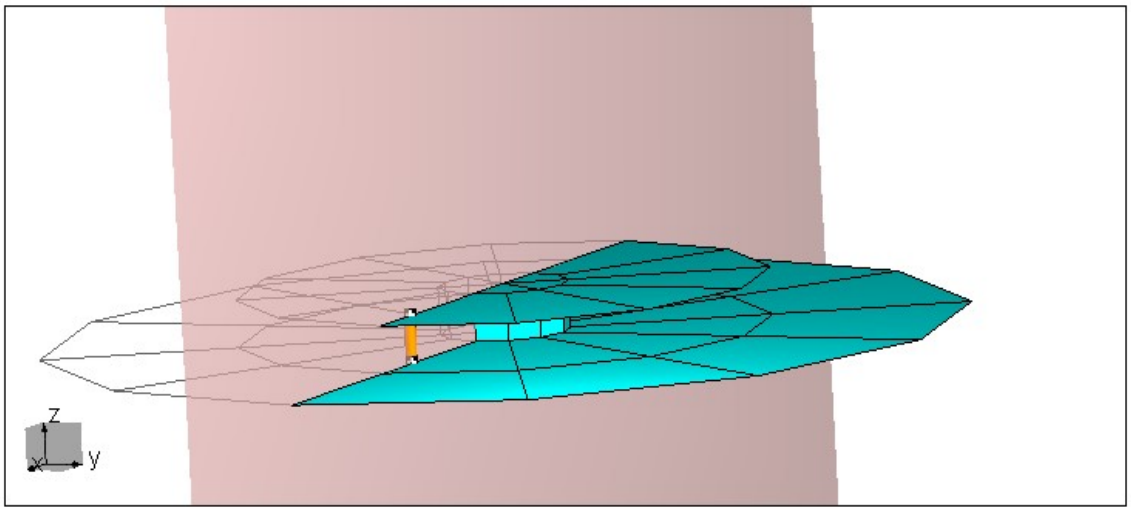

Figure 3-15: WIPL-D Model

3.2.2.1 Evaluation of the influence of the relation between inner and the outer radiuses

Firstly, we are going to simulate the antenna for four different values of the inner and the outer radiuses, so we can see:

- The differences between the results of the analytical model and the model of WIPL-s
- The influence of the dimensions of the antenna on its properties

In all cases, we are going to choose a circular ground plane with a radius of 100mm. Thus, the diffraction effect due to the finite dimensions of the ground plane is negligible.

Case	Inner radius	Outer radius	Ground plane radius
A	7	27.4	100
B	5	24.2	100
C	3	20.6	100
D	1	15.6	100

For the case A, we obtain that the resonant frequency is higher than the resonance frequency calculated with the analytical model. So we have to increase the outer radius in order to achieve a resonance frequency of 2GHz. In the end, the outer radius was set to 27.5mm.

The entrance impedance is mainly determined by the relative position of the feeds. Then, for matching the antenna, we can vary the relative position of the feed respect to the centre of the circular patch.

We observe that the best situation is reached when the position of the feed is quite close to the edge of the patch (d=22 mm). But as we can see, for this case is impossible to achieve a perfect match for the antenna. Another thing we can see is that it exist a weak influence of the position of the feed in the value of the resonant frequency. So although we have designed the antenna in a first time for a resonant frequency of 2GHz, when we vary the position of the feed we obtain a new antenna whose resonant frequency is not exactly the same.

For the analysis, we are going to design the antenna in the three cases for a resonance frequency of 2GHz when the feed is in the initial position (close to the central post). For the rest of the positions of the feed we are going to maintain the same values for the outer and the inner radiuses, so the resonant frequency will vary around the desired frequency. This should be taken into account when we are going to implement the final design, where we have to adjust again the resonant frequency for the final position of the feed.

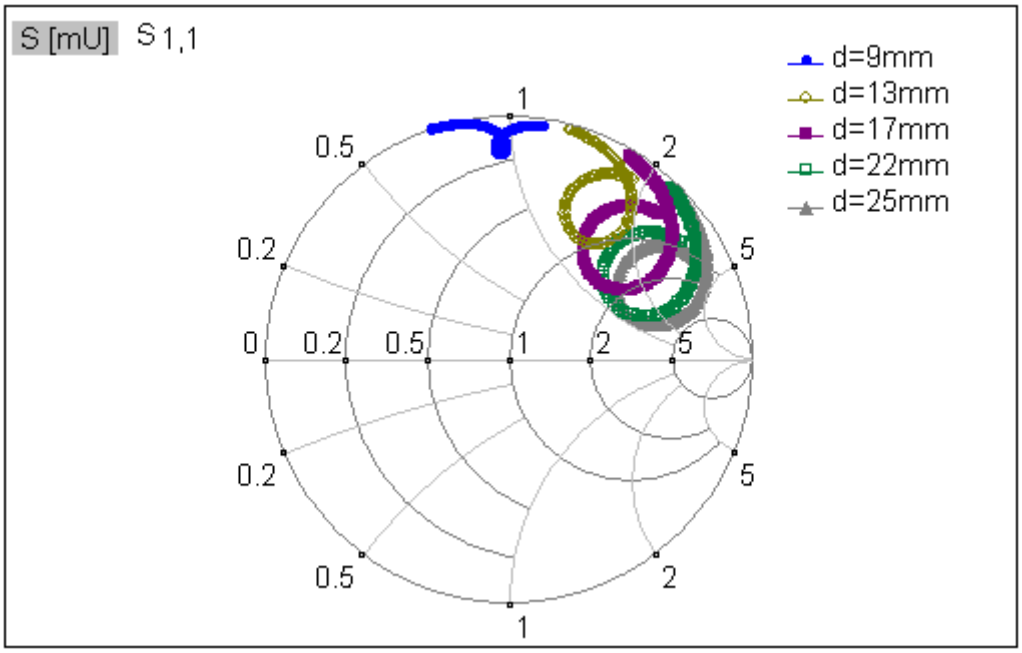

(1) d=distance from the feed point to de centre of the circular patch.

Figure 3-16: Case A. Influence of the feed position in the Smith Chart.

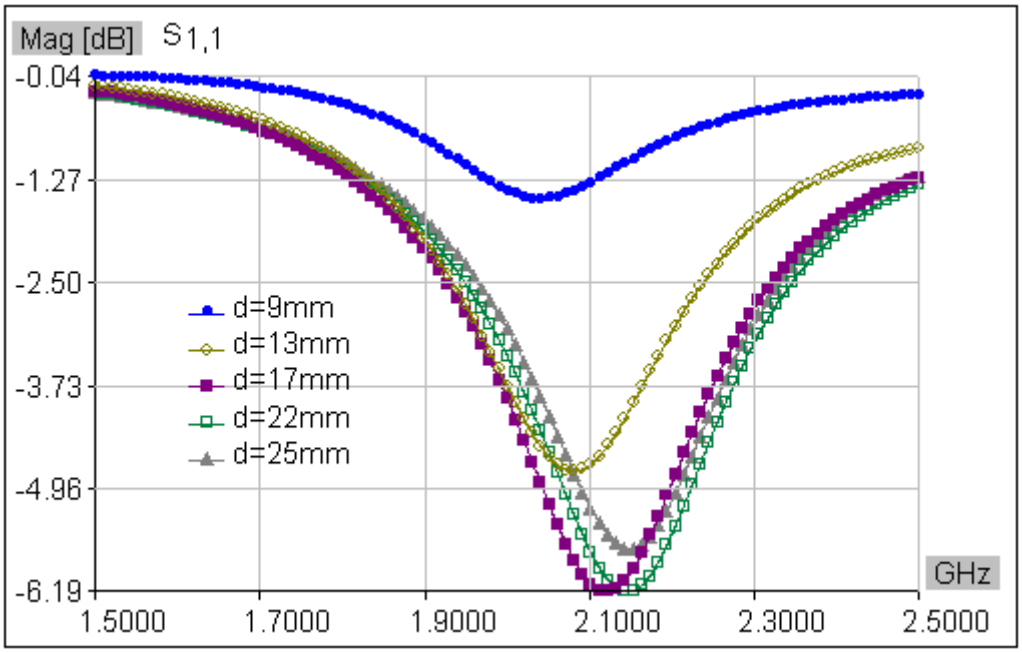

(1) d=distance from the feed point to de centre of the circular patch

Figure 3-17: Case A. Influence of the feed position in the resonant frequency.

Apart from the influence in the input impedance and the influence in the resonant frequency, another property that worth to be analyzed is the influence of the position of the feed in the shape of the radiation pattern.

The radiation pattern has a conical shape which is omnidirectional in the azimuth and has a null in the zenith, which was one of the requirements exposed in the introduction of this project. But the antenna does not have a perfect conical radiation pattern. In fact,

we can see a slight asymmetry in the $\varphi = 0$ plane. Although the influence is not very strong, we can observe a dependency between the position of the feed and the symmetry of the radiation pattern along the $\varphi = 0$ plane. Specifically, when the feed is closer to the edge of the patch, the radiation pattern becomes more asymmetric, and when the feed is closer to the central rod, the radiation pattern becomes more symmetric. But in all cases the radiation pattern is quite asymmetric and this is an undesired situation. The reason because we did not see this asymmetry in the results of the analytical analysis is because, this asymmetry in the radiation pattern is due to the presence of an asymmetric feed schema and we did not consider the feed schema of the antenna in the analytical model

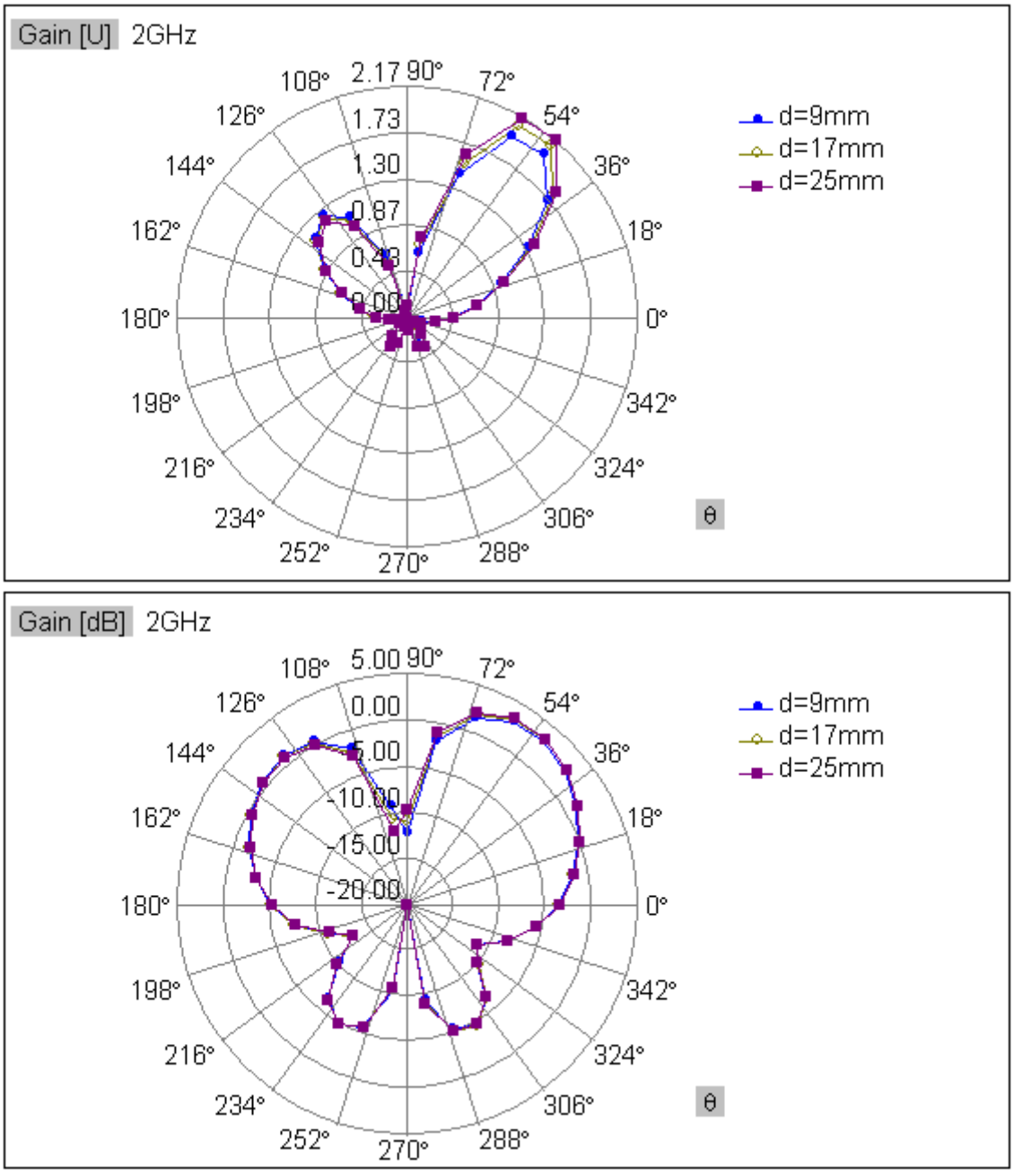

(1) d=distance from the feed point to de centre of the circular patch).

Figure 3-18: Case A. Influence of the feed position in the radiation pattern (φ=0).

For the case B, there is a difference between the result of the MATLAB program for the resonant frequency and the resonant frequency that we can see in the results of the simulation of the WIPL-d model. In fact, in that case the different is still larger (the resonant frequency derived from the WIPL-D simulation is about 200MHz higher). So in order to compensate this difference and get a resonant frequency of about 2GHz we had to increase the outer radius until 25.3mm.

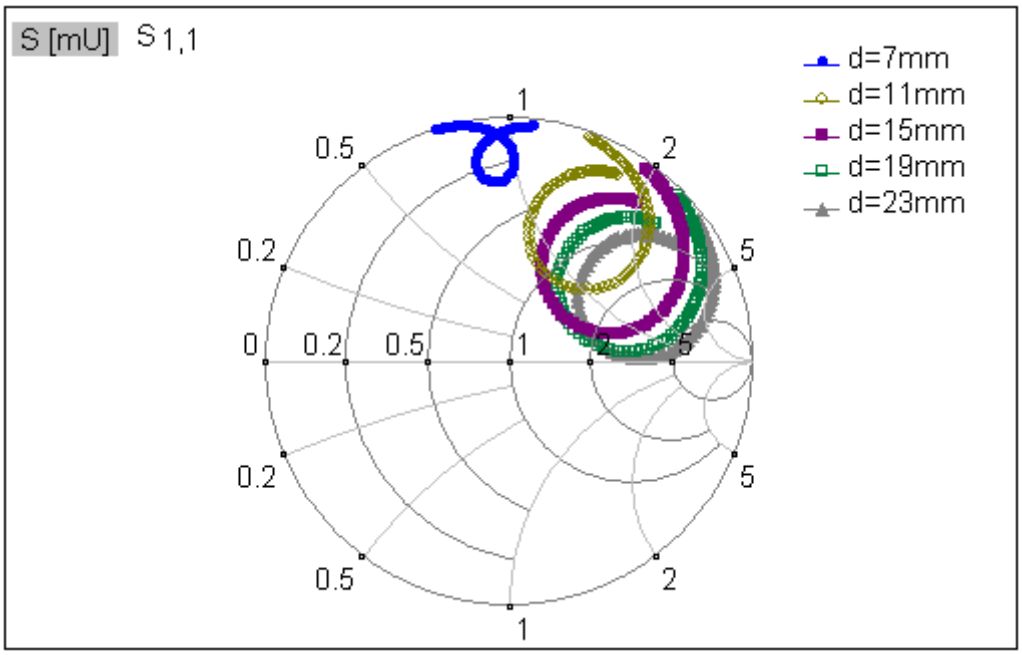

(1) d=distance from the feed point to de centre of the circular patch

Figure 3-19: Case B. Influence of the feed position in the Smith Chart.

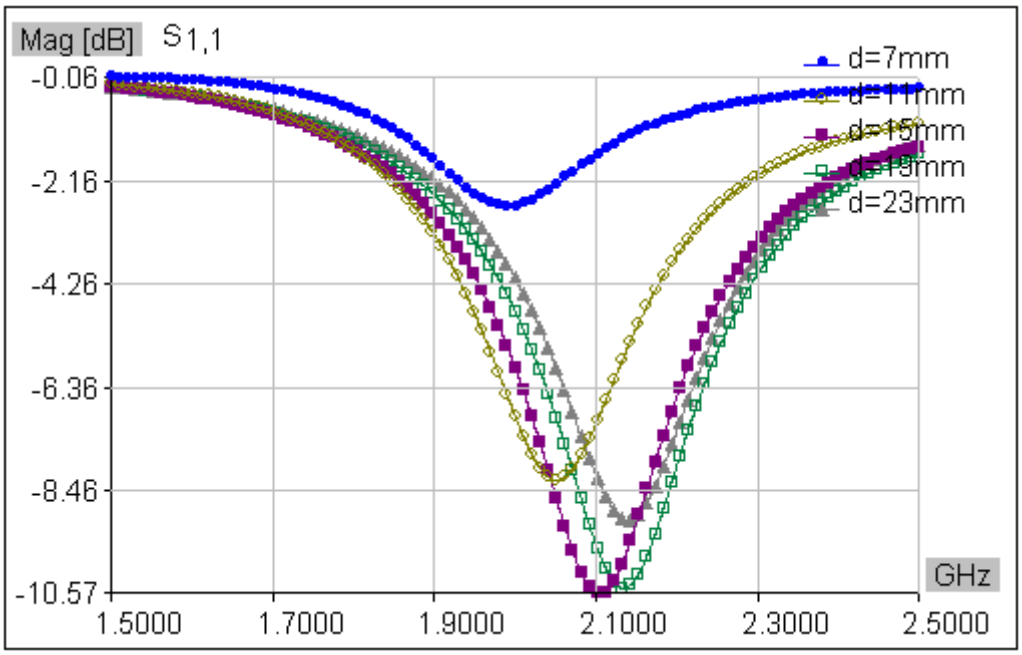

(1) d=distance from the feed point to de centre of the circular patch

Figure 3-20: Case B. Influence of the feed position in the resonant frequency.

The first difference which we can appreciate looking at the Smith chart is that in this case, the matching of the antenna is better, although is not possible to get a perfect matching for the antenna yet. We can see that the best result is obtained when the distance from the feed point to the central metallic rod is about 15mm.
In the other hand, we can see also see, as in the Case A, that in spite of the resonant frequency is determined basically by the dimensions of the antenna, there is a weak influence of the position of the feed that should be considered for the adjustment of the final design.

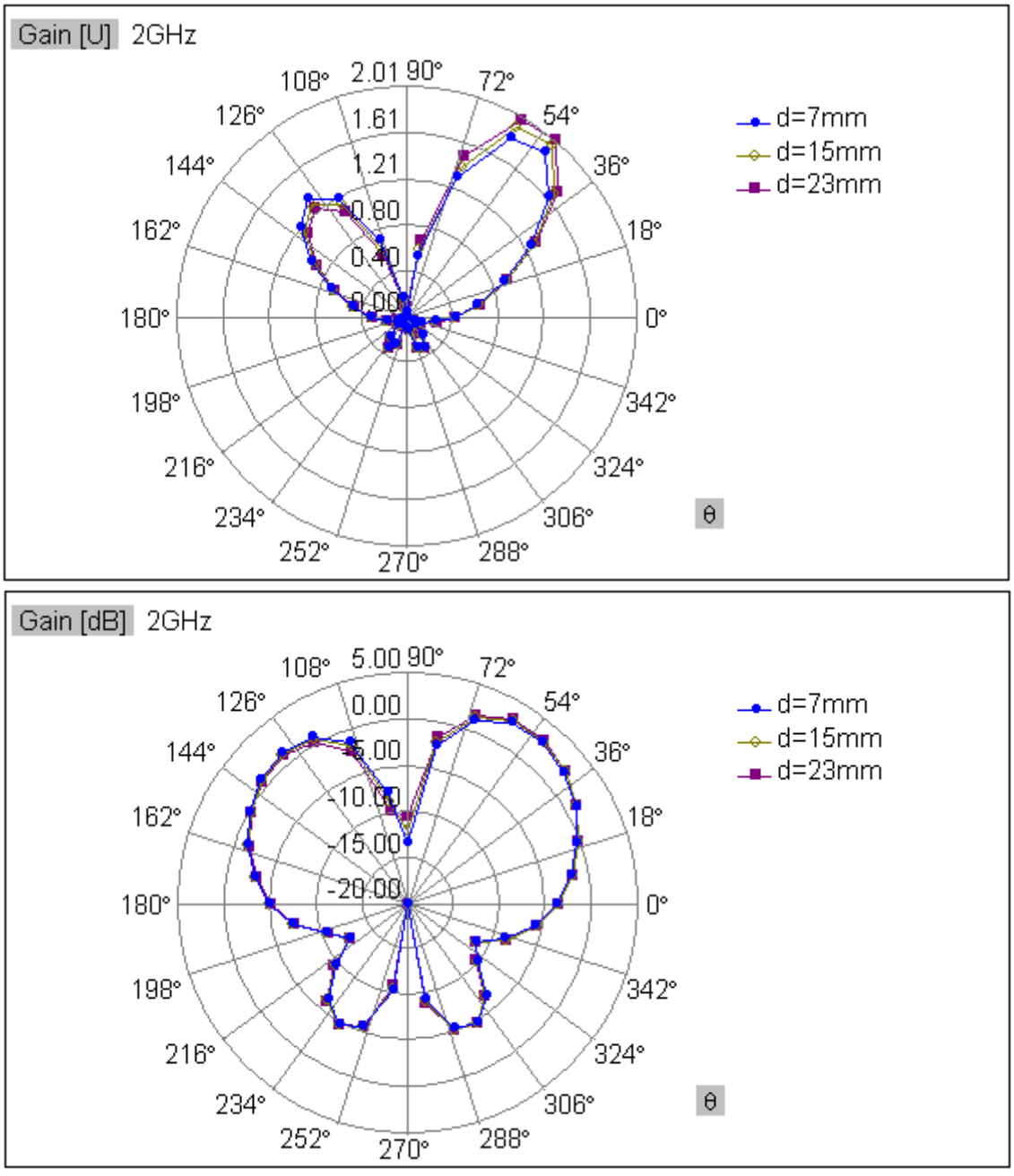

(1) d=distance from the feed point to de centre of the circular patch

Figure 3-21: Case B. Influence of the feed position in the radiation pattern (φ=0).

Finally, as we did in the Case A, we are going to analyze the influence of the position of the feed in the shape of the radiation pattern. In the figure we can see that the position of

the feed affects the symmetry of the radiation pattern. Specifically, when the feed is closer to the edge of the patch, the radiation pattern becomes more asymmetric along the plane $\varphi = 0$, and when the feed is closer to the central rod, the radiation pattern becomes more symmetric.

This is the same behaviour that we observed in the Case A. But much more important than that, is the fact that in this case, with independency of the position of the feed, the radiation pattern is much more symmetric than in the Case B. This coupled with a better matching of the antenna, makes that design better than the design performed in the Case A.

The situation in the Case C is quite better. We can see in the Smith Chart that in this case is possible to get a perfect matching for the design of the antenna (specifically for a distance of 15mm). This is very important, because analysing the plots for the different cases we can conclude that for matching the antenna we need that the central rod has a radius smaller than at least 3mm.

Like in the previous cases, the position of the feed affects the resonant frequency, producing slight variations around the desired resonant frequency. We have to say that in this case, the difference between the expected results and the resonant frequency derived from the simulation is even larger. Specifically, the resonant frequency is about 2.3GHz, so we had to increase the outer radius to correct this difference. In the end, the value of the outer radius was set to 22.3mm.

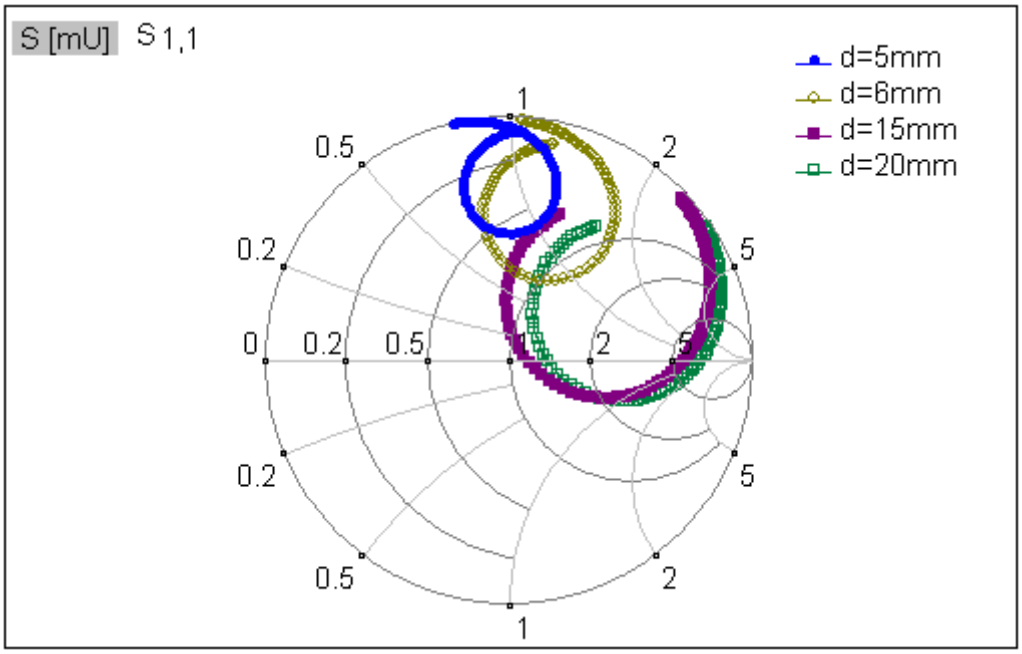

(1) d=distance from the feed point to de centre of the circular patch

Figure 3-22: Case C. Influence of the feed position in the Smith Chart.

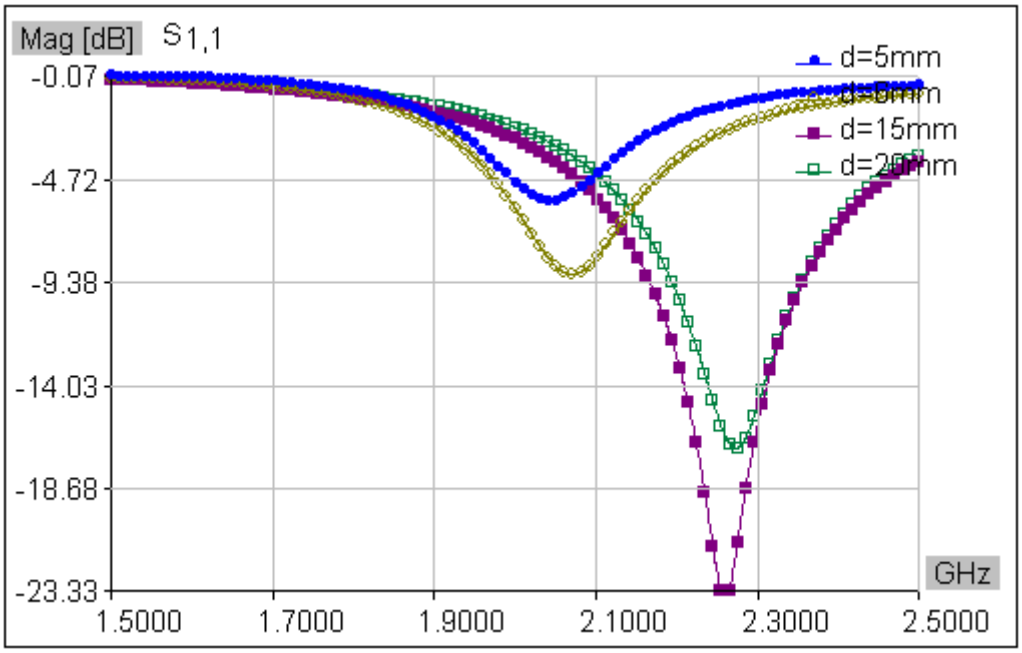

(1) d=distance from the feed point to de centre of the circular patch

Figure 3-23: Case C. Influence of the feed position in the resonant frequency.

Looking at the radiation pattern, we can see that is even more symmetric than the radiation pattern of the case B, which is very interesting for our final design. We can also see, as in the previous case, that there is a weak influence of the position of the feed in the symmetry of the radiation pattern so that, when the feed point is closer to the central post, the radiation pattern is more symmetric.

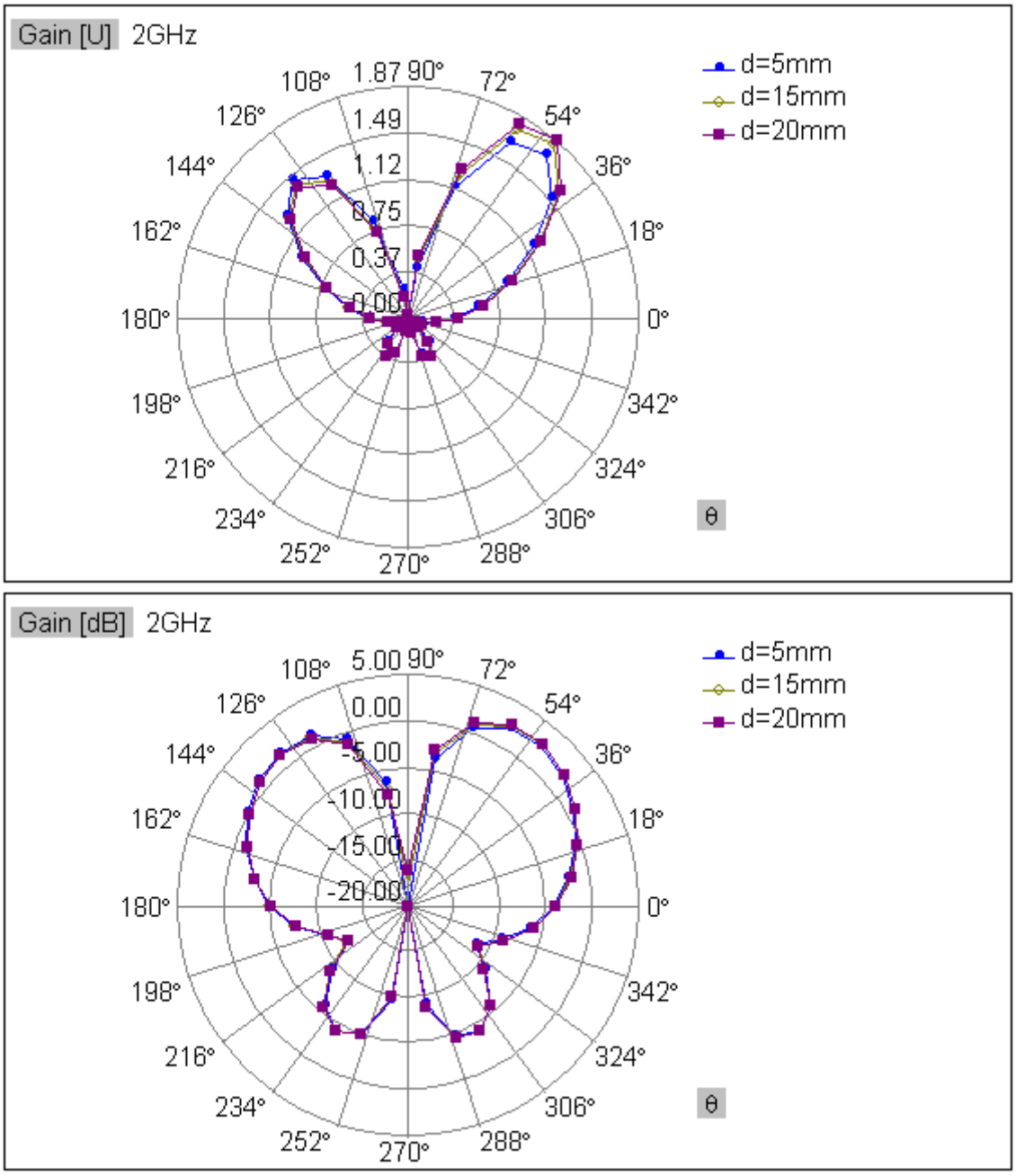

(1) d=distance from the feed point to de centre of the circular patch

Figure 3-24: Case C. Influence of the feed position in the radiation pattern (φ=0).

In the last case (Case D) the smith chart is shown in the next figure, where we can see that is possible to match the antenna, like in the previous case. Specifically in this case, we need to place the feed point very close to the central metallic rod to get a good matching for the antenna (2.7mm from the centre of the patch to the feed point).

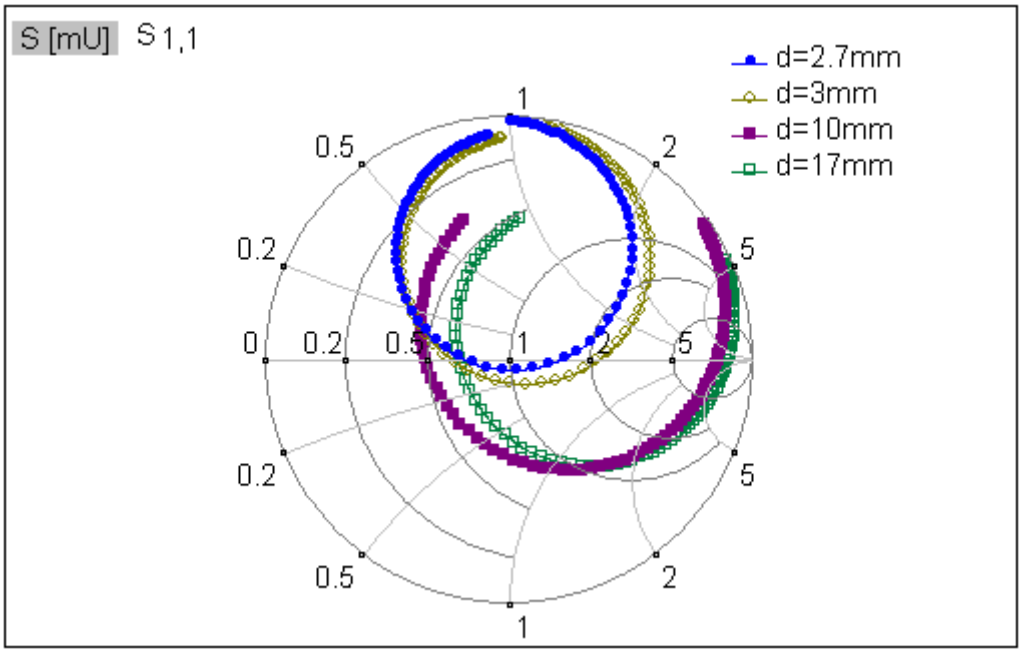

(1) d=distance from the feed point to de centre of the circular patch

Figure 3-25: Case D. Influence of the feed position in the Smith Chart.

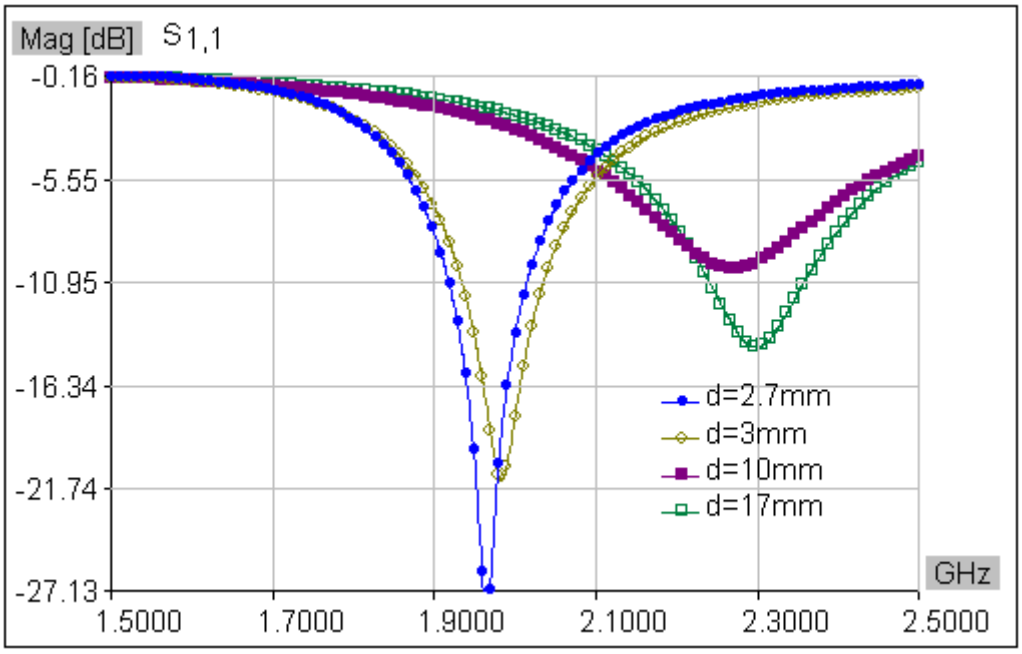

(1) d=distance from the feed point to de centre of the circular patch

Figure 3-26: Case D. Influence of the feed position in the resonant frequency.

After the analysis of the smith charts given by WIPL-D for the last two cases, we can conclude that, when the inner radius is between 1mm and 3mm, there will be a value for the position of the feed that will lead to an antenna which will be matched. Like in the other cases, we have to adjust the value of the outer radius to get a resonant frequency of about 2GHz. The final value for the outer radius in this case is 18.7mm.

Regarding with the radiation pattern, we can see the same behaviour than in the other cases with the position of the feed. Moreover, in this last case, the radiation pattern is the most symmetric. In the following figure we can see this.

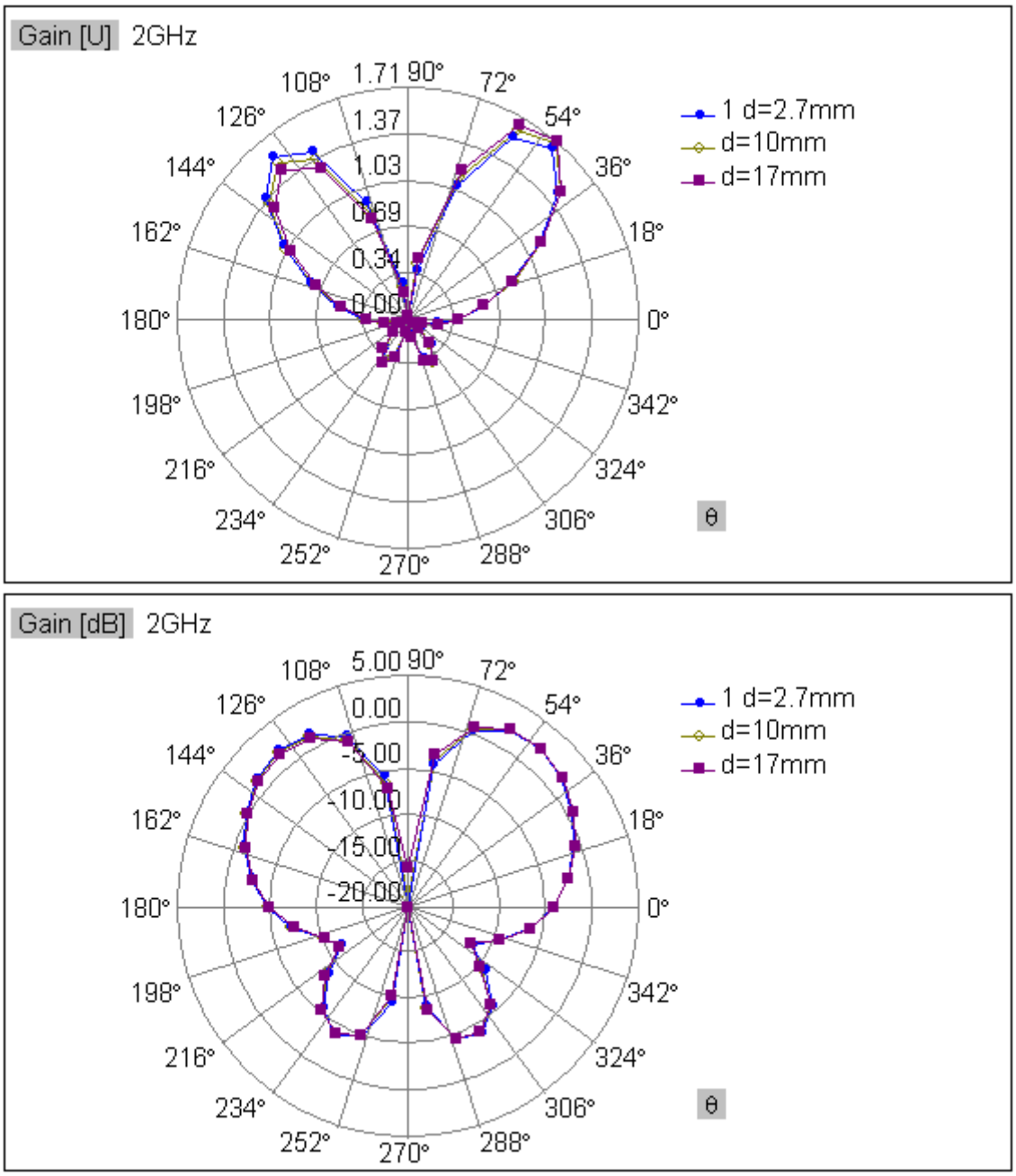

(1) d=distance from the feed point to de centre of the circular patch

Figure 3-27: Case D. Influence of the feed position in the radiation pattern (φ=0).

For finishing this section, we are going to summarize in a table the differences between the four different cases we have been seen. For this we are going to consider, for each case, only the results for the best position of the feed point.

	Feed position (mm)[1]	Elevation Angle (º)[2]	Gain (dB)[3]	Asymmetry (dB)[4]	Half power beam width (º)[5]	VSWR	BW (GHz)[6]
Case A	22	51.5	3.5	2.5	51	2.93	-
Case B	15	52.5	3	2	51.5	1.84	-
Case C	20	52	2.5	1	51.5	1.34	6.76%
Case D	2.7	51.5	2	0	52	1.07	5.34%

1) Distance from the feed point to the centre of the patch
2) Average elevation angle above the horizontal plane in which take place a maximum in the radiation pattern
3) Maximum gain
4) Maximum asymmetry between maximums in the radiation pattern
5) Average half power beam width
6) Bandwidth where the S_{11} remains under 10 dB

Firstly, is important to remark that only the two latest cases lead to a feasible design because only in these two cases is possible to get an antenna matched enough. The first two cases have very bad properties with regards to the matching and also a very asymmetric radiation pattern.

The Case D presents a radiation pattern more symmetric that the radiation pattern of the Case C, which is an advantage from the point of view of the design, but the Case D has a wider relative bandwidth. The width of the beam and the elevation angle are almost the same in the four cases. Finally, the average gain around the elevation angle is also the approximately the same.

In the end, we decided to study in depth the design of the Case C because it presents a group of properties quite good, considering the requirements of the wording. The case D was mainly discarded because it has a very thin central post and this could cause mechanical problem when we had to implement the prototype. Specifically, given that the antenna is going to be placed on the roof of a car, the pressure exercised by the air on the surface of the patch, could finally bend the central post and modifying the behaviour of the antenna.

3.2.2.2 Proposal for the construction of the prototype and analysis of the influence of the ground plane

Based on the results obtained from the previous paragraph, and after some simulations performed to optimize the antenna proposal of the case C, the finals dimensions of the antenna are the followings:

Case	Feed position	Inner radius	Outer radius	Ground plane radius
C	11	3	24.5	100

This parameters lead to a design with the final properties which are summarized in the following table:

	Feed position (mm)[1]	Elevation Angle (º)[2]	Gain (dB)[3]	Asymmetry (dB)[4]	Half power beam width (º)[5]	VSWR	BW (GHz)[6]
Case C	11	51.5	3	1.5	52.5	1.15	1.92-2.08 (5%)

1) Distance from the feed point to the centre of the patch
2) Average elevation angle above the horizontal plane in which take place a maximum in the radiation pattern
3) Maximum gain
4) Maximum asymmetry between maximums in the radiation pattern
5) Average half power beam width
6) Bandwidth where the S_{11} remains under 10 dB

Studying the previous table, we can that see the properties of the antenna are inside the initial requirements. However, the elevation angle of the radiation pattern is still quite higher (around 50º), because we chose as dielectric the air for the simplicity of the design. This led us to try to vary different parameters of the proposal we just presented at the beginning of this section in order to lower the elevation angle of the radiation pattern of the final antenna.

The first idea consisted in add a skirt around the edge of the ground plane, following the conclusions of a previous master thesis [18], which suggested another kind of antenna to satisfies the requirement of the CVIS project. Although the antenna proposed in that thesis is different from the design suggested in this master thesis, we did some simulations for trying if the proposal of a skirt around the ground plane had the same effect for our antenna. However, after some simulations, it was observed that the presence of that skirt barely affect the elevation angle of the radiation pattern. The results of those simulations can be seen in the appendixes.

After that, we tried to vary the dimension of the ground plane. This produced the desired reduction of the elevation angle. So the design of the case C was modified and, after some adjustments of the outer and the inner radiuses values to correct the distortion of the resonance frequency introduced by the variation of the size of the ground plane, three prototypes were proposed for their construction. We can see them in the next table:

Case	Feed position	Inner radius	Outer radius	Ground plane radius
C.1	11	3	24.5	100
C.2	6	3	22.9	50
C.3	6	3	25.9	27

It is necessary to say that this modification of the ground plane size is only a theoretical study only to increase our knowledge about the behaviour of the structure of the antenna, but this is not feasible. In practice, the antenna is going to be placed on the roof of a car, so the ground plane size will be set by the size of the roof which is going to act like a ground plane for the antenna. Nevertheless, if we analyze more closely the following figure, we can do some appreciations.

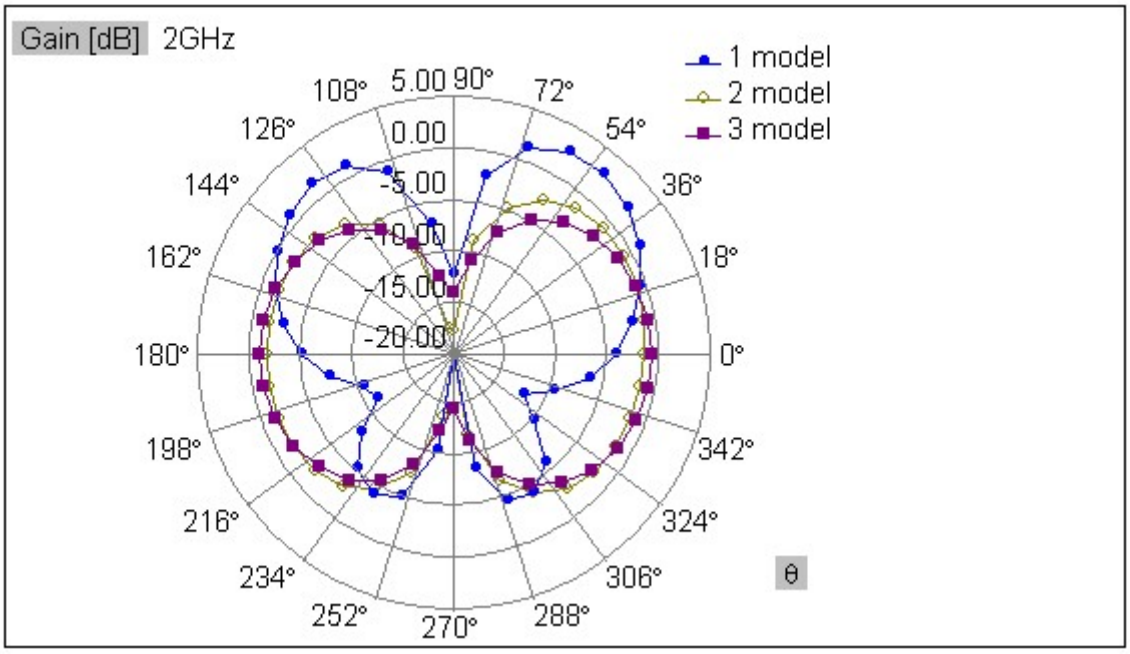

Figure 3-28: Radiation pattern of the prototypes (φ=0).

When the size of the ground plane decreases, we can see how the elevation angle of the radiation pattern also decreases, tending to zero when the size of the ground plane tends to the size of the patch. It is important to say that the size of the ground plane has also some effects over the resonance frequency and the entrance impedance, so we had to make some adjustment in the dimensions of the outer and the inner radius and over the position of the feed, as we saw in the previous table. In the next figure we can see some differences between the three alternatives.

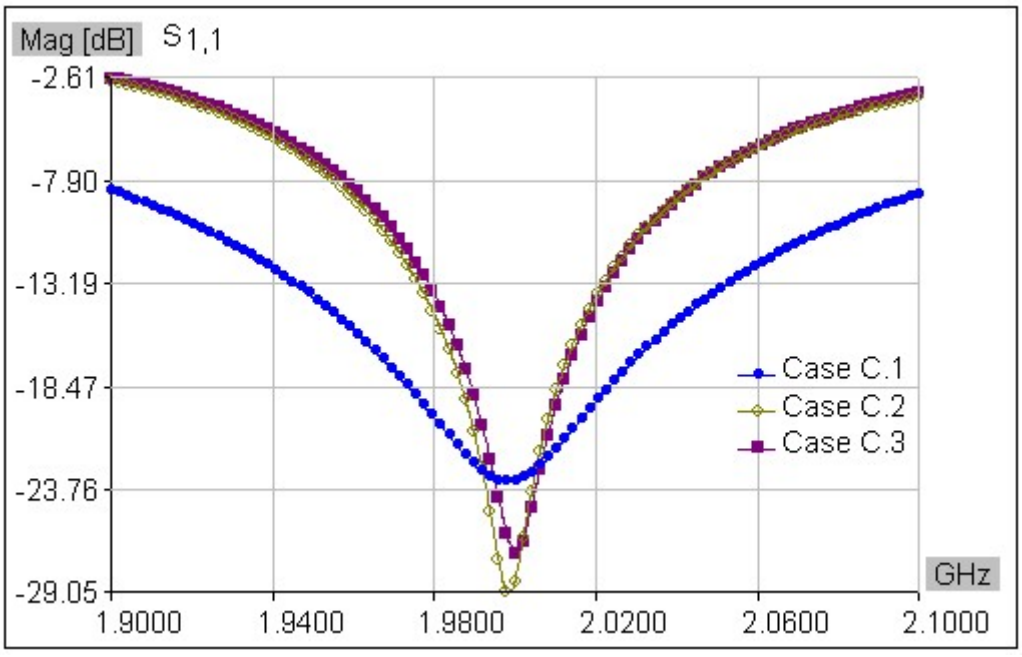

Figure 3-29: Parameter S_{11} of the prototypes.

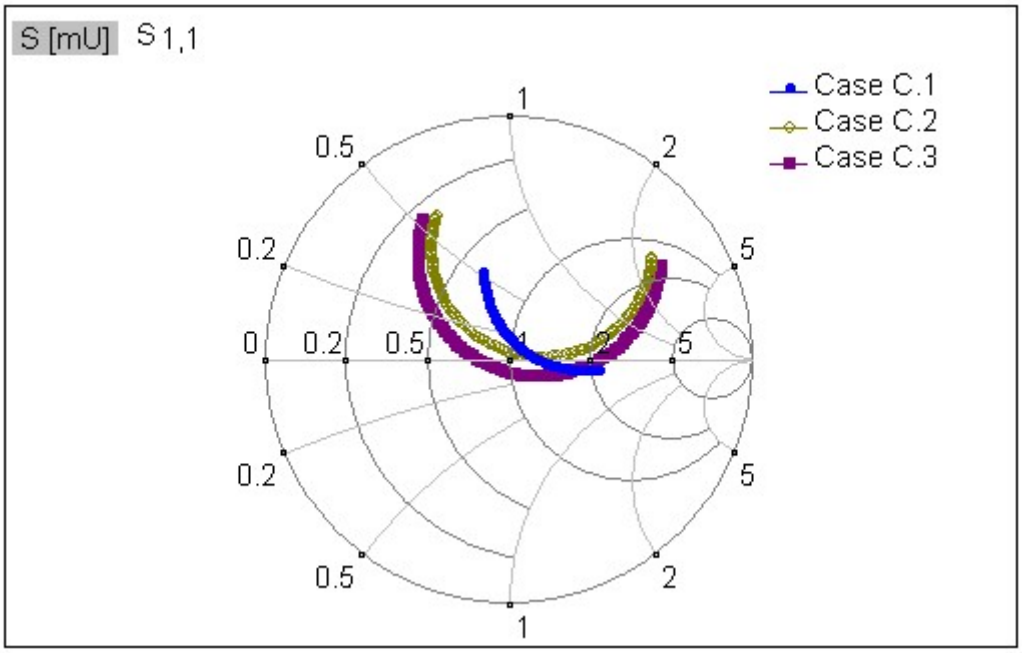

Figure 3-30: Smith chart of the prototypes.

We can see that the bandwidth of the case C.1 is significantly wider than the bandwidth of the cases C.1 and C.2, but C.1 and C.2 have a lower elevation angle in the radiation pattern which was one of the requirements. But it is important to remark that the case C.3 is not a feasible design, given that the roof of the car is going to act like a huge ground plane in comparison with the dimensions of the antenna. The main properties of the three proposals are shown in detail in the next table:

	Feed position (mm)[1]	**Elevation Angle (º)[2]**	**Gain (dB)[3]**	**Asymmetry (dB)[4]**	**Half power beam width (º)[5]**	**VSWR**	**BW (GHz)[6]**
Case C.1	11	51.5	3	1	52.5	1.15	1.92-2.08 (5%)
Case C.2	6	25.5	-1	0.5	120	1.08	1.96-2.03 (3.5%)
Case C.3	6	1	-1	0	104	1.09	1.97-2.03 (3%)

1) Distance from the feed point to the centre of the patch
2) Average elevation angle above the horizontal plane in which take place a maximum in the radiation pattern
3) Maximum gain
4) Maximum asymmetry between maximums in the radiation pattern
5) Average half power beam width
6) Bandwidth where the S_{11} remains under 10 dB

These three variations of the case C are going to be the proposal for the construction of three prototypes which are going to be the final result of this first part of the project.

These prototypes will be tested and compared with the results obtained from the WIPL-D simulation.

3.2.3 Agilent EMDS

Before the construction and the analysis of the three prototypes proposed in the previous section, which is the final goal of this first part of the master thesis, we are going to model and simulate the three models with EMDS. As we explain previously, EMDS is another simulation tool which has the advantage of offering more precise results at the expense of a higher consumption of memory and a longer time of simulation. So the main goal of this section is to check if the results offered by the WIPL-D simulation software are the same that the results of EMDS to be sure that the results are valid, before the construction of the prototypes. In the next figure we can see the model that has been constructed with this tool:

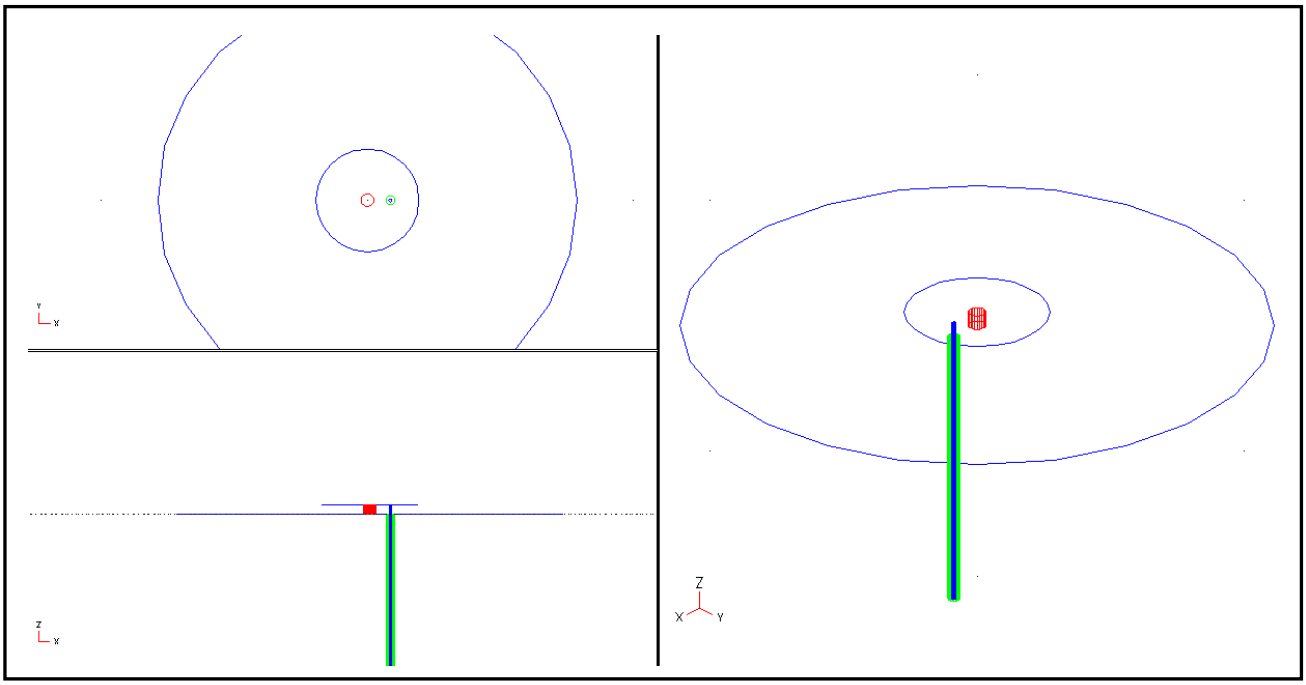

Figure 3-31: EMDS model of the prototypes.

In addition to the input data we used in WIPL-D, for the EMDS model we are going to introduce a more detailed schema of the coaxial feed. Specifically, we are going to use a coaxial feed defined by the following parameters:

- Outer radius: 2.05 mm
- Inner radius: 0.64 mm
- Dielectric: Teflon

This coaxial feed has a characteristic impedance of 50 Ω and it can be found in the market. The rest of the dimensions of the prototypes proposed can be seen in the previous section.

3.2.3.1 EMDS results for the prototypes proposed

First, we are going to simulate and analyze the proposal of the case C.1 which was the one with the largest ground plane. In the next figure we can see the frequency response of the antenna prototype according to the EMDS.

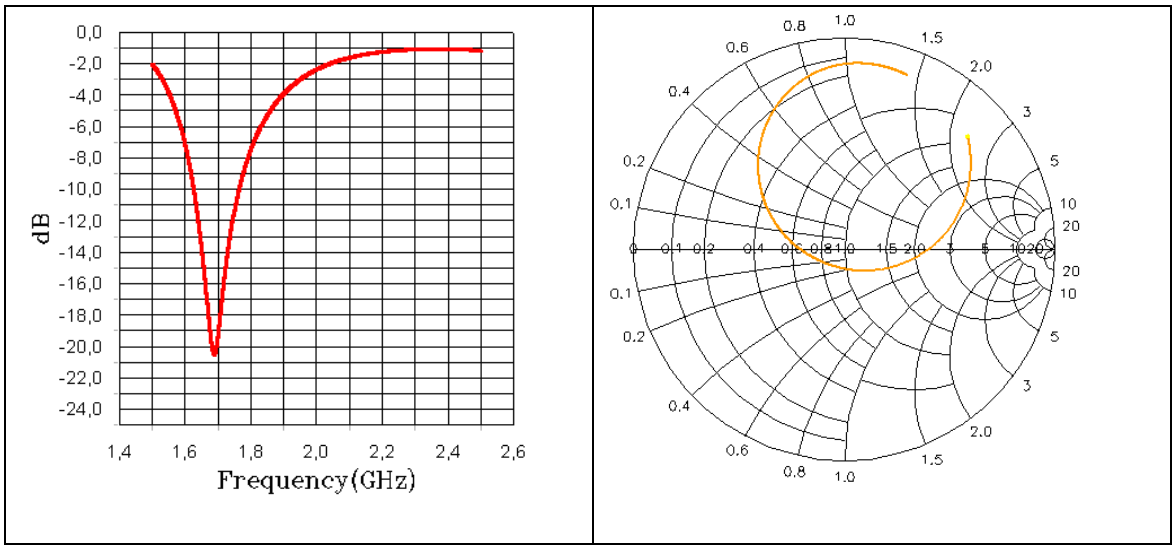

Figure 3-32: Case C.1.S11 parameter and Smith Chart.

The previous figure show that the results offered by EMDS differ a lot from the results we obtained in the previous paragraph with the WIPL-D software. Specifically, we can see how the difference between the resonant frequencies provided by the two simulation tools differs almost 300 MHz. This fact prevents us to trust one hundred percent in the results obtained so far. On the other hand, the Smith chart is almost the same in the two simulation tools. In the following two figures we can see that for the cases C.2 and C.3 the situation is not better. There is a significant difference between the resonance frequencies predicted by the two simulation tools, and in addition, we can see that there is also a significant difference between the Smith charts calculated by the two different programs.

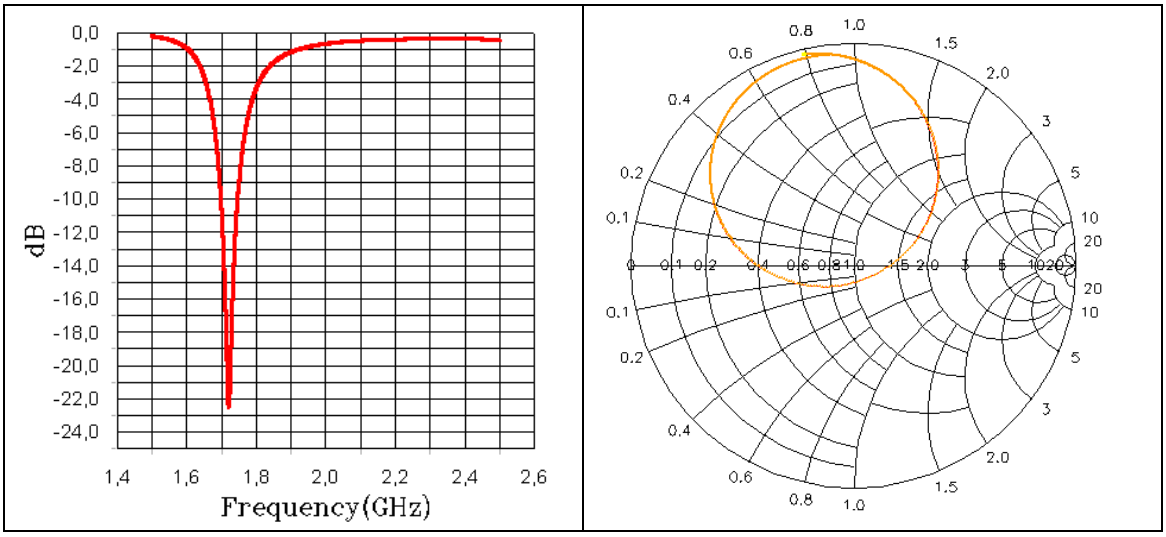

Figure 3-33: Case C.2.Parameter S11 and Smith Chart.

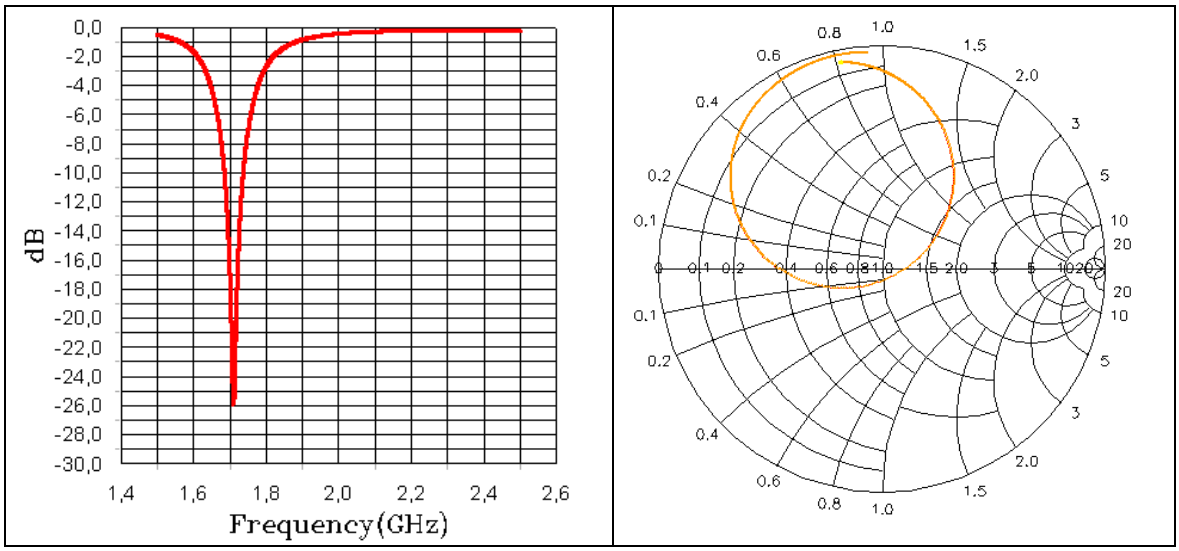

Figure 3-34: Case C.3.Parameter S11 and Smith Chart.

While it is true that EMDS provides more reliable results than WIPL-D, we can not justify, given its magnitude, the appearance of such a difference by a lesser accuracy of the simulation tool. This suggests a malfunction in one of the simulation tools or human error in the process of modelling of the prototypes. This situation finally led to propose the construction of the three prototypes in order to check which simulation tool was supplying wrong results and try to find and solve the source of this problem. Before addressing the construction and measure of the prototypes, is interesting showing and comparing the results obtained by the two simulation tools for the radiation pattern of the prototypes. The results obtained are presented in the following figures.

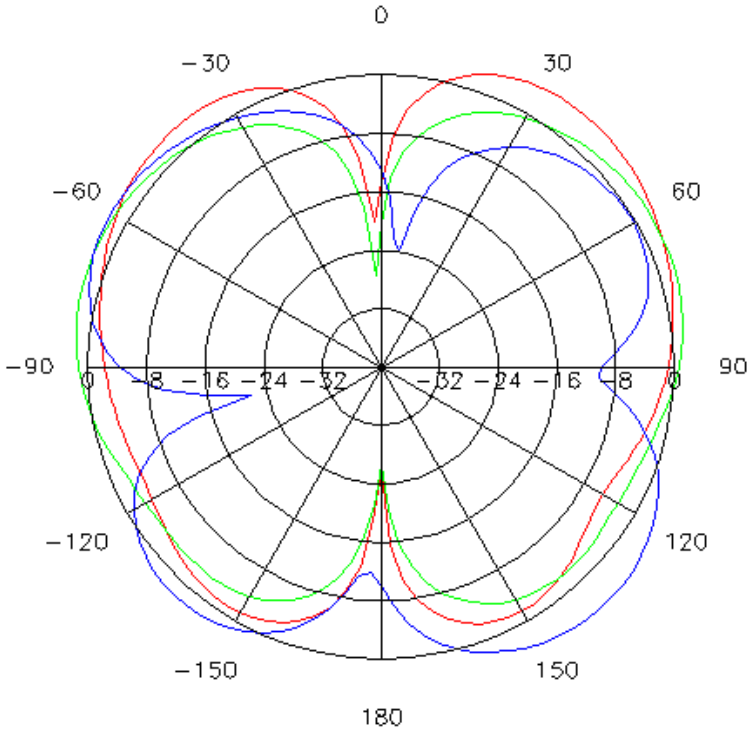

Figure 3-35: Cases C.1, C.2 and C.3.Radiation pattern for the plane φ=0.

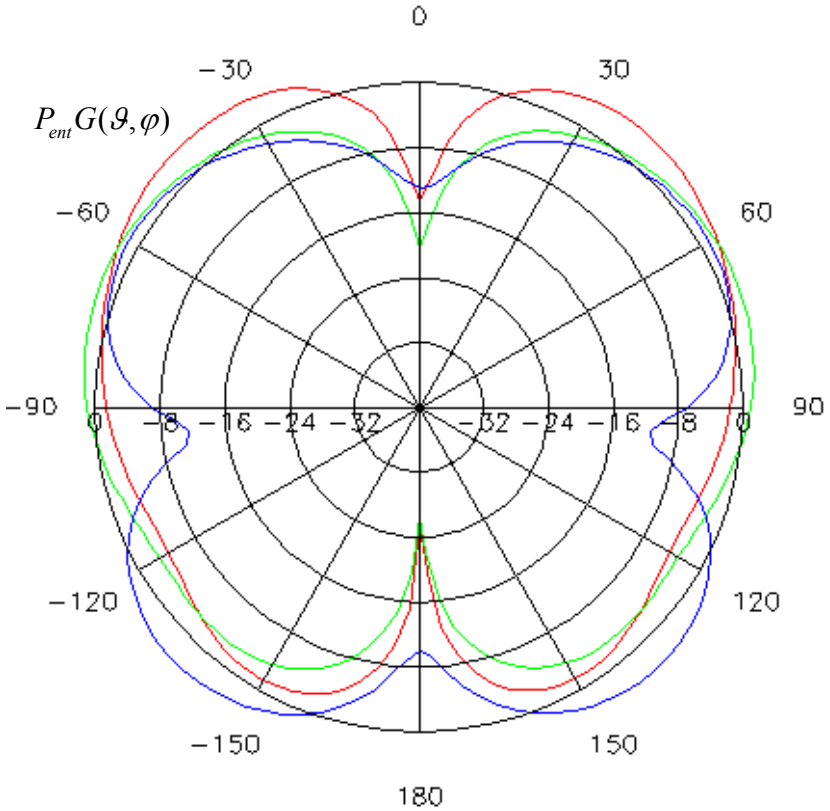

Figure 3-36: Cases C.1, C.2 and C.3.Radiation pattern for the plane φ=90.

It is important to notice that the radiation patterns plotted in the previous figures with EMDS are not normalized for seeing the difference of magnitude between the different

cases. In fact, the value plotted is $P_{in}G(\vartheta,\varphi)$, so we can compare the magnitude between the different cases, given that the input power is the same in the three cases.

We can see the same asymmetry along the plane $\varphi = 90$ which was seen in the results of the WIPL-D model. We can also observe that the elevation angle of the radiation pattern get lower when the size of ground plane decreases, which was the same conclusion that we reach from the WIPL-D simulation. But if we compare the radiation patterns calculated by EMDS with the radiation pattern we saw in the previous chapter, we can see that there is a non negligible difference which becomes more pronounced as the ground plane tends to the size of the patch. In fact, for the case C.3 the radiation patterns obtained by the two tools are completely different.

The main differences between the results of the two simulations tools are summarized in the following table.

		Elevation Angle (º)[1]	**Gain (dB) [2]**	**Asymmetry (dB) [3]**	**Half power beam width (º) [4]**	**VSWR**	**BW (GHz) [5]**
WIPL-D	**Case C.1**	51.5	3	1.241	52.5	1.15	1.92-2.08 (5%)
	Case C.2	25.5	-1	0.8922	120	1.08	1.96-2.03 (3.5%)
	Case C.3	1	-1	0.325	104	1.09	1.97-2.03 (3%)
EMDS	**Case C.1**	51	4.5	1	54	1.20	1.62-1.76 (8.15%)
	Case C.2	21.5	2.5	0	68	1.16	1.7-1.75 (2.79%)
	Case C.3	30	4.5	2	46.5	1.10	1.68-1.74 (3.1%)

1) Average elevation angle above the horizontal plane in which take place a maximum in the radiation pattern
2) Maximum gain
3) Maximum asymmetry between maximums in the radiation pattern
4) Average half power beam width
5) Bandwidth where the S_{11} remains under 10 dB

Seeing the previous table, we can see that the results obtained with the two simulation tools are very different. In fact, we can see how the difference is biggest in the last cases. For the first case, although the resonant frequency is different for the two simulation tools, the rest of the parameters remain almost similar. But for the rest of the cases, there is a large difference in all the properties of the prototypes. We can see how the results for the radiation pattern of the case C.3 are completely different depending on the tool we are using. In the next section, we are going to proceed with the

construction of three prototype according with the specification of the previous three cases, in order to check the results of the simulation tools.

3.3 Prototype construction and analysis

3.3.1 Prototypes

For its analysis, three prototypes were constructed according to the dimensions given for the cases C.1, C.2 and C.3 and taking into account the dimension of the coaxial cable that is going to be used to feed the antenna. In the following figure we can see some pictures of the result of the fabrication process.

A STM-5 probe was used for the coupling of the coaxial feed to the antenna.

The antenna prototypes were mounted in the anechoic chamber through a non metallic support. Specifically, it was made of polyethylene. Two holes were performed to fix the patch antenna to this non metallic support for measuring the radiation pattern in two perpendicular planes. In the prototype for the case C.3, we had to add a plastic arm for fixing the antenna to the anechoic chamber because there was no space between the ground plane edge and the top patch edge to put a screw, in order to fix the antenna to the plastic support.

Although, as we have just explained, some modifications were done on the original prototypes specification due to practical needs, these modifications should not affect the properties of the patch antenna much. In the next figures we can see the prototypes constructed.

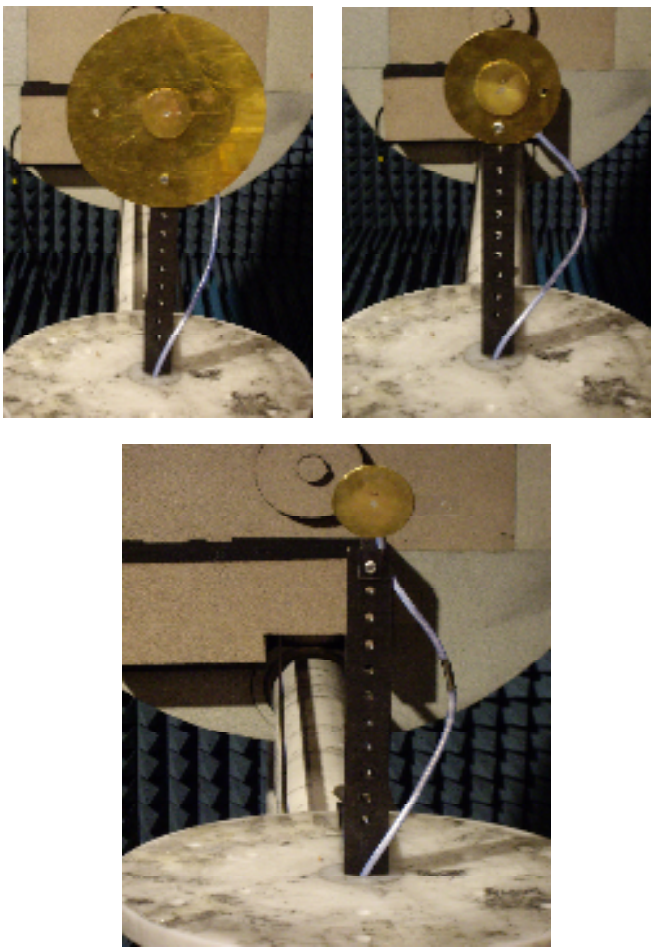

Figure 3-37: Prototypes: C.1 (up-left). C-2 (up-rigth). C.3 (down).

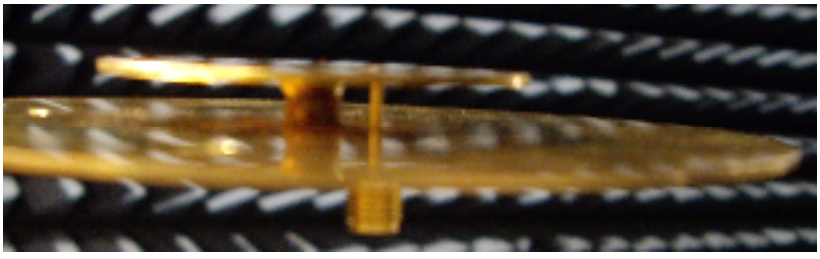

Figure 3-38: Feed schema of the prototypes.

3.3.2 Measure equipment

For measuring the prototypes, we have the following equipment in the antenna laboratory of the NTNU:

- *Natural Analyzer*: With the natural analyzer we can study the properties of the antenna in the range of frequencies of interest. Specifically we are going to use the two natural analyzers which are shown in the next figure.

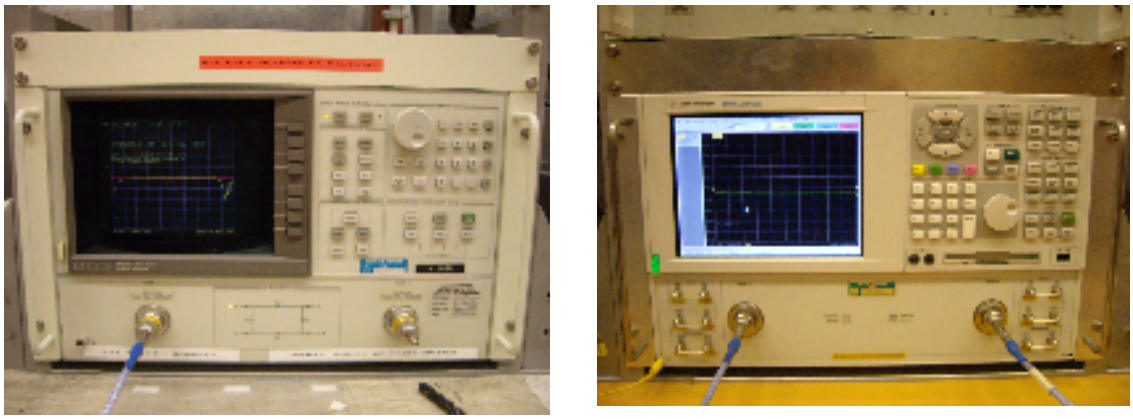

Figure 3-39: Hewlett Packard Network Analyzer 8720C (Left).Agilent Technologies Network Analyzer E8364B (Right).

With the natural analyzers we can study the properties of the antenna in the range of frequencies of interest. The natural analyzer 8720C is going to be used for measuring the scattering parameters (S-parameters) of the prototypes. Is connected to a computer where we can process the data collected from the measured performed. The reference plane for doing the measurement of the input impedance is taken in the ground plane because in the EMDS model, the reference plane was also the ground plane of the patch antenna. On the other hand, the natural analyzer E8364B will be used, in combination with the anechoic chamber, to measure the radiation pattern of the prototypes. In the same way, it is connected to a computer which allows the process of the data collected.

- *Motion controller*: the motion controller allows the movement of the prototype inside the anechoic chamber to measure the radiation pattern in all directions.

Figure 3-40: Newport Motion Controller MM4005.

- *Anechoic chamber:* For obtaining the radiation pattern of the three prototypes, we are going to use the anechoic chamber. It consists in a chamber whose walls are covered by a radiation absorbent material to absorb electromagnetic waves that impinges on the walls, floors and ceilings in the same chamber, offsetting the effects of echo and reverb. In the middle there is a robotic arm where we put the antenna which we want measuring. This robotic arm is controlled by the motion controller that allows moving the antenna in all directions of the space.

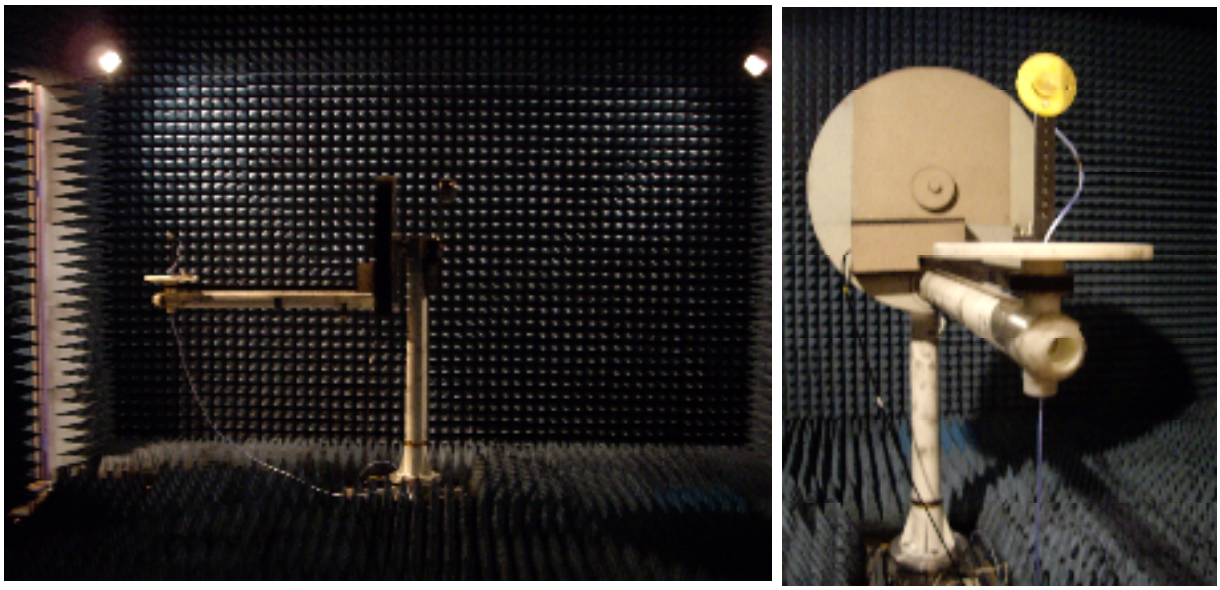

Figure 3-41: Eccosorb Anechoic Chamber.

The transmitter antenna is placed in an aperture performed in one wall of the chamber. The antenna we are going to use as transmitter is a horn antenna, whose gain is well known. This kind of antennas allows doing the necessary measurement in the band of interest (around 1.7GHz). What we measure is the reception radiation pattern of the antenna under test, which will be the same that its transmitter radiation pattern because of the reciprocity theorem.

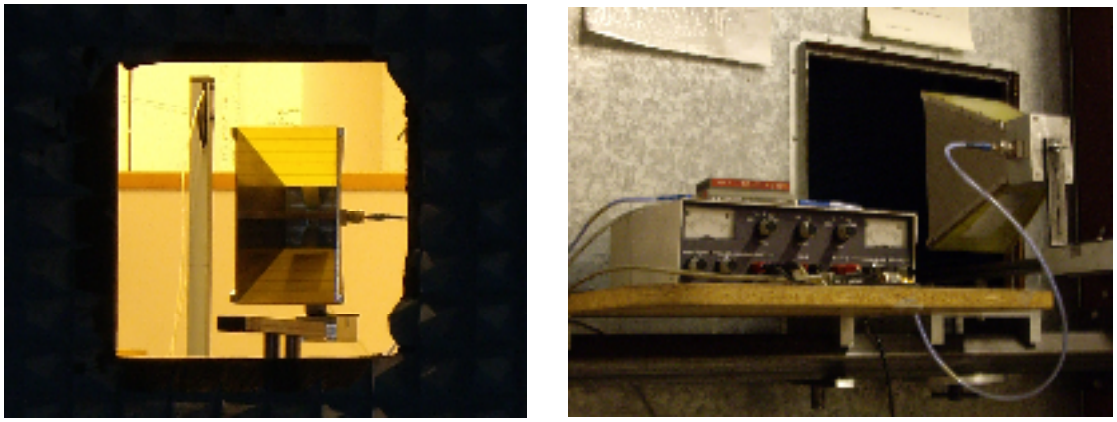

Figure 3-42: Transmitter antenna.

3.3 Results

After the analysis of the prototypes constructed, we could see that the results obtained were quite close to the results obtained by the EMDS software. In this section, we are going to study the differences and similarities between the prototypes and their EMDS models. By the moment, we are going to discard the WIPL-D results because they are not accurate enough. In the next section we will try to perform some modification over the simulation parameters of the WIPL-D software in order to solve the problem. However, although the results of the simulations of the WIPL-D models are not accurate enough, the conclusions extracted in the previous sections about the influence of the feed position, the inner and the outer radiuses over the properties of the antenna are still valid.

First, we are going to compare the results of the first prototype. Seeing the following figures we can see some differences between the properties of the prototypes and the results of the EMDS models.

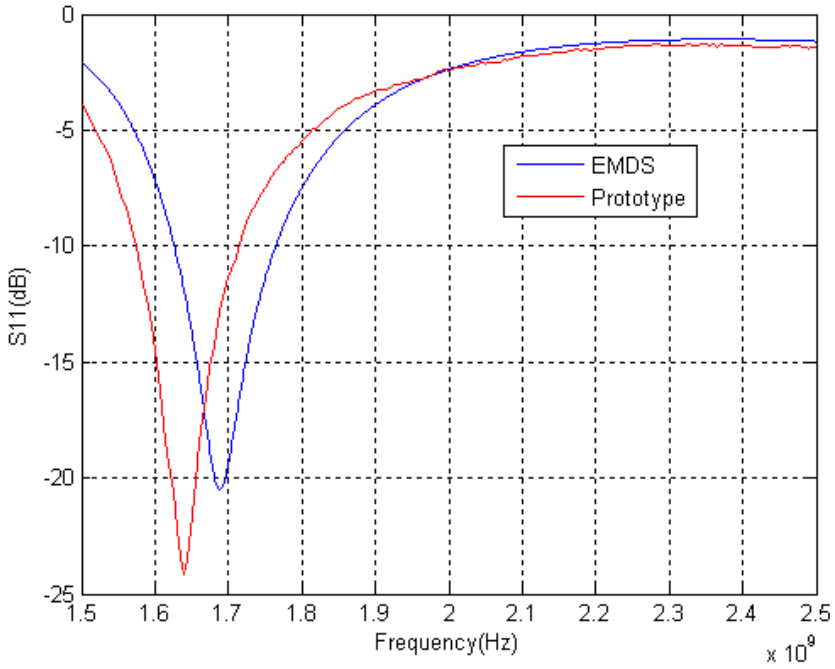

Figure 3-43: Parameter S11 for the case C.1

The resonant frequency predicted by the EMDS model is quite similar to the real resonant frequency of the antenna, for the case C.1. However, we can see that the real resonant frequency is a slightly lower than the predicted one. In addition, we can see that the value of the reflection coefficient for the resonant frequency is about 4dB lower than the predicted. In the next figure we can see the Smith chart where we can appreciate that the matching of the constructed antenna is even better than the matching of the model.

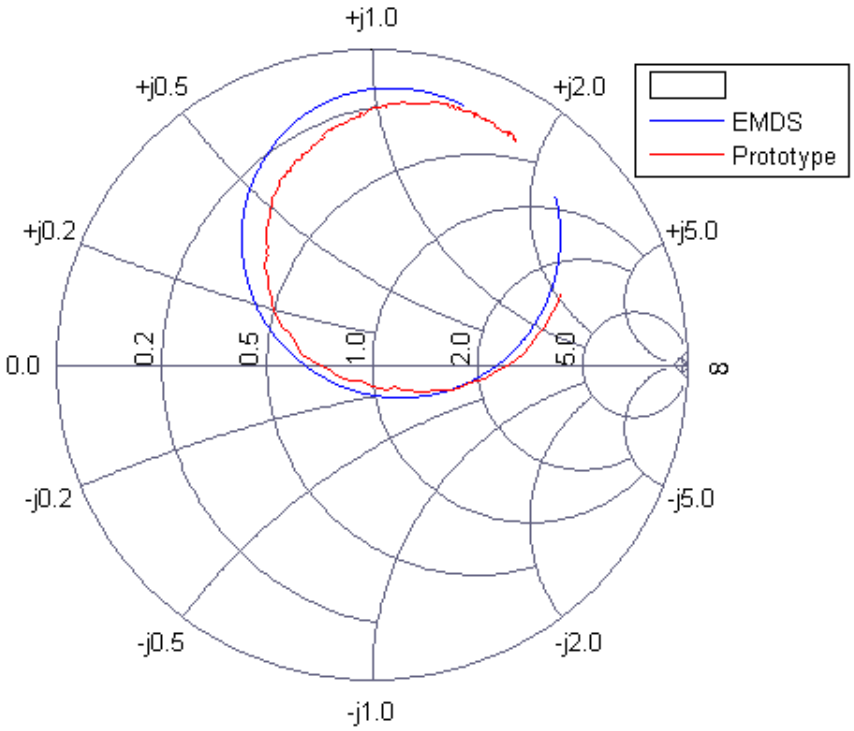

Figure 3-44: Smith chart for the case C.1.

We can appreciate that the constructed prototype has good properties of matching and a relative bandwidth quite close to the predicted with EMDS. Finally, in the following figures we show the comparison between the radiation pattern calculated by EMDS and the radiation pattern measured with the anechoic chamber.

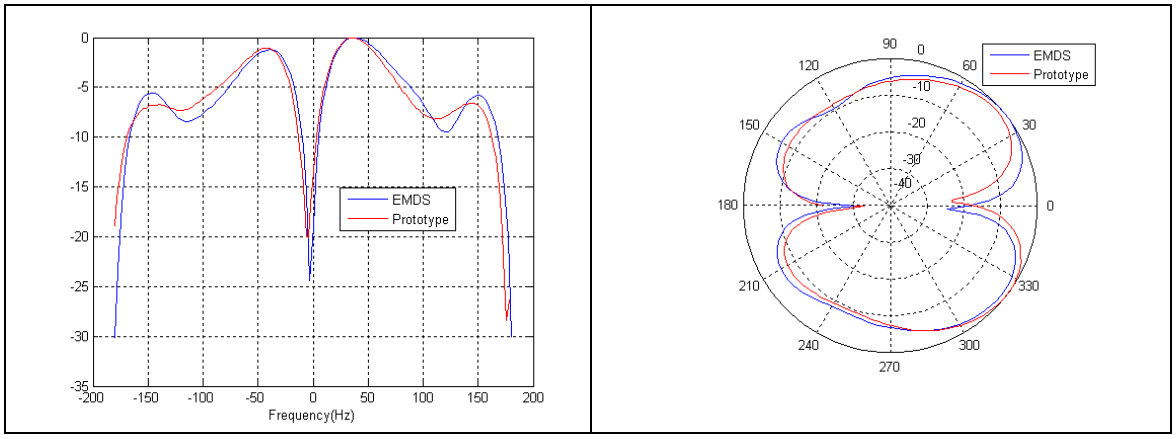

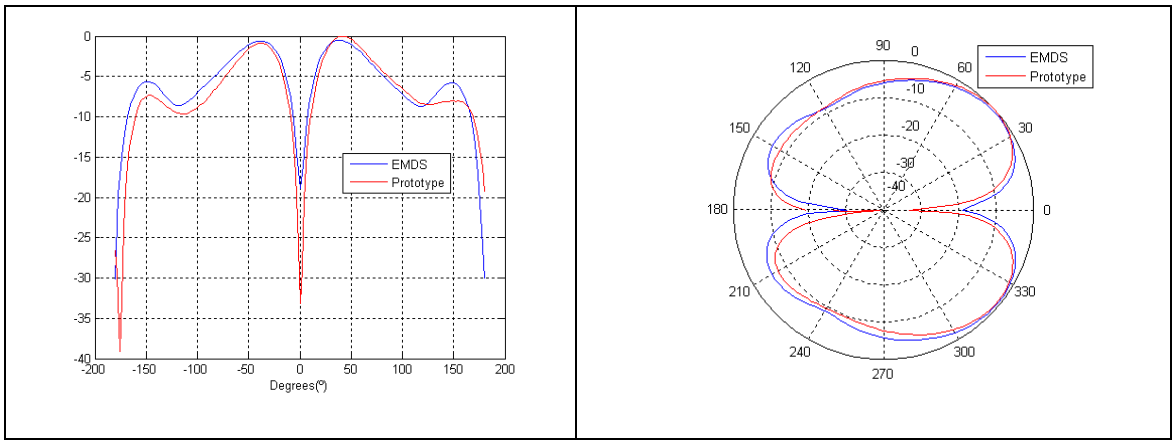

Figure 3-45: Normalized radiation pattern for the plane φ=0.

We can conclude that the radiation pattern measured with the anechoic chamber is very similar to the radiation pattern calculated by EMDS. We can see that both of the radiation patterns have almost the same shape. For the other two cases, the situation is almost the same. We can appreciate a slightly difference between the resonant frequency calculated by EMDS and the resonant frequency of the prototype too. The same occurs with the reflection coefficient for the resonant frequency.

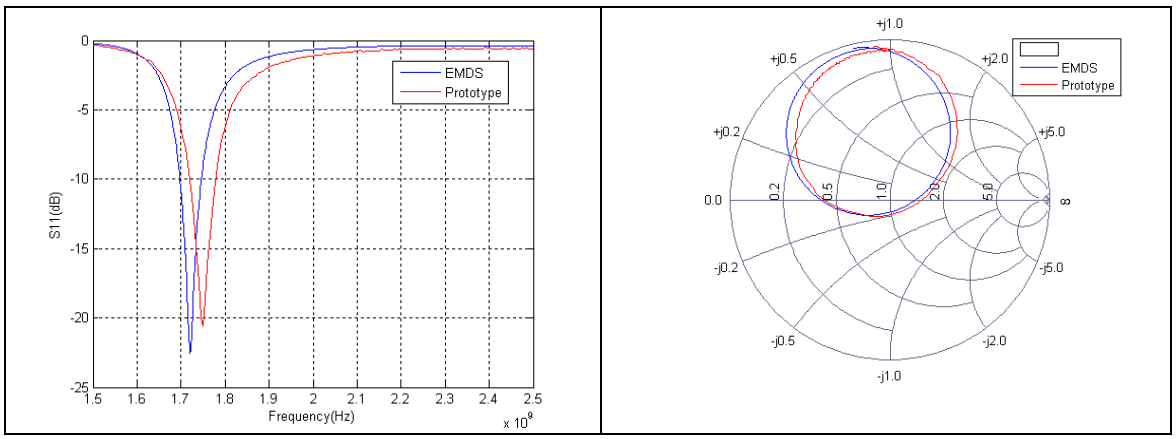

Figure 3-46: Case C.2. Reflection coefficient and Smith chart.

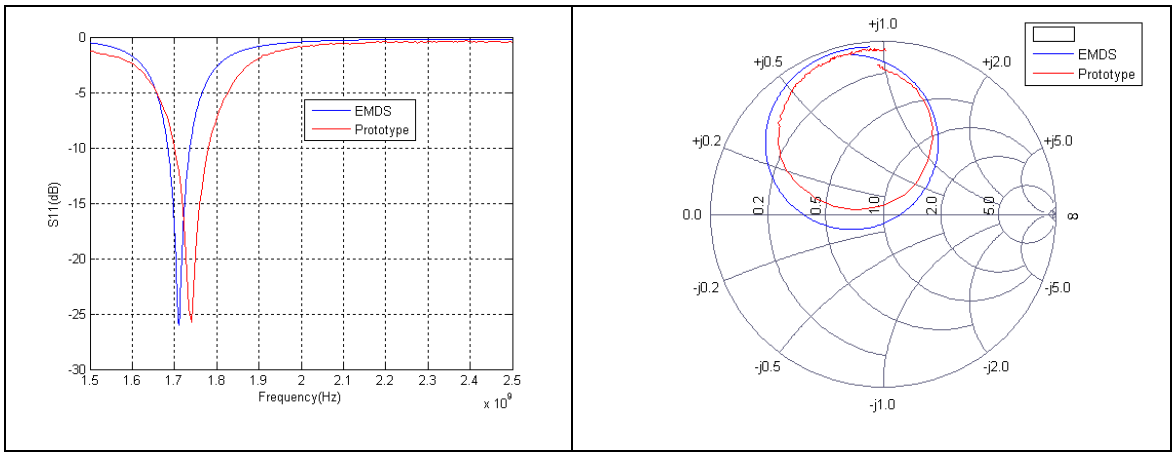

Figure 3-47: Case C.3. Reflection coefficient and Smith chart.

The real resonant frequency of the prototypes is higher than the resonant frequency predicted for the last two cases. The real reflection coefficient is also lower. In the third case, a strong influence in the shape of the smith chart of the prototype due to the presence of objects close to the prototype was observed. The cause was that, as the ground plane had almost the same size that the top patch, some of the radiated energy behind the ground plane was couple to the coaxial cable generating a reflected current. To correct this we had to put a balun around the coaxial cable just before the probe.

Regarding to the radiation pattern, we can see that the shape of the radiation pattern are almost the same for the simulation results and for the measurements. In the following pictures we can see that fact.

For these last cases, the difference between the radiation pattern that we obtained from the measure of the prototypes and the radiation pattern given by EMDS is more important. One of the reasons that explain this fact is the influence of the support. Although a non metallic support was chosen to hold up the antenna, it was observed that it influences a lot in the shape of the radiation pattern. That influence was stronger when the ground plane gets smaller. The shape of the radiation pattern depended on the relative position of the antenna respect with the support. In the next figure we can see this influence:

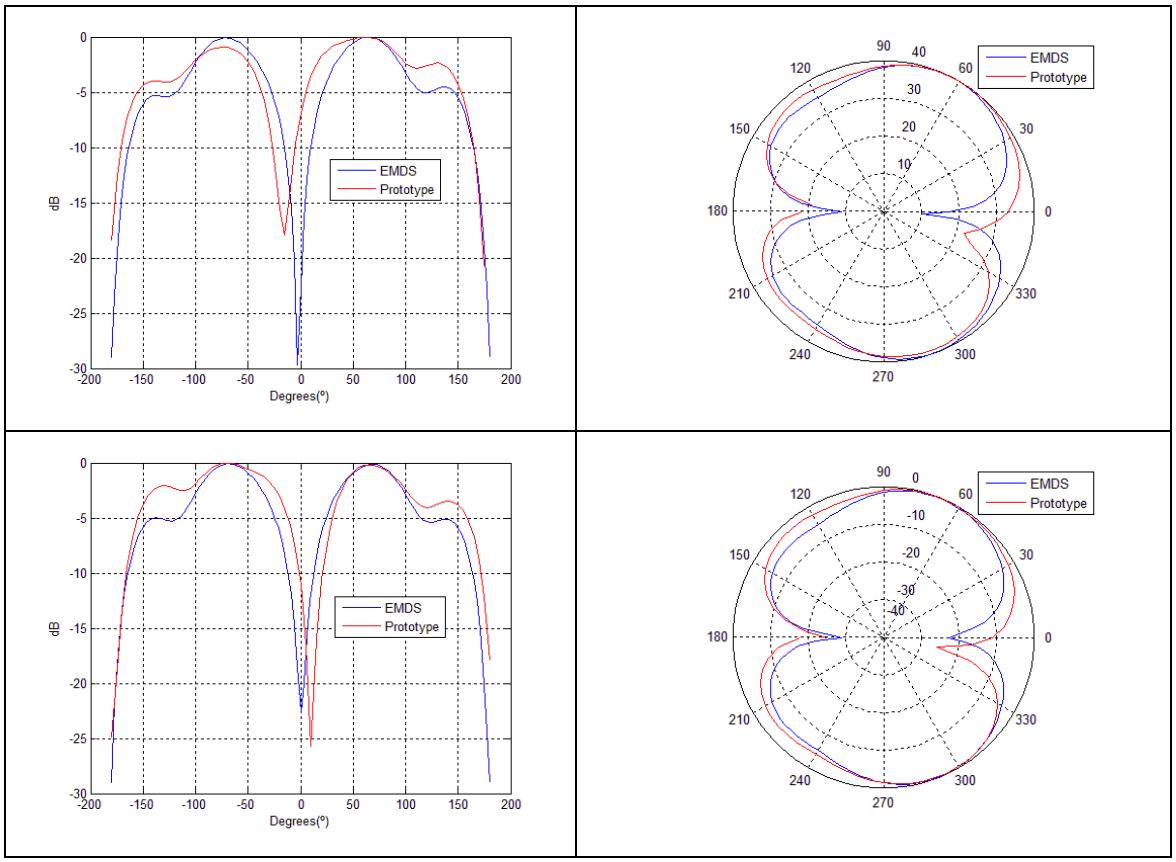

Figure 3-48: Case C.2.Normalized radiation pattern. Plane φ=0 (Up). Plane φ=90 (Down).

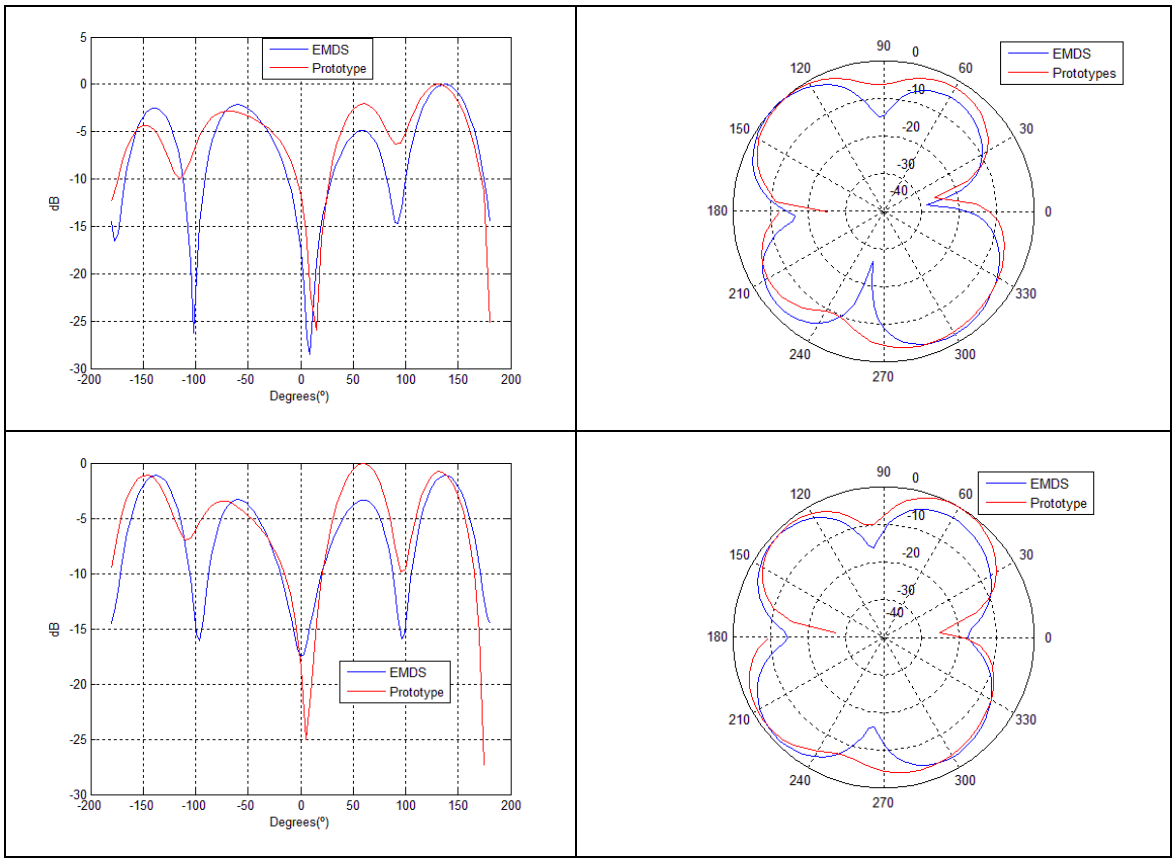

Figure 3-49: Case C.3.Normalized radiation pattern. Plane φ=0 (Up). Plane φ=90 (Down).

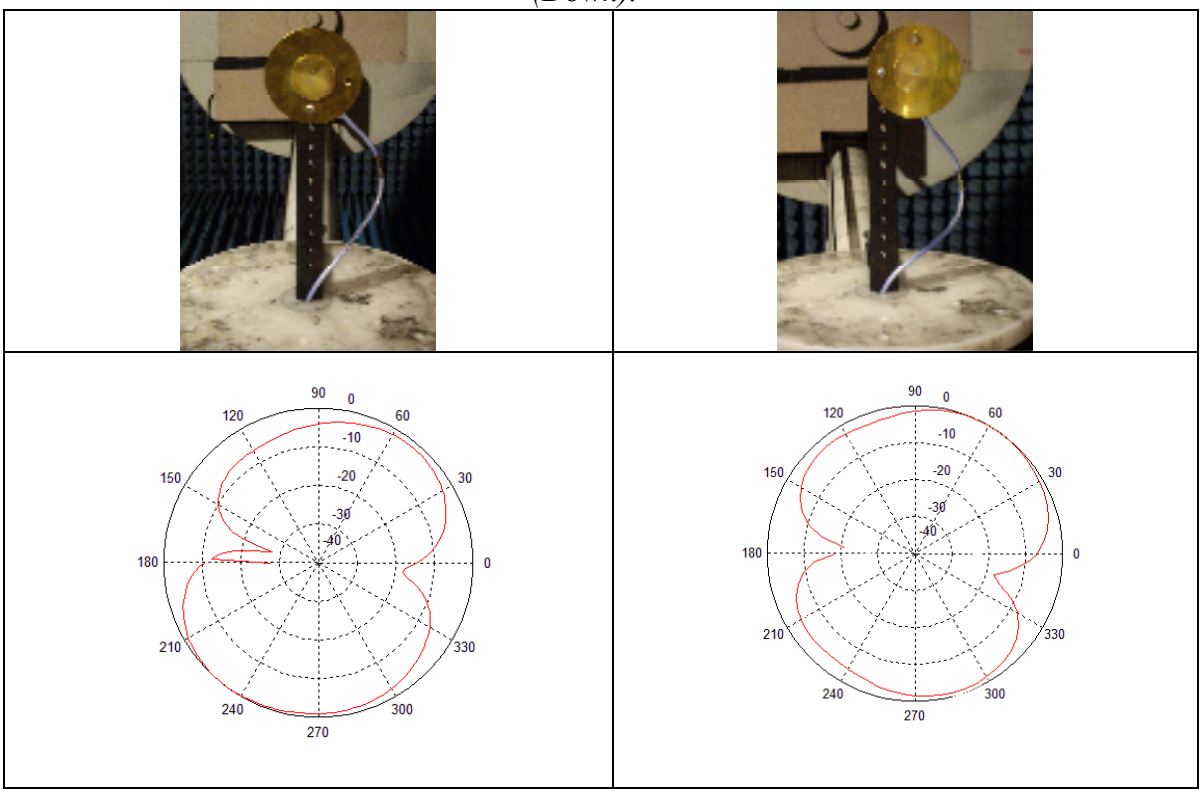

Figure 3-50: Case C.2: Influence of the support position. Radiation pattern for the φ=0 plane.

We can also observe a shift in the position of the zero in the zenith. This could be due to, in addition to the influence of the support, to an error in the calibration of the measure instruments. In spite of those differences, we can see that the radiation patterns of the prototypes are closer to the radiation patterns we obtain with EMDS, so we can discard the results we obtain with WIPL-D.

In the next table we summarize the differences between the prototypes and the EMDS results:

		Elevation Angle (º)[1]	**Gain (dB) [2]**	**Asymmetry (dB) [3]**	**Half power beam width (º) [4]**	**VSWR**	**BW (GHz) [5]**
EMDS	**Case C.1**	51	4.5	1	54	1.20	1.63-1.76 (8.15%)
	Case C.2	21.5	2.5	0	21.5	1.1	1.76-1.75 (2.79%)
	Case C.3	30	4.5	2	46.5	1.10	1.68-1.74 (3.1%)
Measurement	**Case C.1**	50	2.5	1	50	1.13	1.55-1.71 (10.18%)
	Case C.2	26	-1.5	1	104	1.21	1.72-1.78 (3.38%)
	Case C.3	25	- 1.5	3	62	1.11	1.7-1.78 (4.6%)

1) Average elevation angle above the horizontal plane in which take place a maximum in the radiation pattern
2) Maximum gain
3) Maximum asymmetry between maximums in the radiation pattern
4) Average half power beam width
5) Bandwidth where the S_{11} remains under 10 dB

For the case C.1, the properties of the prototype are quite similar to the results obtained from EMDS, but for the last two cases the difference is quite significant. For the measure of the gain of the prototypes, we have used a method called gain transfer method [13]. This method uses a standard gain antenna with a known gain. We calculate the gain of the antenna under test using the next equation:

$$G_t(dB) = G_s(dB) + \frac{P_t}{P_s}$$

Gt(dB) and Gs(dB) are the gains (in dB) of the test and the standard gain antenna. Pt is the received power when the test antenna is acting as the receiving antenna and Ps is the received power when the standard gain antenna is acting as the receiving antenna. The problem is that this method is not very accurate because it does not take into account a

possible mismatch both in the standard gain antenna and the test antenna. This is the reason why the measure gain and the gain given by the EMDS tool are so different.

3.3.4 Correction of the results of WIPL-D

So far, we have concluded that the results offered by WIPL-D were wrong, because the difference between the resonant frequency of the WIPL-D model and the real resonant frequency of the prototype was large enough. After we check that the WIPL-D results were wrong, we decided to investigate it further to figure out why the WIPL-D model had not worked.

After doing some test we discovered that when the number of increases the current expansion parameter (the order of the polynomial approximation of currents) [16], the WIPL-D results become more similar to the EMDS results and the results we got from the measure of the prototypes. So we concluded that we should increase the current expansion parameter in order to improve the accuracy of the WIPL-D model, and thus achieve a model reliable enough. The others advanced options of the simulation like the accuracy of the integrals used in the analysis or the precision do not affect barely the results

However, the WIPL-D results with the current expansion parameter set to the maximum are not accurate enough yet. Especially in the case C.3, where the radiation pattern which is obtained with WIPL-D, is quite different from the real radiation pattern of the prototype. These results are shown in the appendix B.

This happens because we are working with the Lite version of the software WIPL-D which is a limited, low cost version of WIPL-D Pro which performs analysis of projects up to 500 unknowns, so when we try to increase the value of the current expansion parameter over a specific value, we cannot do it because the numbers of unknowns is higher than the maximum number of unknowns allowed. It could be interesting in a future to repeat the simulations of the models with the version Pro of WIPL-D.

This limitation will be the main reason that will lead us to use only the EMDS software to design the stacked antenna for the CVIS project in the second part of this master thesis, discarding the use of the WIPL-D software.

It is important to note that the conclusions of the section 3.2.2 remain valid. The results of that section are not very accurate but the main conclusion we have done about the influence of the dimensions, the substrate and the feed position in the properties of the antenna are still met, when we increase the accuracy of the WIPL-D model.

4. Analysis and design of a stack disk antenna for a compact multi-band antenna solution (Part II).

4.1 Analytical Analysis

Following the same process than we applied for the design of a prototype for the band of 2GHz in the first part, we are going to start the design of the dual-frequency stacked antenna with an analytical analysis.

The schema of the whole geometry of the stacked disk antenna for a compact multi-band antenna solution is shown in the next figure:

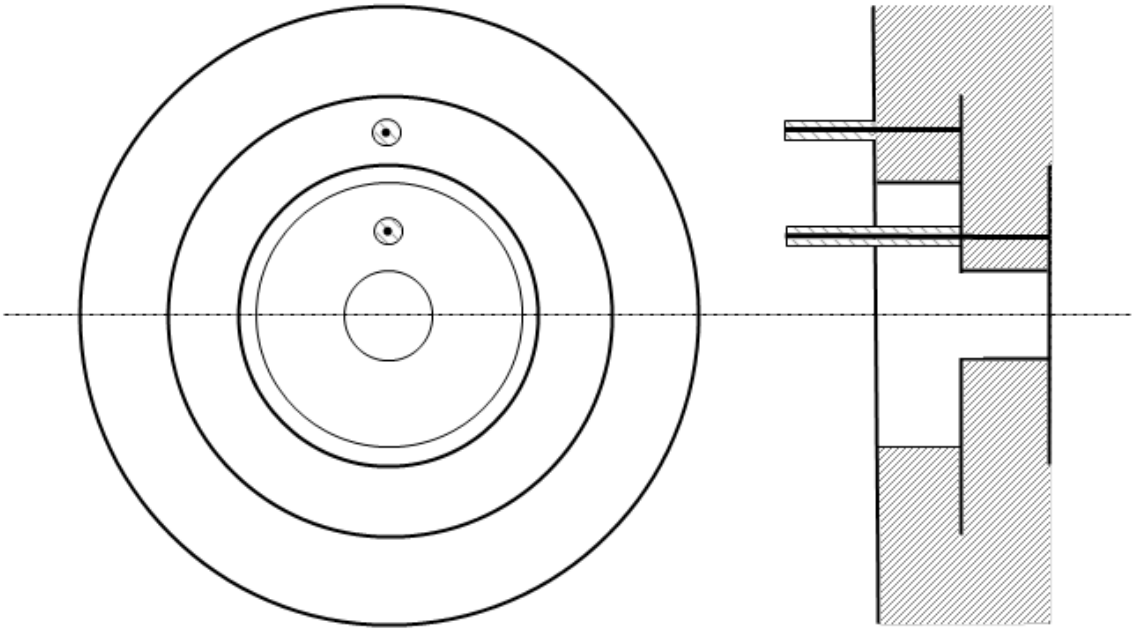

Figure 4-1: Geometry of the dual-frequency stacked antenna

The idea is stacking the antenna which operates in higher frequencies (5.75GHz - 5.95GHz) on the top of the antenna which operates in lower frequencies (2.4GHz – 2.484GHz) so the patch metallization of the second antenna, which will be larger than the patch metallization of the first antenna, acts like the ground plane of the first antenna. One of the ideas that arose while we were working on this geometry was to substitute the solid metallic post of the centre by a hollow metallic post so we could feed the upper antenna, with a coaxial feed which went inside this hollow metallic post.

This is shown in the previous figure and has the advantage, in theory, not affecting the radiation properties of the lower antenna.

In practice, the hollow metal post in the centre of the patch antenna is implemented by means of a set of short pins, which are arranged circularly and connect the patch metallization with the ground plane. This is shown in details in the next figure.

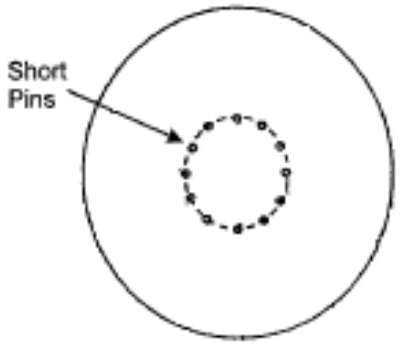

Figure 4-2: Practical implementation of the central post.

The development of a complete analytical analysis which represents the behavior of the entire antenna is not a trivial task. The couplings between the two single patch antennas are complex enough to discard the idea of work in an analytical model for the whole geometry. However, as a first approximation, it is logical to think that we can use the MATLAB program we developed in the section 3.1.5 for designing separately the two single antennas, which form the dual-frequency stacked antenna.

This approach is the one which we are going to use in this section. We are going to design the two patch antennas as if they does not influence each other, and afterward, in the next section, we are going to tackle the problem of the coupling between the two patch antennas with the help of simulation tools.

For the designing of the 2GHz prototype in the first part of this master thesis, we took some previous decisions about the substrate of the antenna (specifically about its permittivity and its height). We based these decisions on practical criteria before using the MATLAB program. Then we are going to review those decisions to adapt them to this new situation:

- *Electrical permittivity*: The main reason that leads to use air as the dielectric between the patch metallization and the ground plane was that this decision leads to a cheaper design and that we could construct the prototypes in a short period of time without the need of a very accurate fabrication process. In this second part, we are not going to construct a prototype. We are going only to design the antenna, so for this part we want to evaluate the possibility of using other different dielectrics than the air. We saw in the analytical design of the section 3.1.4 that we could obtain a radiation pattern with a low elevation angle when you used substrates with a high permittivity. But in the other hand, we saw that the properties of the antenna regarding with its bandwidth and its radiation efficiency get worse when the permittivity of the antenna substrate increase. So

finally, we decided to use duroid with a relative permittivity of 2.33 [19], which is a typical substrate for patch antennas and, as we will see later, it allow reach a compromise between the elevation angle of the radiation pattern and the bandwidth of the antenna.

- *Height*: In the first part we chose a thick enough substrate to avoid that some movements of the plane of the patch metallization due to the impact of the air on the antenna structure when the car is moving, could affect too much the value of the resonant frequency. But in this case, we are going to use a substrate different from air, so the space between the patch metallization and the ground plane is filled with a dielectric which avoids the movements of the plane of the patch metallization by itself. This fact allows us to choose any height for the substrate. As we saw, the height was an important parameter for the bandwidth. Thick substrates lead to broadband antennas. So we will have to select a substrate thick enough to fulfill the bandwidth requirements of the antennas. We are going to start the design with a height of 1.575 mm in the MATLAB program. This is a typical thickness for duroid substrates. In the next section we will have to modify this value to fulfill the bandwidth requirements. However, as we saw in the section 3.1.4, the value of the height barely affects the value of the resonant frequency, so we will still be able to use the results of this section as an approximation.

For the antenna which works in the band of 2.4 GHz -2.484 GHz, we used the MATLAB program of section 3.1.5. We have chosen as input the central frequency of its range of operation (2.442 GHz). The relationships of the inner ('b') and the outer ('a') radiuses that lead to this resonant frequency are shown in the following figure:

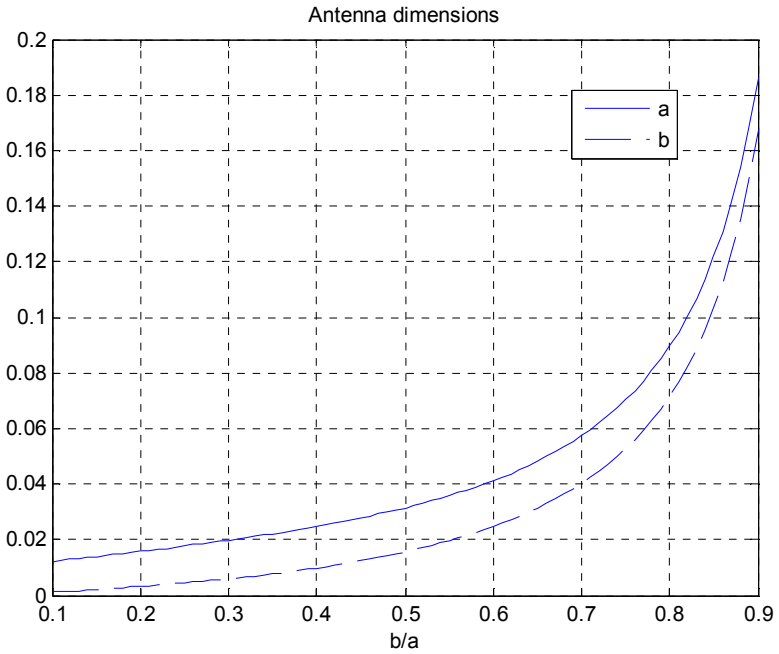

Figure 4-3: Analytical design of the upper antenna (height=1.575 mm, εr=2.33, μr=1).

Regarding with the upper antenna, we used the MATLAB program of section 3.1.5, introducing as input the central frequency of its range of operation (5.85 GHz). The

relationships of the inner ('b') and the outer ('a') radiuses that lead to this resonant frequency are shown in the following figure:

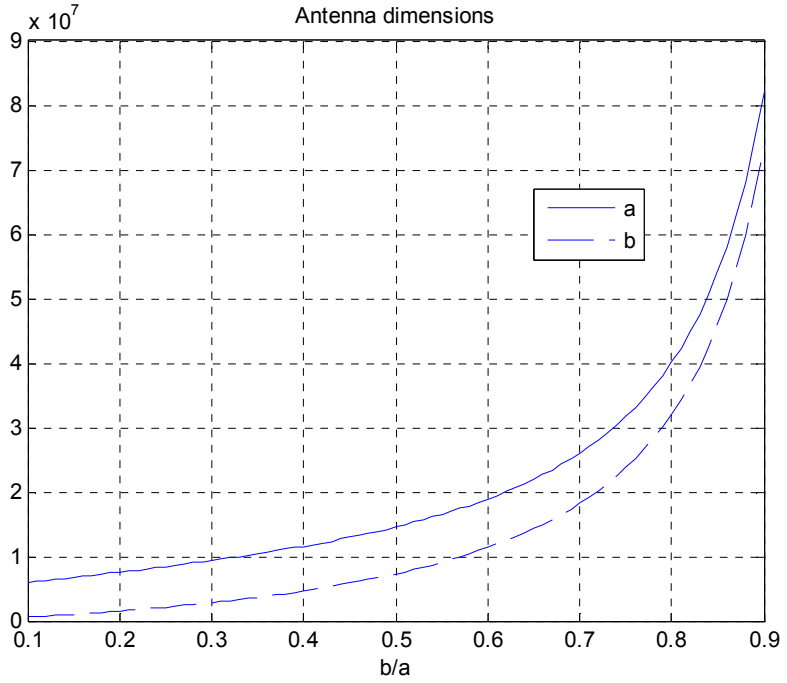

Figure 4-4: Analytical design of the lower antenna (height=1.575 mm, εr=2.33, μr=1).

In the next section we are going to select a specific value for the outer and the inner radius taking into account the analytical design of the two single antennas and the characteristics of the whole geometry. For doing that, we are going to use simulation tools.

4.2 Simulation tools

4.2.1 Introduction

Now, we are going to use only EMDS to simulate the stacked antenna. The main reasons for doing this instead of using WIPL-D first, as we did in the first part of this project, are the followings:

- Accuracy: The results of the WIPL-D software are not accurate enough as we could check through its use for the design of the 2 GHz prototype in the first part.
- Speed: The geometry of the antenna in this part is more complex that the geometry of the antenna of the first part. This makes that the simulations with WIPL-D take more time. In this particular case, the time spent in a WIPL-D simulation, gets quite close to the time spent in an EMDS simulation. So, WIPL-D loses its speed advantage.

So in the next section we are going to modeling and simulate the antenna using EMDS for discussing the results later.

4.2.2 Original stacked antenna

In this section we are going to simulate the geometry of the stacked antenna, which was shown in the section 4.1. We are going to deal this problem in the same way that we did in the analytical design of the section 4.1. First, we are going to design separately the two patch antennas and afterward, we are going to simulate the whole structure.

4.2.2.1 Single patch antenna for 2.4GHz-2.484GHz

Inside the possible values which were supplied by MATLAB program for the patch antenna with a resonant frequency of 2.442GHz, we need to choose a specific value for the inner and the outer radiuses. For doing this choice, we have to observe and analyze again the geometry of the stacked antenna.

In the first part of this master thesis we discovered than the resonant entrance impedance depended on the position of the feed point, so we can match the antenna choosing a suitable position for the feed. So, if we can vary the position of the feed in a wide range, then is easier to get a perfect matching for the antenna.

Coming back to the previous section, we observe the geometry of the stacked antenna and we can see that the possible values of the feed position for the upper antenna are:

- Between the inner radius of the upper antenna and the inner radius of the lower antenna, in the case that the outer radius of the upper antenna was larger than the inner radius of the lower antenna.
- Between the inner radius of the upper antenna and the outer radius of the upper antenna, in the case that the outer radius of the upper antenna was smaller than the inner radius of the lower antenna.

So we are interested in choosing a large inner radius for the lower antenna in order to facilitate the matching of the upper antenna.

The problem appears, when we tried to increase the inner radius of the antenna, because the radiation pattern became more asymmetric, as we can see in the next figure.

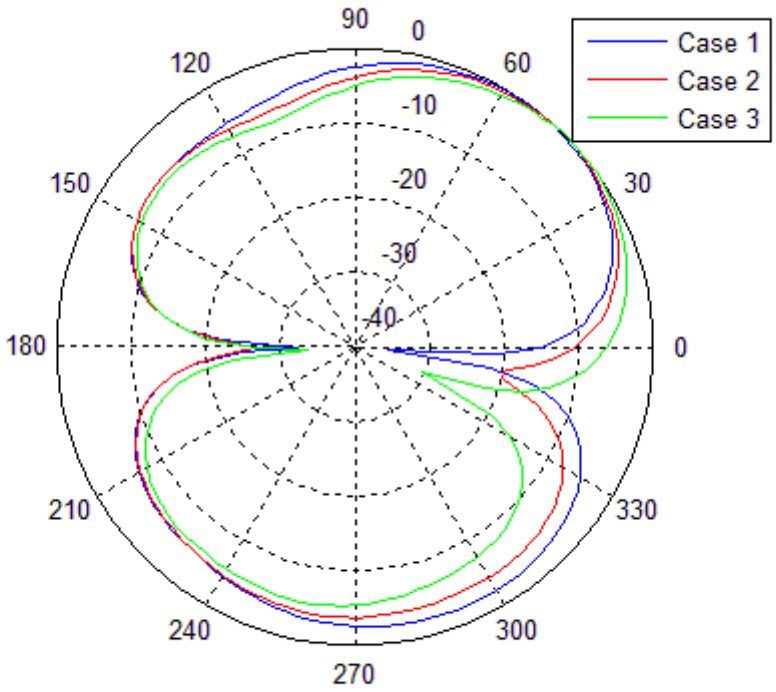

Figure 4-5: Cases 1, 2 and 3: Radiation pattern for the plane φ=0.

The characteristics of the three cases simulated are shown in the next table:

Case	**Feed position**	**Inner radius**	**Outer radius**	**Dielectric radius**	**Ground plane radius**
1	8.4	5	15.7	50	100
2	17.5	8	19.6	50	100
3	21	10	22.3	50	100

Up to now, the radius of the ground plane had been chosen following the indications of [1]. According to those indications, we selected a radius for the ground plane twice larger than the outer radius. Thus, the diffraction effect due to the finite dimensions of the ground plane is negligible. From now, we are going to differentiate between the dielectric radius (approximately twice larger than the outer radius), and the ground plane which is still larger for modeling better our antenna, given that it is going to be placed on the roof of a car.

The resonant frequency for all of those antennas is 2.442 GHz and the position of the feed was chosen to get a good matching for each. If we look at the figure and the table again, we can see the following appreciations:

- The radiation pattern becomes more asymmetric when the inner radius increases.
- The matching of the antenna becomes more difficult when the inner radius increases. If we wanted to design an antenna with an inner radius larger than the case 3, we could not get a good matching, as we can deduce when we observe the evolution of the feed position for the three cases.

The second problem appears because the antenna had a very narrow band so it was no appropriate for our application. In order to meet the width band requirements, we had to replace the original substrate with a new one with a thickness of 4.75 mm. Since manufacturers do not offer substrates with that thickness; we decided stacking two substrates of 1.575 mm and 3.175 mm [19].

Finally, we decided to choose an inner radius for the lower antenna of 5 mm which was the maximum radius we could choose without a big deterioration of the symmetry of the radiation pattern of the patch antenna, and a duroid substrate of 4.75 mm. In the next figures we can see the properties of the final design of the antenna:

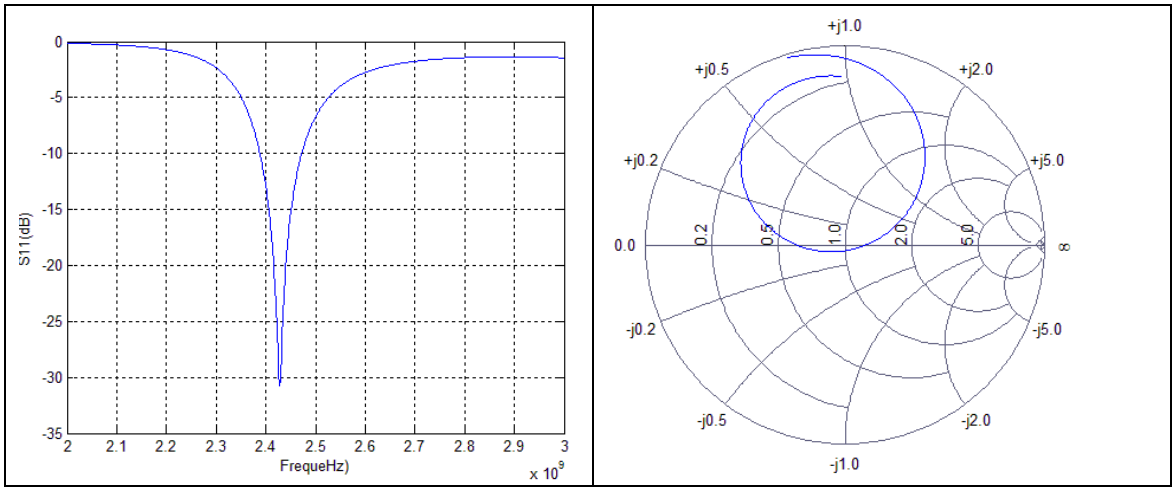

Figure 4-6: Case 1. Parameter S_{11} and Smith Chart.

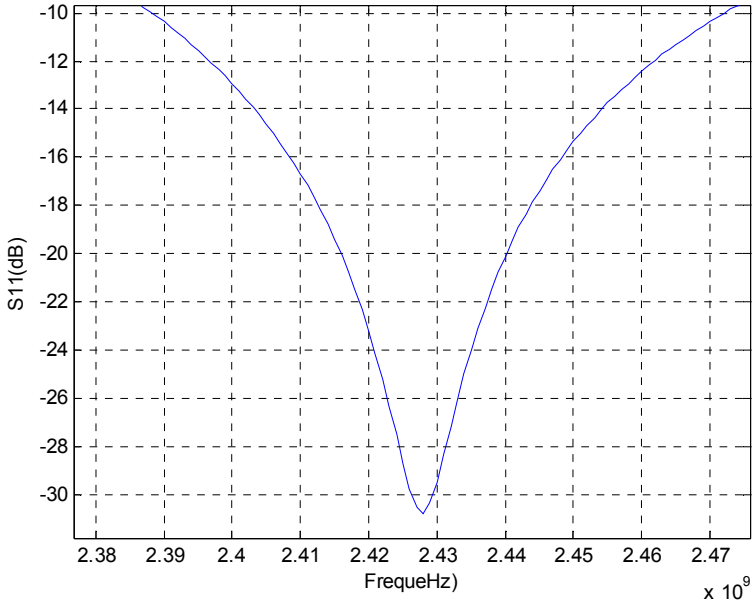

Figure 4-7: Case 1.Bandwidth.

We can see in the final figure how the S_{11} parameter remains under 10 dB in the band of interest, which is enough for fulfilling the bandwidth requirements for this antenna. Finally, the radiation pattern is almost the same that was presented by the antenna with a substrate of 1.575 mm. In the next figure we can see the radiation pattern.

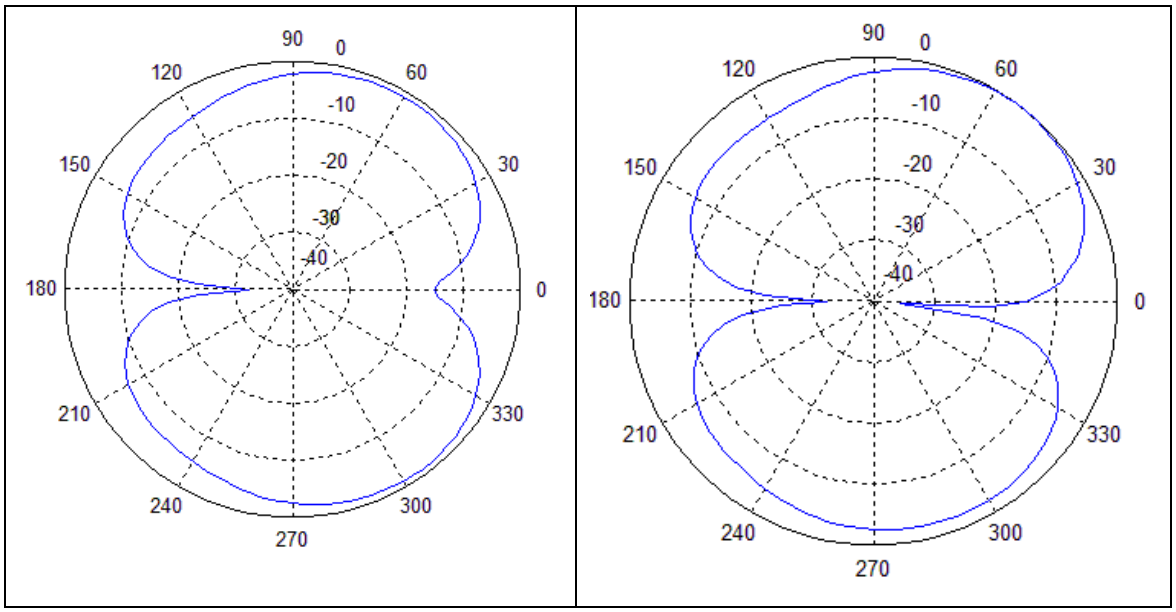

Figure 4-8: Case 1: Normalized radiation pattern. Plane φ=0 (Right). Plane φ=90 (Left).

4.2.2.2 Single patch antenna for 5.75GHz-5.95GHz

For this antenna, we are interested in a small value for the inner radius and a big value for the outer radius. Specifically, we are looking for an outer radius of the same size of about the inner radius of the lower antenna.

Finally, we chose an inner radius of 0.5 mm. For this value of the inner radius and considering the dimension of the coaxial feed, the closest position to the centre where we can put the feed point is about 2.60 mm. Then the minimum outer radius for this antenna is about 3.30 mm. The value of the resonant frequency for this antenna is 3.3GHz, so we would need a smaller outer radius to get a resonant frequency of 5.85 GHz. This is no possible given the dimensions of the antenna.

This supposed a quite hard limitation that has not been predicted previously, and involves the need of do some modifications over the original design in order to develop a feasible antenna design for the multi-channel terminal for the CVIS project. These modifications over the original design are presented in the following sections.

4.2.3 Stacked antenna with 2 coaxial feed points

The first modification made on the original stacked antenna was to add a second feed point in front symmetrically placed with respect to the central metallic post. The idea was to get a more symmetric radiation pattern and therefore, be able use a larger inner radius for the lower antenna which allows us more possibilities to match the upper antenna. In the following figure we can see this new model:

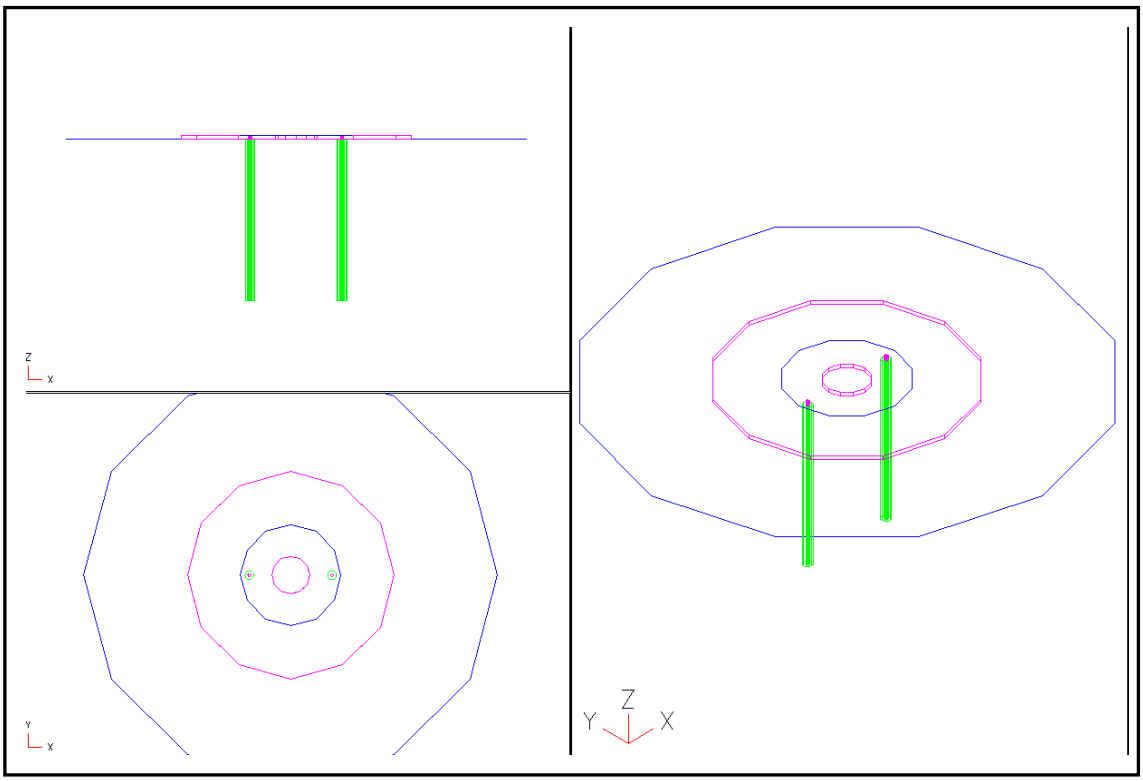

Figure 4-9: EMDS model of a single patch antenna with 2 feeds

In addition, this new model with two feeds had other especial advantages which were very interesting. Here are shown the advantages of this model with respect to the original one:

- *Wider bandwidth*: It was noticed a quite important increase of the bandwidth of the antennas with respect to the original model with one feed. This allowed selecting a thinner substrate to reduce the dimension of the stacked antenna. This is important because the ultimate aim of this project is studying the viability of use this design for its use in the future in the CVIS project. The multi-channel terminal which is needed for the CVIS project should work with a high number of frequency bands. Then it would be needed stacking a lot of single patch antennas instead of only two. So a reduction of the height of each single patch antenna is very important to reduce the dimension of the multi-channel terminal.
- Radiation pattern: As we said just before, the radiation pattern becomes much more symmetric.

However, this new model presents some disadvantages over the original one:

- *Economical cost*: The production of this antenna would be more expensive than the original one because of the introduction of a more complex feed schema with two feeds.
- *Complexity*: The design of an antenna for a given resonant frequency is more difficult when we work with two feeds. The results of the simulations are quite far from the results obtained from the analytical design, so we cannot use the analytical model to obtain an approximation of the dimensions of the patch antenna for a particular resonant frequency. In addition, the process of matching the antenna becomes slightly more difficult.

4.2.3.1 Single patch antenna for 2.4GHz-2.484GHz

Taking the dimensions of the patch with one feed as the starting point, we had to modify the outer radius of the patch to get a resonance frequency of 2.442 GHz. In addition, as we explained before, we discovered a quite significant increment of the bandwidth of the patch antenna when we incorporated the second feed, so we studied the possibility of reducing the height of the substrate without leaving to fulfil the bandwidth requirements. Finally, we chose a duroid substrate with a height of 1.575 mm, which was the thinner one, among the offer of the manufactures which allows the fulfilling of the requirements.

The choice of a new height for the substrate, combined with the fact that we incorporated the second feed point, caused that we had to modify the position of the feed point for matching the patch antenna. In the next table we can see the final dimensions of the lower single patch antenna:

Feed position	**Inner radius**	**Outer radius**	**Dielectric radius**	**Ground plane radius**
20	9.1	24.3	50	100

In the following figures we can see the properties of this patch antenna:

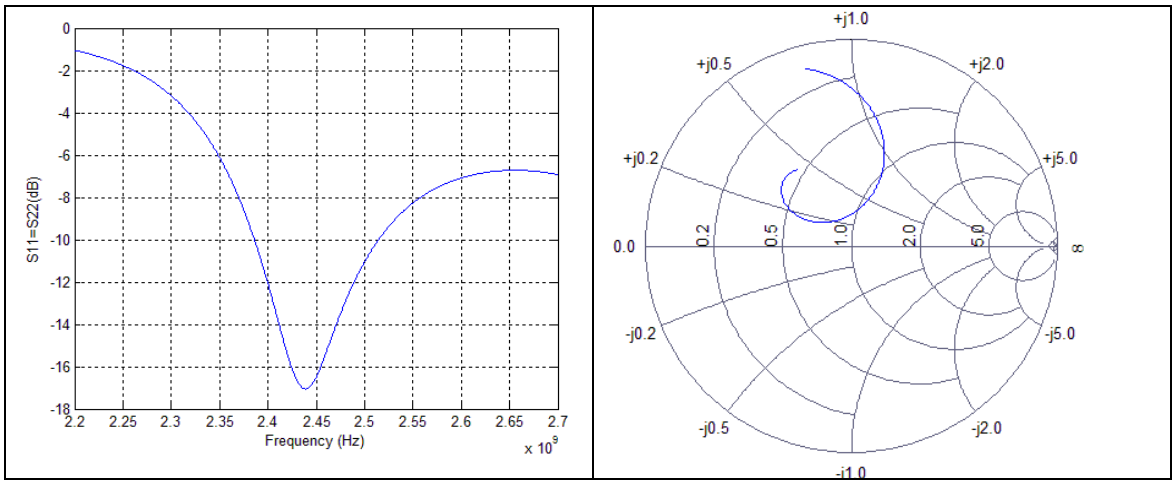

Figure 4-10: Lower antenna with 2 feeds. Parameter S_{11} and S_{22} (Left). Smith chart (Right).

We can see how the bandwidth is slight wider, even when we have reduced the height of the substrate until 1.575mm. In the Smith chart we can see that the antenna present a quite acceptable matching. In addition, if we see the Smith chart for a wider range of frequencies, we can see some differences with the original model.

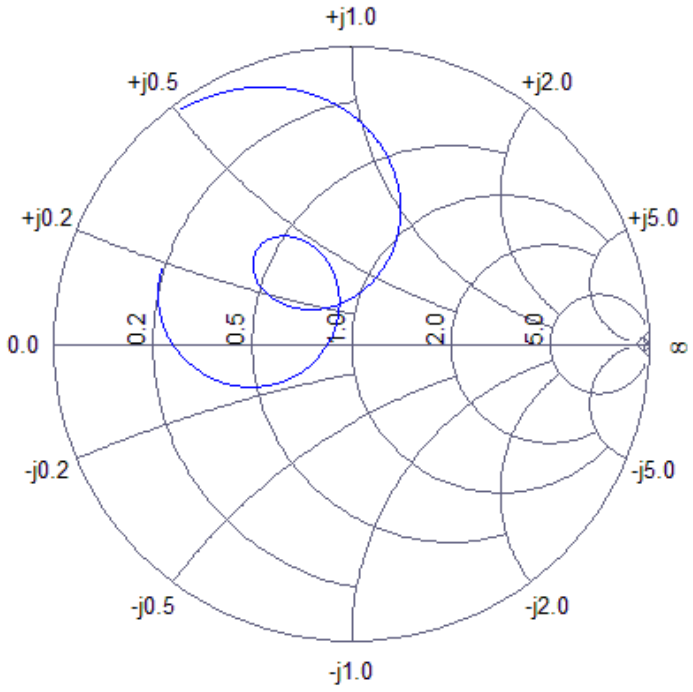

Figure 4-11: Lower antenna with 2 feeds. Smith chart.

In the previous figure, we can see how the plot of the entrance impedance in the Smith chart presents a loop much smaller than the original antenna with one feed. Thus, the curve remains quite close to the centre of the Smith chart for a wider band. Specifically, we can see two points where the reflection coefficient presents a local minimum. Although this antenna is not perfectly matched, we can see it fulfils the requirements in

the band of interest. So, although the matching of the antenna at the resonant frequency is worse than in the case of the patch antenna with only one feed, due to a major complexity that make more difficult the antenna matching, the bandwidth of the antenna increases a lot and the S_{11} parameter remains below 10 dB in the band of interest, which was the initial requirement.

Regarding to the radiation pattern, we can see that it is perfectly symmetric in each φ plane due to the presence of the two feed. The asymmetry between the plane φ and the plane φ is almost negligible. The main reason of choosing an inner radius of 9.1 mm is that it was the larger radius we could use without a distortion in the shape of the radiation pattern. If we use a larger inner radius, the null in the zenith of the radiation pattern disappears, which is no desirable. In the following figure we can see the final radiation pattern:

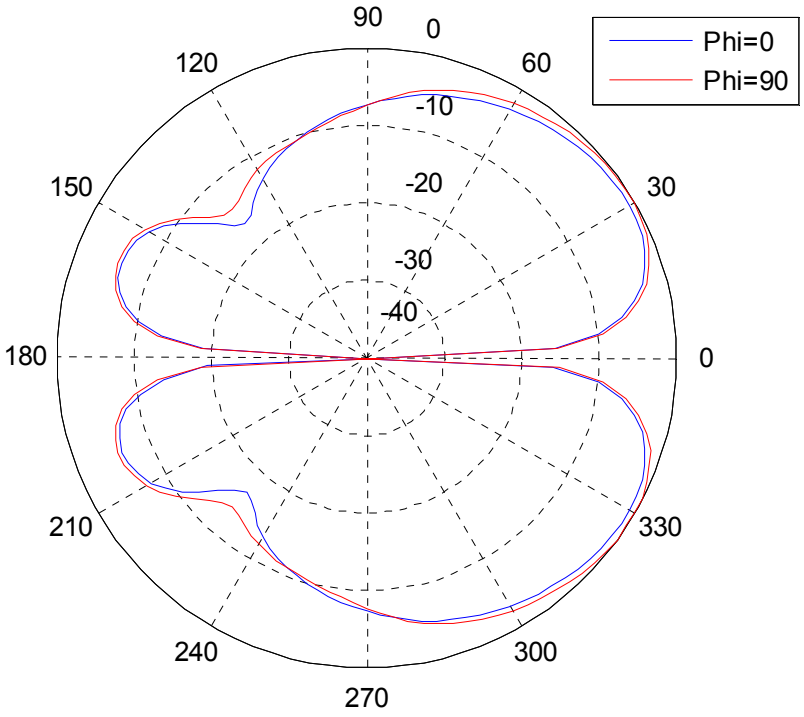

Figure 4-12: Lower antenna. Normalized radiation pattern. Plane φ=0 and φ=90.

Finally, in the following table we can see the summary of the most important properties of this antenna:

Elevation Angle (º)[1]	Gain (dB) [2]	Asymmetry (dB) [3]	Half power beam width (º) [4]	VSWR	BW (GHz) [5]
57	2	1	52	1.33	2.39-2.51 (5.22%)

1) Average elevation angle above the horizontal plane in which take place a maximum in the radiation pattern
2) Maximum gain
3) Maximum asymmetry between maximums in the radiation pattern
4) Average half power beam width
5) Bandwidth where the S_{11} remains under 10 dB

One of the disadvantages of this patch antenna is that the elevation angle is higher than elevation angle of the patch antenna with one feed, but it is still quite acceptable.

4.2.3.2 Single patch antenna for 5.75GHz-5.95GHz

As we did previously in the original design, we are going to choose an outer radius approximately equal to the inner radius of the lower antenna in order to maximize the range of positions where we can put the feed. The difference with respect to the original design is that now we have a larger inner radius in the lower antenna, so it is possible to get a quite good matching upper antenna.

As in the lower antenna, we observed that the incorporation of the second feed produced an increment in the bandwidth of the antenna, so we could reduce the height of the substrate until 1.575 mm. The ground plane of this upper antenna is going to be the patch metallization of the lower antenna. The radius of the dielectric is the same than in the lower antenna. The final dimensions of the upper antenna are specified in the following table:

Feed position	Inner radius	Outer radius	Dielectric radius	Ground plane radius
7.3	3	8.7	50	24.3

In the following figure we can see the behavior of this single patch antenna inside the band of frequencies where we are interested:

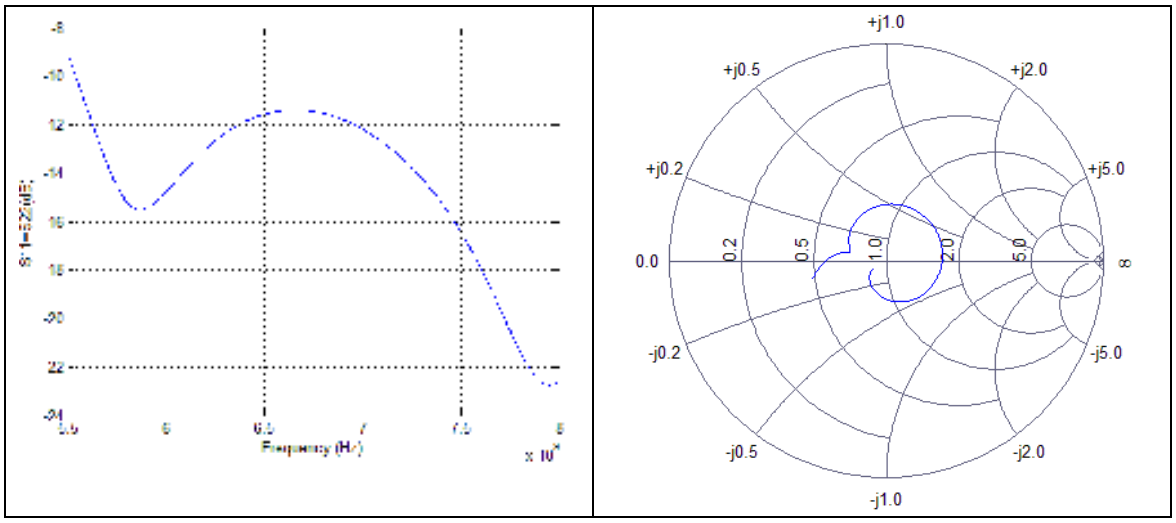

Figure 4-13: Upper antenna with 2 feeds. Parameter S_{11} and S_{22} (Left). Smith chart (Right).

In this case, the influence of the second feed in the bandwidth of the antenna is even stronger. We can see that the size of the loop in the Smith chart is very small and how the curve remains close to the central point surrounding it over a wide range of frequencies.

Although the S_{11} parameter stays under -10 dB in the whole range of frequencies where we have done the simulation, we are interested in the range between the starting of the curve and the local maximum, because after this last frequency the mode changes (a mode different from TM_{01} appears), and therefore the shape of the radiation pattern.

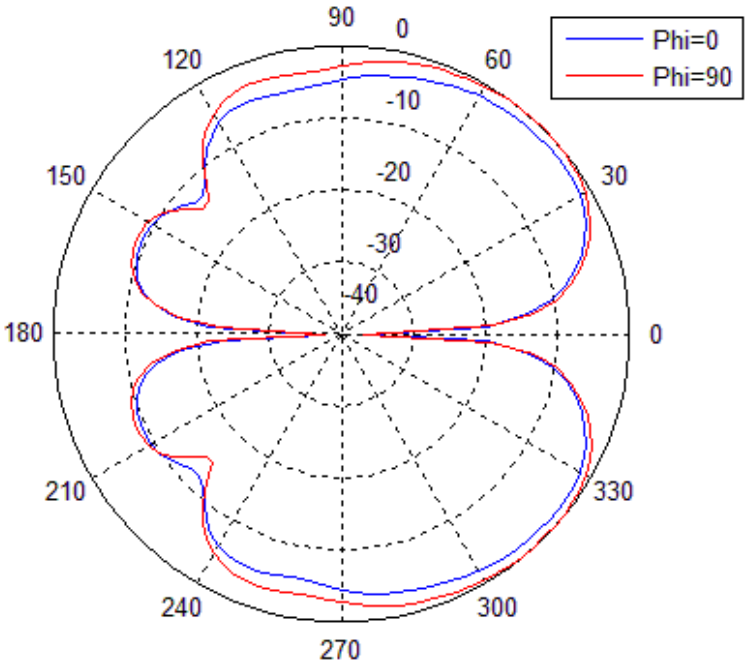

Figure 4-14: Lower antenna. Normalized radiation pattern. Plane φ=0 and φ=90.

The previous figure shows the final radiation pattern for the upper antenna. As we saw in the lower antenna, we can see that it is perfectly symmetric in each φ plane due to the presence of the two feed. The asymmetry between the plane φ and the plane φ is almost negligible. We can see that in this case, the elevation angle is even lower than in the case of the lower antenna.

We can see that the radiation pattern for this antenna also fulfils the requirements. The following table shows the most important properties for this single patch antenna:

Elevation Angle (º)[1]	**Gain (dB)[2]**	**Asymmetry (dB)[3]**	**Half power beam width (º)[4]**	**VSWR**	**BW (GHz)[5]**
44	2	1	72	1.40	5.54-6.65 (35%)

1) Average elevation angle above the horizontal plane in which take place a maximum in the radiation pattern
2) Maximum gain
3) Maximum asymmetry between maximums in the radiation pattern
4) Average half power beam width
5) Bandwidth where the S_{11} remains under 10 dB

In this case, the elevation angle is lower than in the lower antenna and the improvement of the bandwidth is much bigger. The matching of the antenna is worse than in the lower antenna because the limitations imposed by the geometry of the antenna are stricter and it makes more difficult to get a perfect matching.

4.2.3.2 Final design of the stacked antenna

Once we have designed separately the two single patch antennas with the 2 feeds, we are ready to tackle the global design of the stacked antenna for covering both bands of frequencies (2.4GHz-2.484GHz-5.75GHz-5.95GHz).

In this section we are going to analyze the differences between the behaviour of the patch antennas when they are stacked and when they are separated

We can see how the upper antenna is feeding by two coaxial feeds inside the central post of the lower antenna to avoid the influence in its radiation pattern, which was one of the design requirements.

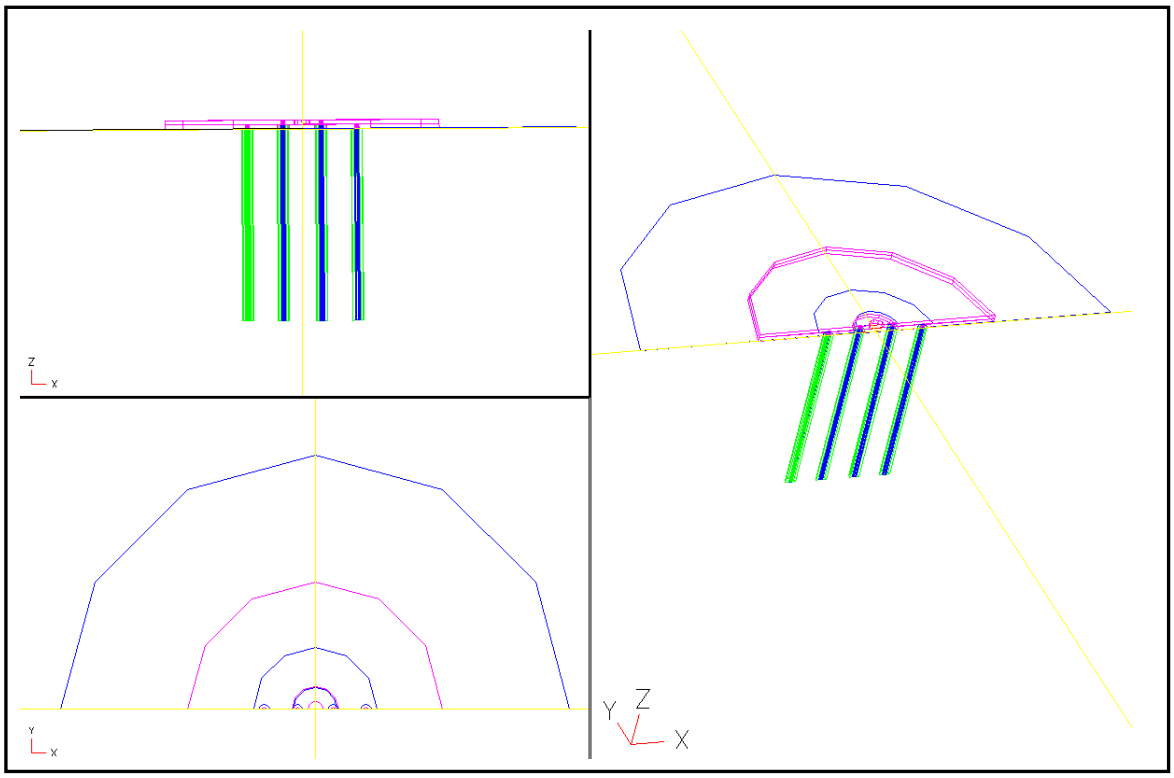

Figure 4-15: EMDS of the stacked antenna with 2 feeds.

As we said previously, we had to modify slightly the dimension of the patch antennas because when we put it together the resonant frequency and the entrance impedance, slightly change. So, we maintain the same height for the patch antennas and the inner radius, but we varied the size of the outer radius. The following table shows the dimensions of the patches that form the stacked antenna:

	Feed position	**Inner radius**	**Outer radius**	**Dielectric radius**	**Ground plane radius**
Lower antenna	20	9.1	24.3	50	100
Upper antenna	7	3	8.9	50	24.3

The simulation of this structure with EMDS gives results slightly different from the results we obtained when we modeled the patch antennas separately. One of the goals of this section is to analyze the differences between the behavior of the two antennas when they are separated and its behavior when they are stack.

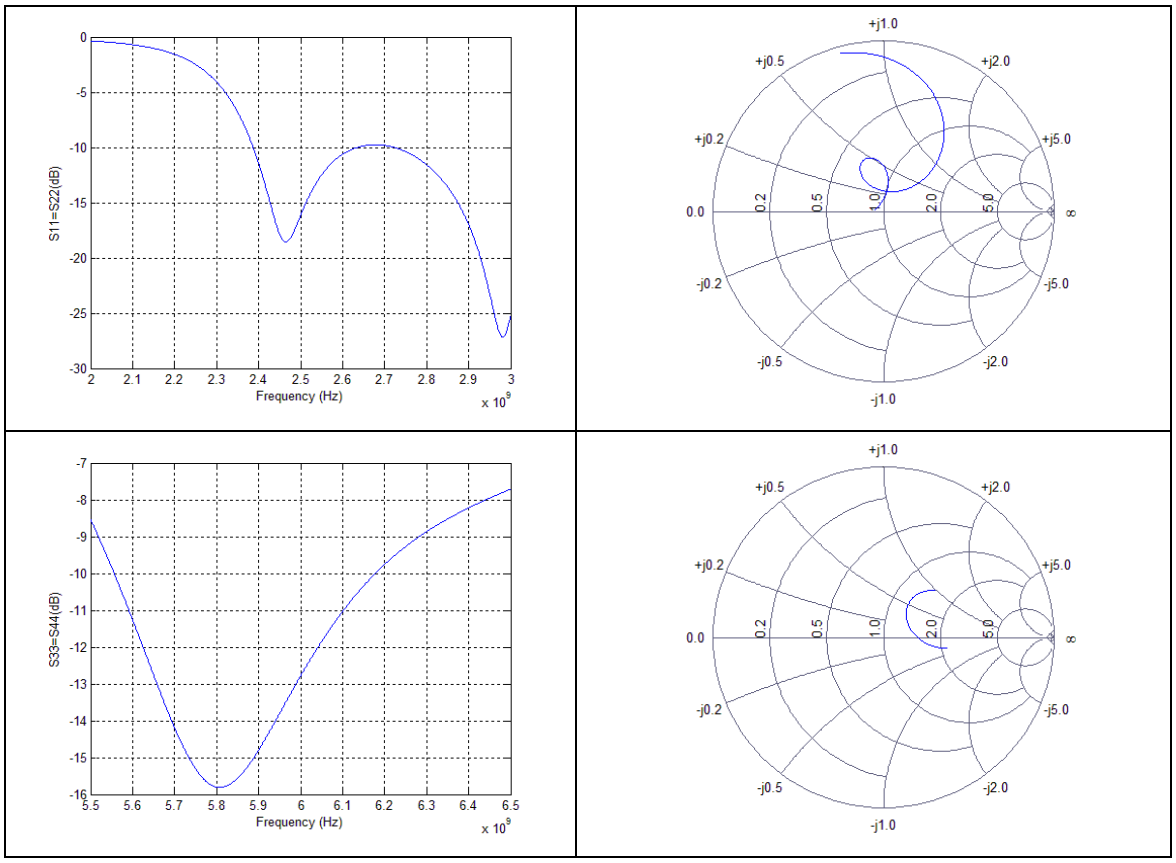

Figure 4-16: Stacked antenna. S-Parameters in the band of 2.442 GHz (Up) and 5.85 GHz (Down).

In the previous figure we can see the behavior of the stacked antenna in the two bands of frequencies. We can see how the behavior of the stacked antenna in the two bands of interest fulfils the requirements (S_{11} < 10 dB). In the lower band, we can see that the smith chart is quite similar to the Smith chart of the lower antenna when it was simulated separately. However, in the higher band we can observe that the Smith chart we obtain change a lot compare to the Smith chart of the upper antenna obtained in the previous section. So the influence of the lower antenna in the upper antenna is stronger than the influence of the upper antenna in the lower antenna.

If we look at the following figures where we can see the radiation pattern of the stacked antenna in the bands of interest, we observe the same fact.

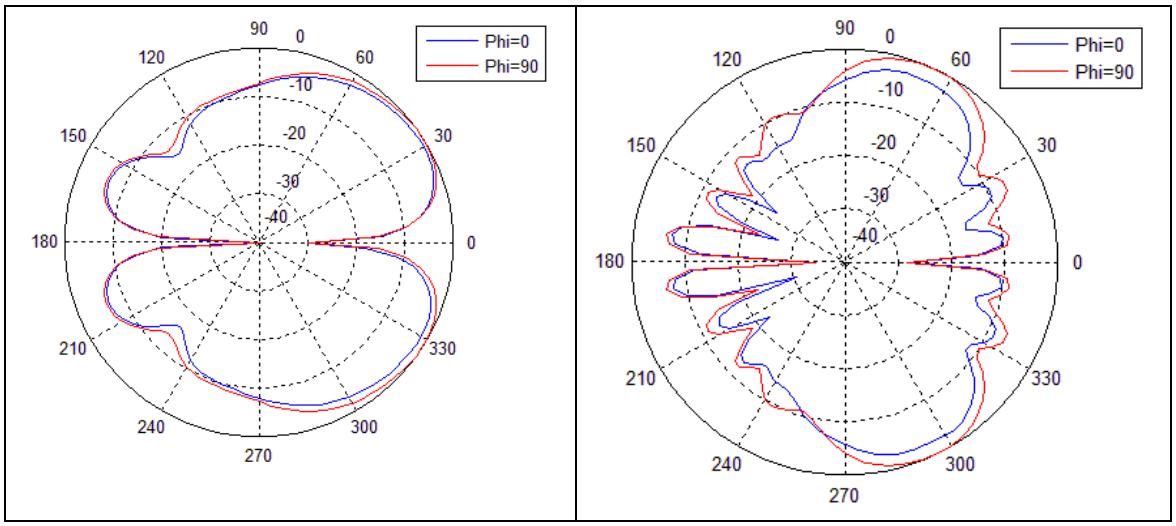

Figure 4-17: Stacked antenna. Radiation pattern in the band of 2.442 GHz (Left) and 5.85 GHz (Right).

The radiation pattern of the stacked antenna in the band of 2.442 GHz is quite close to the radiation pattern we obtained for the upper patch antenna in the previous section. So, we can conclude that the influence of the upper antenna in the lower patch antenna is weak. The problem arises when we deal with the upper antenna. We can see that the radiation pattern has changed. The stacked antenna still has a conical radiation pattern with a null at the zenith direction, but in this case, the radiation pattern presents an important ripple. This is because the ground plane of the upper patch antenna is formed by the patch of the lower antenna and the ground plane, so the complexity of the fields inside this structure is bigger than in the lower patch antenna.

Once we obtained this result for the upper antenna, some other tests were performed in order to determine the cause of the ripple. We tried to modify first the outer radius of the patch antenna but the effect over the ripple was not significant. Afterward, we modified the size of the ground plane of the lower antenna and it was found that the modification of the size of the ground plane of the lower antenna had a strong influence over the radiation pattern of the upper antenna. We decided to construct a new EMDS model with the supposition of an infinite ground plane which is a more real condition if we consider that the stacked antenna is going to be placed on the roof of a car, which is much larger than the dimensions of the antenna.

The radiation pattern we got from the simulation of this new EMDS model is shown in the following figure.

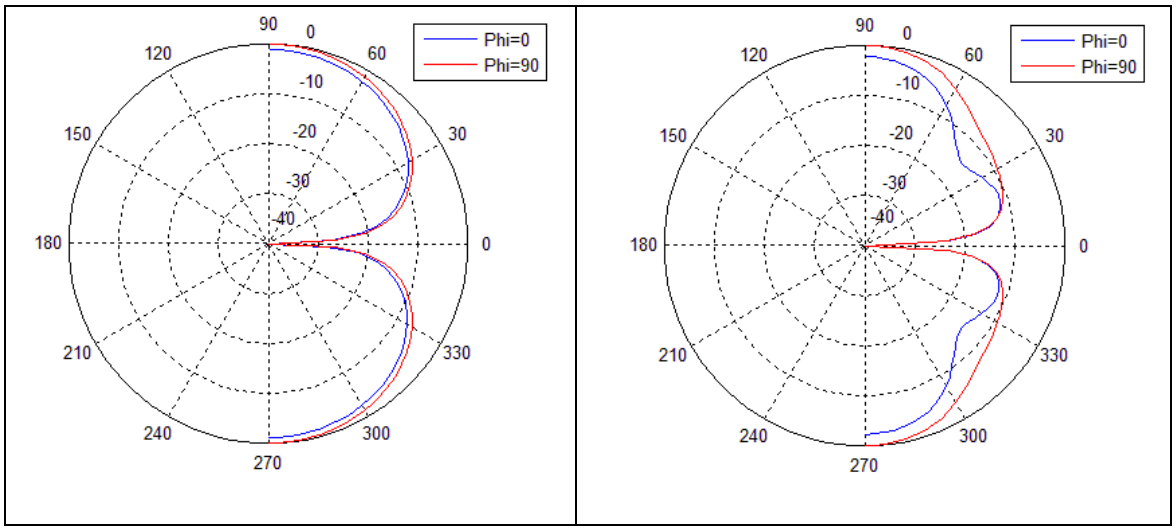

Figure 4-18: Stacked antenna (Infinite ground plane). Radiation pattern in the band of 2.442 GHz (Left) and 5.85 GHz (Right).

The radiation pattern for the antenna in the band of 2.442 GHz fulfils the requirements. It is a conical radiation pattern with a null at the zenith direction. In addition, the maximum radiation direction is ϑ=90º (elevation angle of 0º), which is very interesting for the application of our antenna. The elevation angle of the upper antenna is also 0, but in this case, the shape of the radiation pattern in the plane φ=0 is slightly different from the expected radiation pattern (it presents a local minimum for ϑ=45º). However, the differences between the expected radiation pattern and the radiation pattern obtained, do not involve a serious problem since the difference is not very significant. In addition the radiation pattern starts to be different for an elevation angle larger than 30º, so it can be discard given that for this kind of system the most transmissions occurs in low elevation angles.

The bandwidth and the reflection coefficient for the stacked antenna with an infinite ground plane are shown in the following figure:

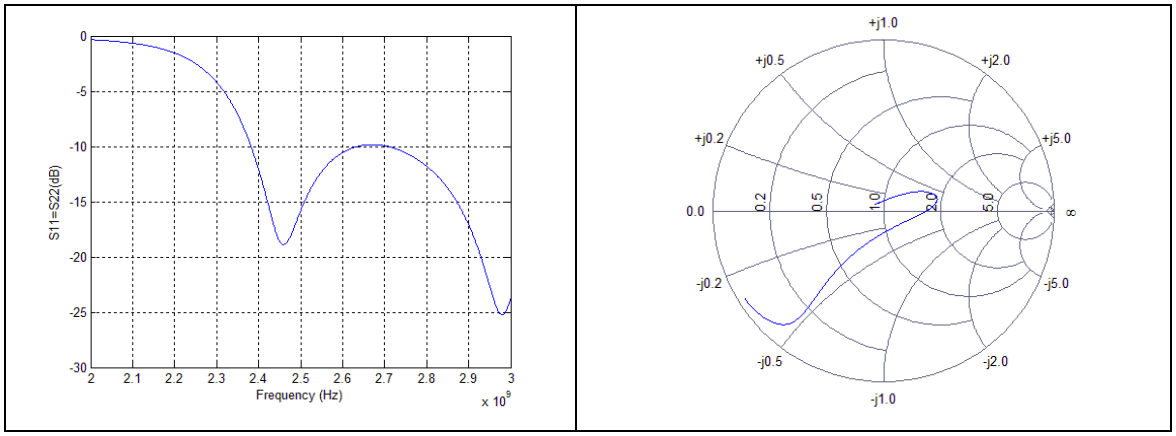

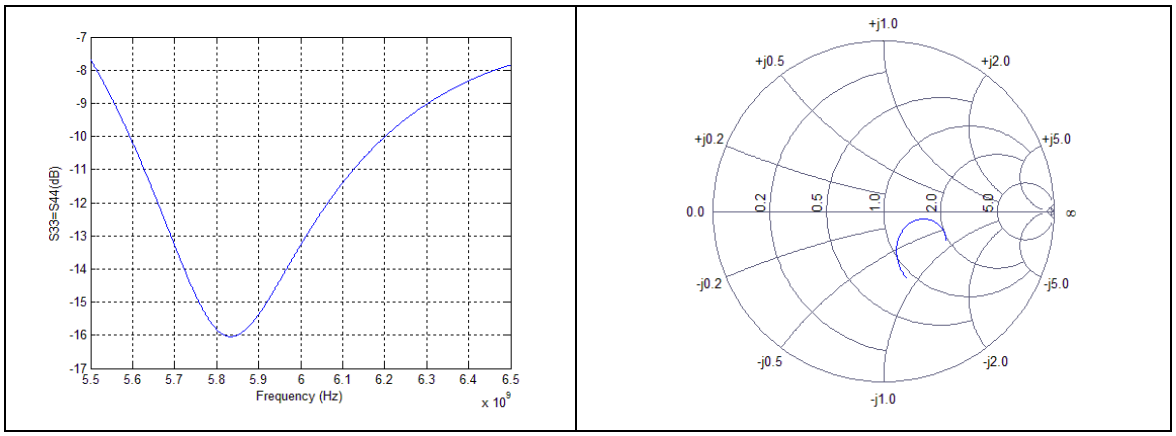

Figure 4-19: Stacked antenna. S-Parameters in the band of 2.442 GHz (Up) and 5.85 GHz (Down).

We can see that the properties of the stacked antenna with an infinite ground plane are still valid inside the bands of interest. So this model was chosen as the final design for the stacked antenna, which was the main goal of the second part of this master thesis.

Finally, in the following tables we can find the characteristics of the final design of the stacked antenna:

Frequency band expected (GHz)	**Elevation Angle (º)[1]**	**Gain (dB)[2]**	**Asymmetry (dB)[3]**	**Half power beam width (º)[4]**	**VSWR**	**BW (GHz)[5]**
2.4-2.484	0	2.7	1.13	39	1.26	2.38-2.64 (10.12%)
5.75-5.95	0	2.5	2.33	25.5	1.37	5.59-6.20 (10.27%)

1) Average elevation angle above the horizontal plane in which take place a maximum in the radiation pattern
2) Maximum gain
3) Maximum asymmetry between maximums in the radiation pattern
4) Average half power beam width
5) Bandwidth where the S_{11} remains under 10 dB

The previous table shows that the S_{11} parameter remains under 10 dB in the bands of interest, which was one of the requirements. Regarding to the shape of the radiation pattern, we can see that the elevation angle is 0º which was a desirable characteristic for our application. In addition the radiation pattern inside each frequency band is quite symmetric. So, this model fulfils all the requirements which were set at the beginning of this master thesis and therefore, constitute a solution for the problem of the design of a dual-frequency stacked antenna dealt in this second part of the master thesis.

4.2.4 Monopole stacked on the top of the patch antenna

Although the solution achieved in the previous section satisfies all the requirements which were presented at the beginning of this master thesis, in this section we are going to analyze another alternative. This alternative arose as a consequence of the impossibility of carrying out the original design proposed at the beginning of the second part of this master thesis, which was studied and analyzed in the section 4.2.2. It consists in placing a monopole on the top of a compact circular patch antenna, so that the monopole acts as an antenna for the band of 5.75 – 5.95 GHz while the circular patch antenna acts as an antenna for the band of 2.4 – 2.484 GHz. In the following figure we can see the EMDS model of this new alternative:

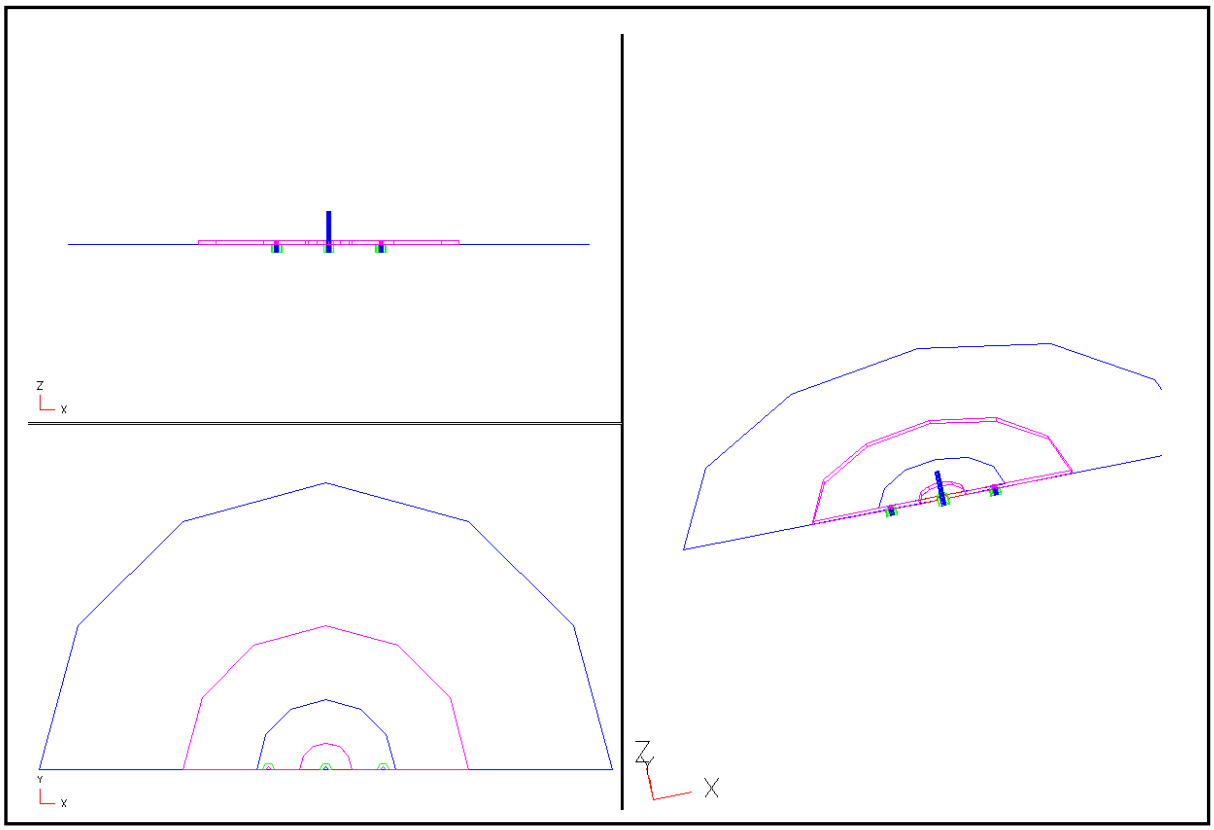

Figure 4-20: EMDS model of the monopole alternative

So, we substitute the compact disk antenna for the highest frequency band, for a monopole which has the patch of the lower antenna as its ground plane. The resonant frequency of a monopole is determined by the next equation:

$$l = \frac{\lambda}{4} = \frac{c}{4f}$$

So if we want a resonant frequency of 5.85 GHz we need a monopole of 12.82 mm.

After some simulation, we concluded that the optimum length that leads to a resonant frequency close to 5.85 GHz is 12.4 mm. We can see that both values are quite similar. In the following tables we can see the final dimensions of this new prototype:

	Feed position	Inner radius	Outer radius	Dielectric radius	Ground plane radius
Lower antenna	23	9.1	24.5	50	Infinite

	Length	Width (Radius of the monopole)
Monopole	12.4	1.5

Concerning to the lower antenna, we had to make some slight modifications. This is because the presence of the monopole slightly affects the properties of the antenna. So, the resonant frequency and the input impedance were a bit different compared to its properties when it was analyzed as a separate entity.

However, once we perform these slight modifications, the properties of the antenna remain quite similar to its properties when it was simulated separately in section 4.2.2.1. In the following figure we can see it:

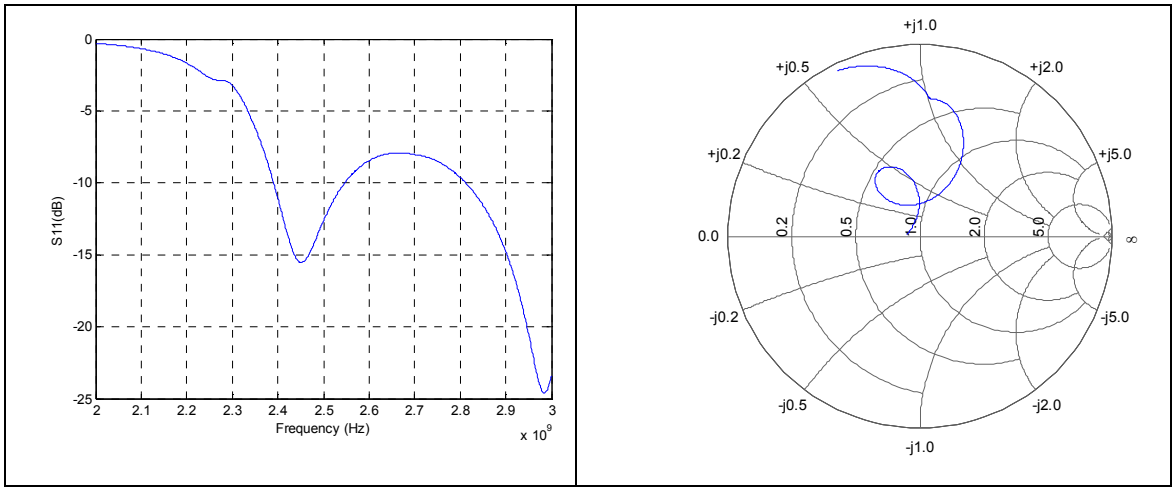

Figure 4-21: Lower antenna. Parameter S_{11} and Smith chart.

We can observe that the properties of the antenna remain similar in the surroundings of the resonant frequency. If we look at the radiation pattern in the following figure it is possible to see that the plot is quite similar to the plot of the section 4.2.3.2. So we can conclude that the presence of the monopole barely affects the properties of the patch

antenna.

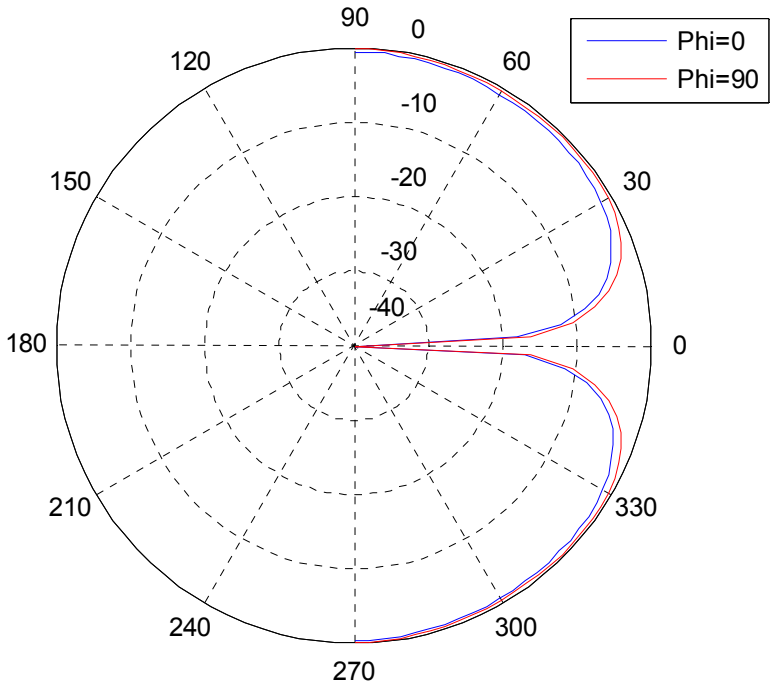

Figure 4-22: Lower antenna. Radiation pattern.

Regarding to the design of the monopole for the band of frequencies between 5.75 GHz and 5.95 GHz, we can see its properties inside the band in the next figure. The first design we did was not valid because it was not enough matched. So we decided to vary the width of the monopole to get a more adequate matching for the monopole antenna. We observed that when the width of the monopole increases, the matching of the antenna gets better. Finally, we chose a radius of 1.5 mm because with this value we obtain a quite good matching for the monopole.

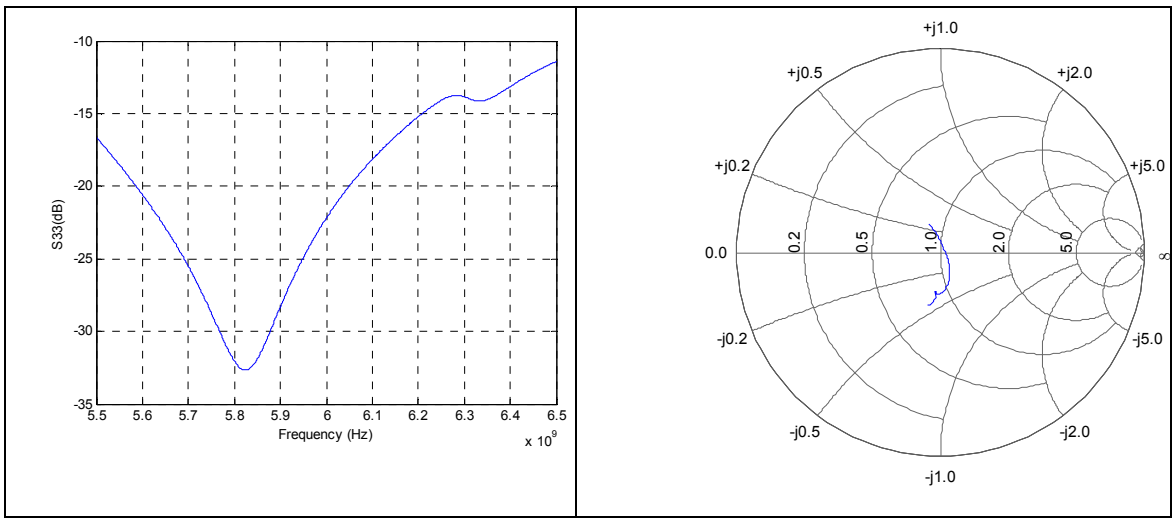

Figure 4-23: Monopole. Parameter S_{11} and Smith chart.

The previous figure shows that the reflection coefficient remains below 10 dB in the band of interest. In fact, the bandwidth of the monopole is wider than the bandwidth of a compact circular patch antenna, so it fulfils the requirements without problems.

Concerning to the radiation pattern, it is not as we could expect. Instead of the classic radiation pattern of a monopole, we obtain the radiation pattern shown in the following figure. The reason is that the ground plane of this monopole is not a simple one. It comprises the ground plane of the lower patch antenna and its metallization patch, so the fields which appear are more complex than the ones which appear in a classical monopole.

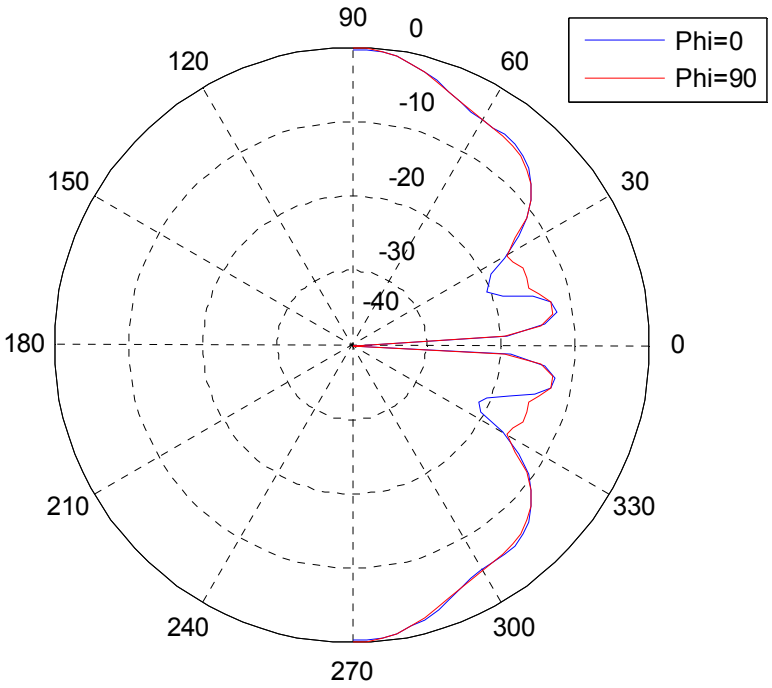

Figure 4-24: Monopole. Radiation pattern.

We can notice a significant ripple when the elevation angle is higher than 45º. In fact, this ripple is higher than the one which appears in the design of the section 4.2.3.1. But as we explain before, this ripple is not a serious problem because the deformation of the radiation pattern due to this ripple is not very high. In addition, if we compare this radiation pattern with the conical radiation pattern with a null in the zenith that we expected, the most important differences appear when the elevation angle is higher than 45º so they can be discard given that in this kind of applications, the most transmissions occur in lower elevation angles ($\varphi<30º$).

If we look again the Smith chart and the radiation pattern of the monopole, we can see that there are important differences with respect to the properties of a classical monopole [13], so we can conclude that the influence of the lower antenna on the monopole is quite strong. The situation is similar to what happened when we tried stacking the two patch antennas in the section 4.2.3.1. The influence of the upper

antenna on the lower antenna was weak but the influence of the lower antenna on the upper antenna was quite strong.

The advantage of this new approach, the use of a monopole to transmit in the band of 5.75-5.95 GHz, is its simplicity. Instead of a complex structure with two patch antennas stacked, we only have to construct a single patch antenna and then, put a monopole on the top. But this new design has the disadvantage that we cannot stack more antennas on the top because of the presence of the monopole. So this kind of design is not suitable for the CVIS project due to the fact that this project need a multi-band terminal which transmits information in more than two band of frequency.

In the following table, the most relevant properties of this alternative are shown:

Frequency band expected (GHz)	**Elevation Angle (º)[1]**	**Gain (dB)[2]**	**Asymmetry (dB)[3]**	**Half power beam width (º)[4]**	**VSWR**	**BW (GHz)[5]**
2.4-2.484	0	1	0.5	70	1.35	2.39-2.55 (6.5%)
5.75-5.95	0	1.5	6	20.5	1.05	5.2-6.28 (18.8%)

1) Average elevation angle above the horizontal plane in which take place a maximum in the radiation pattern
2) Maximum gain
3) Maximum asymmetry between maximums in the radiation pattern
4) Average half power beam width
5) Bandwidth where the S_{11} remains under 10 dB

To summarize, this alternative also fulfils the requirement raised at the beginning of this second part of this master thesis. However, it is not practical for the implementation of a multi-band terminal for the CVIS project given that it is not possible to cover more than two frequency bands. So finally, the design of the section 4.2.3.1 is the most suitable for our objectives.

5. Conclusion

Through this master thesis we have studied the possibility of stack several compact patch antennas to construct a multi-band terminal for the CVIS project. This studied has been carried out by means of two main parts.

In the first part we have studied in depth the patch antenna proposed in [1], firstly with an analytical model. We applied the cavity model to the geometry of our patch antenna so that we could establish the influence of the different parameters of the patch antenna on its properties. The main conclusions we have reached are:

- When we increase the outer radius of the circular patch antenna, it resonant frequency decreases.
- When we increase the inner radius of the circular patch antenna, it resonant frequency increases as well.
- When we increase the electrical permittivity of the circular patch antenna, it resonant frequency decreases.
- When we increase the height of the circular patch antenna, it resonant frequency decreases.

We also discovered that the influence of the height on the resonant frequency was weaker than the influence of the rest of the parameters. So it is more useful basing the choice of the height on other criterions such as the bandwidth of the antenna. In fact, there is a direct relationship between the height of a patch antenna and its bandwidth as we could see in many articles. Another important conclusion we did with the help of this analytical model was the existence of a relationship between the electrical permittivity of the substrate and the elevation angle above the horizontal plane of the radiation pattern. It has been proved that when we increase the electrical permittivity, the elevation angle of the radiation pattern decreases. This is quite important because for the application of the CVIS project, it is important to have a low elevation angle.

With the help of two different simulation tools, WIPL-D and EMDS, we have studied others properties of this kind of antennas which cannot be studied with only the use of the analytical model. We discover a dependency between the position of the feed and the entrance impedance. It was also discovered a dependency between the symmetry of the radiation pattern along the feed plane and the size of the central post. Through the simulation of several cases it was proved that when the inner radius of the patch antenna increases, the radiation pattern becomes more asymmetric. The position of the feed also affects the symmetry of the radiation pattern, but its influence was much weaker, so in order to set a design process, it is more useful choosing the feed position to get a good matching and choosing the inner radius of the patch antenna to obtain a symmetric enough radiation pattern.

Once we had studied, through the use of the analytical model and the simulation tools, we construct some prototypes to check the results we had obtained. In fact, the results obtained with the two simulation tools were quite different, so it was necessary checking which one offers the right results. In addition, we decided to use air as

dielectric in the prototypes so we had to figure out another way of get a low elevation angle. Two main conclusions were derived from the construction of these prototypes:

- The influence of the size of the ground plane on the elevation angle. Although in [1] al the patch antennas have a ground plane twice larger than the patch, we construct three different prototypes with three different ground planes size. It was proved that when the ground plane was decreased and it becomes more similar to the size of the patch, the elevation angle of the radiation pattern becomes lower.
- It was also discovered that the version Lite of the WIPL-D software was not suitable for the simulation of this kind of antenna. The results of this tool were very far of the real properties of the prototypes. It is possible to improve the accuracy of the results if we increase the current expansion parameter, but even in this case the results were not accurate enough.

In the second part we applied the conclusions reached in the first part for the construction of a multi-band terminal. Specifically, we designed a dual-frequency terminal. For doing that, we stack two compact circular patch antennas. The process is the same that in the first part. We use an analytical model for designing each of the two patch antenna, and afterward, we used simulation tools to see what happened when we stack the two patch antennas. In this case we did not use WIPL-D because in the first part we concluded its results were not accurate enough. Finally, it was concluded that it was not possible to build a terminal for the proposed bands (2.4-2.484 GHz and 5.75-5.95GHz). Given that the feed of the upper patch antenna should go inside the central post of the lower patch antenna, we needed that the lower antenna had a large inner radius to allow the variation of the feed position over a wide range, so that we could easily get a good matching for the upper antenna. But when we tried to increase the inner radius of the lower antenna, its radiation pattern becomes quite asymmetric. To solve two modifications over the original design was performed:

- *2 feeds model*: We added a second feed point which was symmetrically placed with respect to the central metallic post.
- *Monopole on the top of the patch antenna*: It is a simplification of the first alternative. It consists in replacing the upper antenna by a monopole.

The first alternative, the 2 feeds model, leads to a symmetric radiation pattern along the feed plane. There was a small asymmetry between the plane feed and the perpendicular plane, but it was almost negligible. So this alternative allows us to increase the inner radius and in this way, we can get a good matching for the upper antenna. In addition it was discovered that when we introduced the second feed, the bandwidth of the patch antennas becomes wider. This is very important because generally, the bandwidth of this kind of antennas is very narrow and the only ways to expand it is increasing the height of the substrate or reducing the electrical permittivity. But we saw before, that we were interested in low electrical permittivity substrates because they lead to low elevation angles. And of course we want that the antenna have a low profile because it makes the antenna more attractive to the final users. So with the introduction of the second feed we could reduce the height of the substrate until 1.575 mm, which is a quite reasonable value. The final design is shown in section 4.2.3.2, where we can check that it fulfils all the requirements which were raised at the beginning of this master thesis. We can also see that the influence of the upper antenna on the lower antenna is almost

negligible, but the influence of the lower antenna on the upper antenna is significant. An important ripple appears in the radiation pattern of the upper antenna when we put it on the top of the lower antenna. This is due to the fact that the ground plane of the upper patch antenna is formed by the patch of the lower antenna and the ground plane, so the complexity of the fields inside this structure is bigger than in the lower patch antenna. However, the differences between the expected radiation pattern and the radiation pattern obtained start for an elevation angle larger than 30º, so it can be discarded given that for this kind of system the most transmissions occurs in low elevation angles.

The second alternative is a simplification of the 2 feeds model. It has the advantage that it is a more simple design, but it is not possible to cover more than two frequency bands with this schema, so finally we decided to propose the 2 feeds model as our final design. In the section 4.2.4 we can see the properties of this new model.

6. Future work

As the main result of the second part of this master thesis we obtained a design of a dual-frequency terminal through the two compact circular patch antennas stacked. Specifically, this stack antenna operates in the band of 2.4-2.484 GHz and in the band of 5.75-5.95 GHz, which are two of the frequencies band used by the protocol CALM. But this protocol, which is used in the CVIS project, uses other wireless technologies which use others frequency bands. So it could be interesting to study the feasibility of stacking more than two patch antennas in order to build a commercial terminal which could be used by the users of the CVIS system. Moreover, the second part of this master thesis ends with the design of the prototype through the use of the analytical model and the EMDS software, but no prototype was built. So it was interesting to build a physical prototype and check the possible differences between the results of the simulation software and the real properties of the final prototype.

On the other hand, it could be interesting to figure out a way to avoid the influence of the lower patch antenna of the stack antenna on the upper antenna. It does not suppose a critical problem, but it could be useful to analyze closer the configuration of the fields inside this complex structure. Finally, it would be interesting to incorporate more than two feed points in order to see how this affects the bandwidth, the radiation pattern, and in summary, if this leads to a better solution.

7. References

1. McEwan N.J., Abd-Alhameed R.A., Ibrahim E.M., Excell P.S., Ali N.T. "*Compact WLAN disc antennas*". IEEE. December 2002.
2. Cooperative Vehicle-Infrastructure System. http://www.cvisproject.org/.
3. U. Balaji. "*Circular patch antenna for radio LAN*". IEEE. 2003.
4. Guo, Y.J., Paez, A., Sadeghzadeh, R.A., Barton, S.K. "*A circular patch antenna for radio LAN*". IEEE. January 1997.
5. Keith R. Carver, James W. Mink. "*Microstrip Antenna Technology*". IEEE. January 1981.
6. Garg R., Reddy V.S. " *Edge feeding of microstrip ring antennas".* IEEE. August 2003.
7. Mehrotra A.R., Jackson D.R, Williams J.T., Long S.A. "*An annular-ring reduced surface wave microstrip antenna*". IEEE. August 1999.
8. Y. Lin, L. Shafai. "*Characteristics of concentrically shorted circular patch microstrip antennas*". IEEE. February 1990.
9. Rodney G. Vaughan. "*Two-Port Higher Mode Circular Microstrip*". IEEE. March 1988.
10. Jawad Y . Siddiqui, D. Guha. "*Improved Formulas for the Input Impedance of Probe Fed Circular Microstrip Antenna*". 2003.
11. Stuart A. Long, Mark D. Walton. "*A Dual-Frequency Stacked Circular-Disc Antenna*". IEEE. 1979.
12. R. Garg, P. Barthia, I. Bahl, A. Ittipiboon. "*Microstrip Antenna Design Handbook*". Archtech House. Norwood, 2001.
13. Constatine A. Balanis. "*Antenna Theory Analysis and Design*". John Wiley & Sons. New York, 1997.
14. Constatine A. Balanis. "*Advanced Engineering Electromagnetics*". John Wiley & Sons. New York, 1997.
15. K. Fong Lee, W. Chen. "*Advances in Microstrip and Printed Antennas*", John Wiley & Sons. New York, 1997.
16. Branko M. Kolundzija, Jovan S. Ognjanovic, Tapan K. Sarkar. "*WIPL-D Microwave: Software and User's Manual*". Archtech House. Belgrade, 2005.
17. "EMDS User guide". Agilent Technologies. 2008. http://eesof.tm.agilent.com/products/emds_main.hyml
18. Svein Vikan. "Steerable Antenna Solution for Communication between Cars". Master's thesis, Norwegian University of Science and Technology. June 2008.
19. Rogers Corporation (Advanced Circuit Materials). "RT/duroid®5870 /5880 High Frequency Laminates". http://www.rogerscorporation.com/mwu/pdf/5000data.pdf

8. Appendix A: MATLAB programs

Influence of the outer radius

```
%Description: This program obtains the resonant frequency of a
circular patch antenna given its dimensions. Specifically, this
program analyzes the influence of the outer radius.

clear all
format long

%Constants
c = 2.998e8;
mr=1; %Permeability
er=1; %Permittivity
h=5e-3; %Height
b=linspace(3e-3,3e-3,100); %Inner radius

%Imputs
a=linspace(10e-3,30e-3,100); %Outer radius
psi=b./a;

%Bessel condition for the resonant frequency
for psiindex=1:length(psi)
    x=[0:0.001:20];
    %TM0
    F=besselj(-1,x).*bessely(0,psi(psiindex)*x)-
besselj(0,psi(psiindex)*x).*bessely(-1,x);
    Fabs=abs(F);

    i=0;
    j=1;
    k=2;
    ind=0; %index of the zeros of the function
    for i=1:[length(x)-3]
        j=j+1;
        k=k+1;

        if ((Fabs(i)>Fabs(j)) && (Fabs(j) < Fabs(k))); %local minimum
            ind=ind+1;
            ceros(ind)=x(j);
        end
    end

    %Effective outer radius calculation
    am=sqrt(a(psiindex)^2-b(psiindex)^2);
    aef=a(psiindex)*sqrt(1+( ((2*h)/(pi*am*er))*
(log((pi*am)/(2*h))+1.7726) ));


    betap=ceros(1)/aef;

    %Resonant frequency
    fr(psiindex)=(betap*c)/(sqrt(mr*er)*2*pi);

end

%Plot
```

```
plot(a*1000,fr/1e9)
title('Influence of the outer radius in the resonant frequency')
xlabel('a(mm)')
ylabel('fr(GHz)')
grid on
```

Inner radius influence

```
%Description: This program obtains the resonant frequency of a
circular patch antenna given its dimensions. Specifically, this
program analyzes the influence of the inner radius.

clear all
format long

%Constants
c = 2.998e8;
mr=1; %Permeability
er=1; %Permittivity
h=5e-3; %Height
a=linspace(30e-3,30e-3,100); %Outer radius

%Imputs
b=linspace(5e-3,25e-3,100); %Inner radius
psi=b./a;

%Bessel condition for the resonant frequency
for psiindex=1:length(psi)
    x=[0:0.001:20];
    %TM0
    F=besselj(-1,x).*bessely(0,psi(psiindex)*x)-
besselj(0,psi(psiindex)*x).*bessely(-1,x);
    Fabs=abs(F);

    i=0;
    j=1;
    k=2;
    ind=0; %index of the zeros of the function
    for i=1:[length(x)-3]
        j=j+1;
        k=k+1;

        if ((Fabs(i)>Fabs(j)) && (Fabs(j) < Fabs(k))); %local minimum
            ind=ind+1;
            ceros(ind)=x(j);
        end
    end

    %Effective outer radius calculation
    am=sqrt(a(psiindex)^2-b(psiindex)^2);
    aef=a(psiindex)*sqrt(1+( ((2*h)/(pi*am*er))*
(log((pi*am)/(2*h))+1.7726) ));


    betap=ceros(1)/aef;

    %Resonant frequency
    fr(psiindex)=(betap*c)/(sqrt(mr*er)*2*pi);

end
```

```
%Plot
plot(b*1000,fr/1e9)
title('Influence of the inner radius in the resonant frequency')
xlabel('b(mm)')
ylabel('fr(GHz)')
grid on
```

Height influence

```
%Description: This program obtains the resonant frequency of a
circular patch antenna given its dimensions. Specifically, this
program analyzes the influence of the height of the substrate.

clear all
format long

%Constants
c = 2.998e8;
mr=1; %Permeability
er=1; %Permittivity
a=25e-3; %Outer radius
b=3e-3; %Inner radius
psi=b/a;

%Imputs
h=linspace(1e-3,5e-3,100); %Height

%Bessel condition for the resonant frequency
for hindex=1:length(h)
    x=[0:0.001:20];
    %TM0
    F=besselj(-1,x).*bessely(0,psi*x)- besselj(0,psi*x).*bessely(-
1,x);
    Fabs=abs(F);

    i=0;
    j=1;
    k=2;
    ind=0; %index of the zeros of the function
    for i=1:[length(x)-3]
        j=j+1;
        k=k+1;

        if ((Fabs(i)>Fabs(j)) && (Fabs(j) < Fabs(k))); %local minimum
            ind=ind+1;
            ceros(ind)=x(j);
        end
    end

    %Effective outer radius calculation
    am=sqrt(a^2-b^2);
    aef=a*sqrt(1+( ((2*h(hindex))/(pi*a*er))*
(log((pi*a)/(2*h(hindex)))+1.7726) ));


    betap=ceros(1)/aef;

    %Resonant frequency
    fr(hindex)=(betap*c)/(sqrt(mr*er)*2*pi);

end
```

```
%Plot
plot(h*1000,fr/1e9)
title('Influence of the heigth of the substrate in the resonant
frequency')
xlabel('h(mm)')
ylabel('fr(GHz)')
grid on
```

Permittivity influence

```
%Description: This program obtains the resonant frequency of a
circular patch antenna given its dimensions. Specifically, this
program analyzes the influence of the outer radius..

clear all
format long

%Constants
c = 2.998e8;
mr=1; %Permeability
h=5e-3; %Height
a=25e-3; %Outer radius
b=3e-3; %Inner radius
psi=b/a;

%Imputs
er=linspace(1,10,100); %Permittivity

%Bessel condition for the resonant frequency
for erindex=1:length(er)
    x=[0:0.001:20];
    %TM0
    F=besselj(-1,x).*bessely(0,psi*x)- besselj(0,psi*x).*bessely(-
1,x);
    Fabs=abs(F);

    i=0;
    j=1;
    k=2;
    ind=0; %index of the zeros of the function
    for i=1:[length(x)-3]
        j=j+1;
        k=k+1;

        if ((Fabs(i)>Fabs(j)) && (Fabs(j) < Fabs(k))); %local minimum
            ind=ind+1;
            ceros(ind)=x(j);
        end
    end

    %Effective outer radius calculation
    am=sqrt(a^2-b^2);
    aef=a*sqrt(1+( ((2*h)/(pi*am*er(erindex)))*
(log((pi*am)/(2*h))+1.7726) ));


    betap=ceros(1)/aef;

    %Resonant frequency
    fr(erindex)=(betap*c)/(sqrt(mr*er(erindex))*2*pi);
```

```
end

%Plot
plot(er,fr/1e9)
title('Influence of the electrical permittivity of the substrate in
the resonant frequency')
xlabel('Relative electrical permitivity')
ylabel('fr(GHz)')
grid on
```

General influence of the different parameters

```
%Description: This program plots the possible dimensions and
substrates materials that lead to a particular resonant frequency.

clear all
format long
%Constants
c = 2.998e8;
mr=1; %Permeability
h=1.524e-3; %Height

%Imputs
er=[1 3 5]; %Permittivity
fr=input ('Enter the resonant frequency:'); %Resonant frequency

%Graphic colors
colores=['b' 'r' 'g' 'c' 'm' 'y' 'k' 'b' 'r' 'g' 'c' 'm' 'y' 'k'];

for erindex=1:length(er)

%betap for each er
betap=sqrt(mr*er(erindex))*(2*pi*fr)/c;

%for each psi=a/b, I calculate the function for the x=betap*a vector

x=[0:0.01:30];
psi=[0.1:0.01:0.9];

psiindex=[1:length(psi)];

for psiindex=1:length(psi)

    %Bessel function

    F=besselj(-1,x).*bessely(0,psi(psiindex)*x)-
besselj(0,psi(psiindex)*x).*bessely(-1,x);

    %First zero calculation. I look for the first local minimun of the
bessel function

    Fabs=abs(F);
    i=0;
    j=1;
    k=2;
    ind=0; %index of the zeros of the function
    for i=1:[length(x)-3]
        j=j+1;
        k=k+1;
```

```
        if ((Fabs(i)>Fabs(j)) && (Fabs(j) < Fabs(k))); %local minimum
            ind=ind+1;
            ceros(ind)=x(j);
        end
    end

%From the first zero of the bessel function I obtain the value of a
a(psiindex)=ceros(1)/betap;

%Correction factor for considering the fringing field at the edges of
the patch.

aef=a(psiindex)/10;

am=sqrt(aef^2*(1-psi(psiindex)^2));
a(psiindex)=aef/(sqrt(1+(2*h/(pi*er(erindex)*am))*(log(pi*am/(2*h)+1.7
726))));

a(psiindex)=a(psiindex)*10;

%Once we know a we can find the value b with the relation b=K*a
b(psiindex)=psi(psiindex)*a(psiindex);


end %for

%Once I have the a and b for each psi, I plot the results

plot(psi,a,colores(erindex))
hold on
plot(psi,b,[colores(erindex) '--'])
grid on
title('Antenna dimensions');
xlabel('b/a');

end
hold off
```

Radiation pattern

```
%Description: This program plots the radiation pattern of the antenna.

clear all
format long
%Constants
c = 2.998e8;
mr=1; %Permeability
fr=2e9; %Resonant frequency
%Inputs

%For choosing this values, we should use the previous programs in this
%appendix
a=input('Introduce outer radius:');
b=input('Introduce inner radius:');

%Calculation of the radiation pattern

K0=2*pi*fr;
theta=linspace(0,pi,100);
F=abs(besselj(1,K0*a*sin(theta))).^2;
```

```
F=F/max(F);


%Plot
polar(theta,F)
```

9. Appendix B: WIPLD-D Corrections

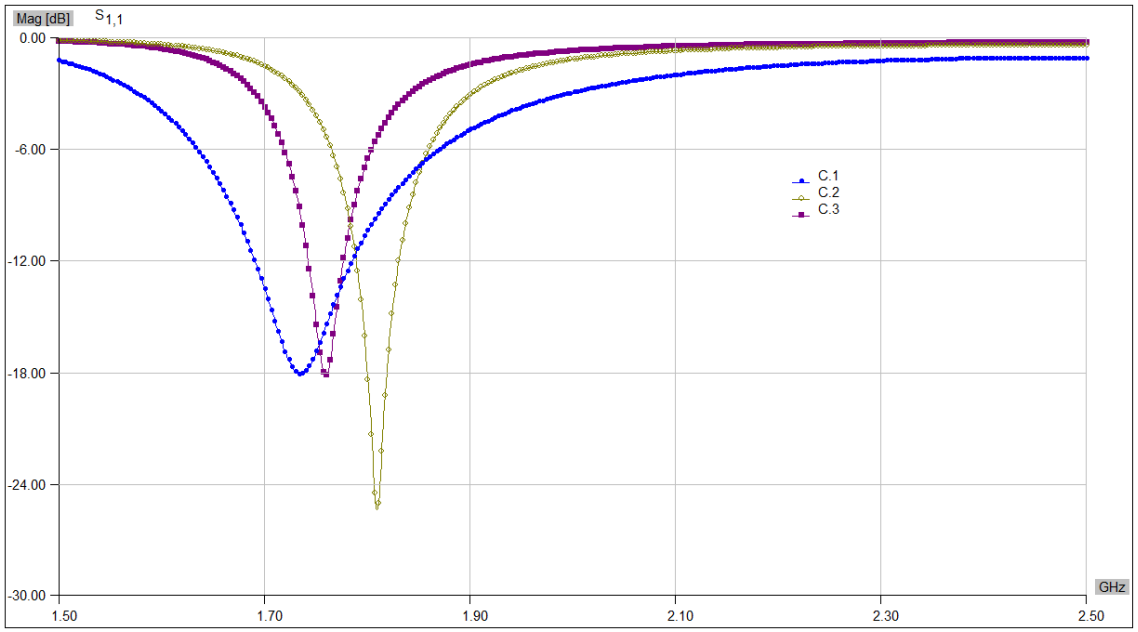

Figure 9-1: Parameter S_{11} of the prototypes.

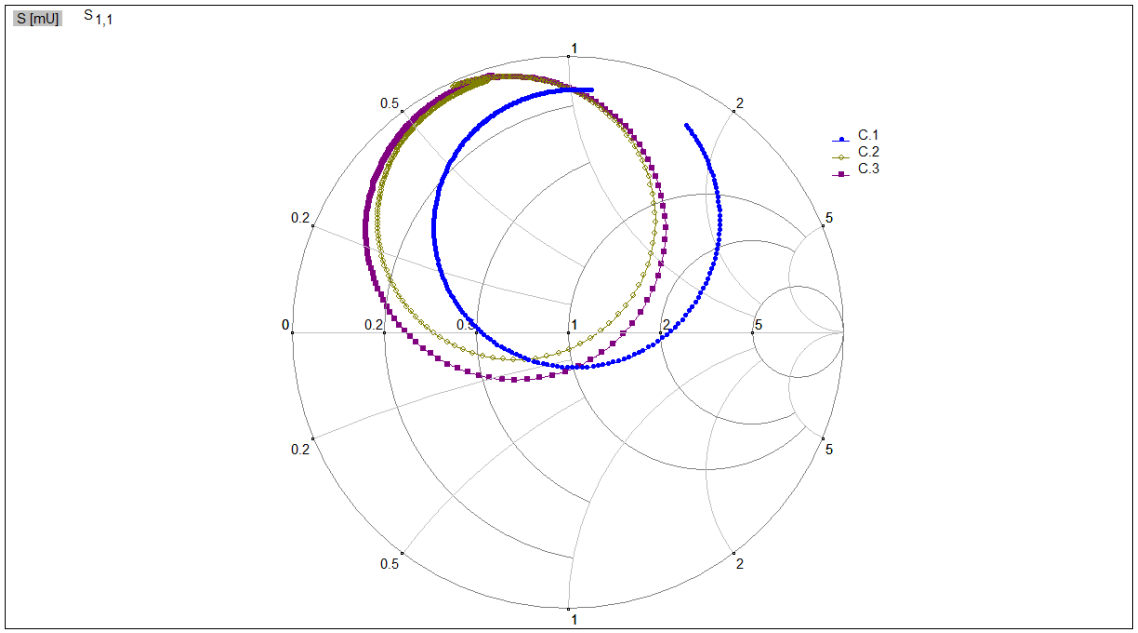

Figure 9-2: Smith chart of the prototypes.

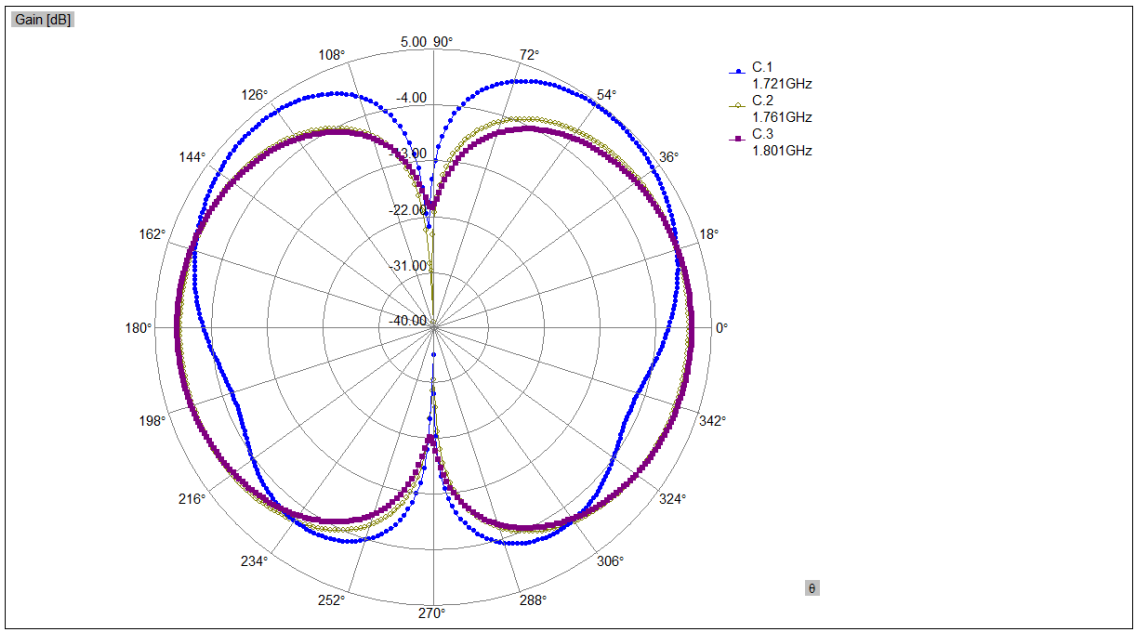

Figure 9-3: Radiation pattern of the prototypes (Plane φ=0).